# Dual-wavelength control via phase-controlled optical feedback

Pawlus, Robert

(2020)

Vrije
Universiteit
Brussel

FACULTY OF ENGINEERING
Department of Applied Physics and Photonics

# Dual-wavelength control via phase-controlled optical feedback

A thesis submitted in fulfilment of the requirements for the award of the degree of Doctor in Engineering by

Robert Pawlus

March 2020

Promoters: Prof. Dr. Martin Virte
Prof. Dr. Ir. Hugo Thienpont
Priv. Doz. Dr. rer. nat. Stefan Breuer

TECHNISCHE
UNIVERSITÄT
DARMSTADT

# Dual-wavelength control via phase-controlled optical feedback

To the faculty of Physics
of the Technische Universität Darmstadt

to obtain the academic degree
of a Doctor rerum naturalium (Dr. rer. nat.)

Dissertation of
M.Sc. Robert Pawlus
born in Darmstadt, Germany

First reviewer: Priv.-Doz. Dr. rer. nat. Stefan Breuer
Second reviewer: Prof. Dr. Martin Virte

Darmstadt 2020
D17

M.Sc. Robert Pawlus: Dual-wavelength control via phase-controlled optical feedback
Vrije Universiteit Brussel, Belgium & Technische Universität Darmstadt, Germany
Year of publication: 2020
Date of public defence: 15.06.2020

# Members of the Jury

**Prof. Dr. Ir. Yves Rolain, chairman**
Department of Fundamental Electricity and Instrumentation,
Vrije Universiteit Brussel, Belgium

**Em. Prof. Dr. Ir. Roger Vounckx, vice-chairman**
Department of Fundamental Electricity and Instrumentation,
Vrije Universiteit Brussel, Belgium

**Prof. Dr. Ir. Nathalie Vermeulen, secretary**
Department of Applied Physics and Photonics,
Vrije Universiteit Brussel, Belgium

**Prof. Dr. Erwin Bente, examiner**
Photonic Integration group,
Eindhoven University of Technology, Netherlands

**Dr. Yanhua Hong, examiner**
School of Computer Science and Electronic Engineering,
Bangor University, United Kingdom

**Prof. Dr. Benno Liebchen, examiner**
Institute of solid-state physics,
Technische Universität Darmstadt, Germany

**Prof. Dr. Martin Virte, promoter**
Department of Applied Physics and Photonics,
Vrije Universiteit Brussel, Belgium

**Prof. Dr. Ir. Hugo Thienpont, co-promoter**
Department of Applied Physics and Photonics,
Vrije Universiteit Brussel, Belgium

**Priv. Doz. Dr. rer. nat. Stefan Breuer, co-promoter**
Institute of Applied Physics,
Technische Universität Darmstadt, Germany

## ABSTRACT

Lasers with the capability to emit simultaneously at two distinct wavelengths - so-called dual-wavelength lasers - are highly desirable in several applications ranging from data communication, to the field of THz or sensing, but remain challenging to manufacture. Current solutions can typically be categorized in two groups. On the one hand, external forcing can be used to make a largely multi-mode laser emit at only two wavelengths. These are highly versatile and flexible solutions but are typically obtained through complex and/or bulky setups. On the other hand, laser structures with intrinsic wavelength selection appear to be way more robust but suffer from a lack of external control and flexibility; in short, these devices cannot be fine-tuned. In this PhD thesis, we propose, implement and experimentally demonstrate a simple technique for controlling the output of dual-wavelength lasers relying on a compact external structure that can be easily integrated monolithically with the laser.

This new technique is based on the Fabry-Perot effect of a phase controlled external feedback cavity. In short, the external cavity will slightly boost resonant modes while the non-resonant modes will see a slight increase of their losses. The phase control then allows to select the resonating modes. As a result, setting the feedback cavity length to ensure that the two distinct wavelengths emitted by the lasers are out-of-phase after a cavity round trip allows to selectively boost or suppress one or the other wavelength on demand.

To demonstrate the feasibility and relevance of the approach, we have first designed and implemented dual-wavelength lasers on a Photonic Integrated Circuit (PIC), using a generic foundry platform. Because the proposed control technique would have the advantage of being particularly compact, we rely on Distributed Bragg Reflectors (DBRs) as wavelength selective elements of the laser, thus obtaining a compact laser as well. We have designed different lasers using DBRs, placed sequentially or in parallel, to achieve dual-wavelength emission combined with a broadband reflector or a third DBR. We then coupled these devices with specifically designed external cavities including an electro-optic phase modulator and a semiconductor optical amplifier in order to control both, the feedback strength and the feedback phase.

After a detailed characterization of the dual-wavelength lasers and, in particular, a confirmation that these were indeed successfully emitting at two distinct wavelengths, we have then explored the effect of the phase controlled optical feedback on the laser emission. Thus, we were able to confirm that the proposed technique could be consistently used to achieve complete extinction of each mode with suppression ratios as high as 50 dB. Despite varying performances across the different devices, the switching ap-

peared to be particularly robust against most experimental variables. Moreover, we have recorded switching times below 4 ns, which appeared to be mostly limited by the own response time of the phase modulator, and which could potentially be reduced below the nanosecond timescale making it one of the fastest switching techniques currently available. Next, we have investigated the limitations of both the dual-wavelength laser and the control technique. Taking advantage of the large amount of measurements performed across several PICs and lasers, combined with a thorough numerical exploration of the parameter space, we were able to identify different directions of research for further optimizations. Improvements of the DBRs could lead to an improved wavelength tunability that the external cavity could withstand, while the laser and external cavity structure could potentially be optimized to achieve higher output power, higher side mode suppression ratio and a more compact design. Last, but not least, the current results strongly suggest that going from dual to multi ($\geqslant 3$) wavelength lasers could be realistically considered without significant conceptual changes.

To conclude, in this thesis, we propose a new solution to control dual-wavelength lasers through a highly compact and efficient external structure which allows to balance or switch the wavelength emission at will using a single control parameter: the optical feedback phase.

## SAMENVATTING

Lasers met de mogelijkheid om gelijktijdig uit te zenden op twee verschillende golflengten zijn zeer wenselijk in verschillende toepassingen, variërend van datacommunicatie tot het veld van THz of van detectie, maar blijven een uitdaging om te vervaardigen. Huidige oplossingen kunnen doorgaans in twee groepen worden onderverdeeld. Enerzijds kan externe forcering worden gebruikt om een grotendeels multi-mode laser te laten uitzenden op slechts twee golflengten. Dit zijn zeer veelzijdige en flexibele oplossingen, maar worden meestal verkregen door complexe en / of omvangrijke opstellingen. Aan de andere kant lijken laserstructuren met intrinsieke golflengteselectie veel robuuster, maar lijden ze onder een gebrek aan externe controle en flexibiliteit; kortom, deze apparaten kunnen niet worden verfijnd. In dit proefschrift suggereren, implementeren en demonstreren we experimenteel een eenvoudige techniek voor het regelen van de output van lasers met dubbele golflengte op basis van een compacte externe structuur die gemakkelijk monolithisch kan worden geïntegreerd met de laser.

Deze nieuwe techniek is gebaseerd op het Fabry-Perot-effect van een fasegestuurde externe trilholte. Kortom, de uitwendige trilholte zal de resonantiemodi enigszins versterken, terwijl de niet-resonerende modi een lichte toename van hun verliezen zullen zien. De faseregeling maakt het vervolgens mogelijk om de resonerende modi te selecteren. Als resultaat, laat het instellen van de lengte van de trilholte, zodat dat de twee verschillende golflengten die door de lasers worden uitgezonden uit fase zijn na een rondreis in de trilholte, toe om op verzoek selectief de ene of de andere golflengte te versterken of te onderdrukken.

Om de haalbaarheid en relevantie van de aanpak aan te tonen, hebben we eerst lasers met dubbele golflengte ontworpen en geïmplementeerd op een fotonisch geïntegreerd circuit (Photonic Integrated Circuit, PIC), met behulp van een generiek platform. Omdat de voorgestelde regeltechniek het voordeel zou hebben dat deze bijzonder compact is, vertrouwen we op verdeelde Bragg-reflectoren (distributed Bragg reflectors, DBRs) als golflengte-selectieve elementen van de laser, waardoor we ook een compacte laser krijgen. We hebben verschillende lasers ontworpen die DBRs gebruiken, zij het sequentieel of parallel geplaatst, om emissie met dubbele golflengte te bereiken in combinatie met een breedbandreflector of een derde DBR. Vervolgens hebben we deze apparaten gekoppeld aan speciaal ontworpen externe trilholtes, waaronder een elektro-optische fasemodulator en een halfgeleider optische versterker om zowel de terugkoppelsterkte als de terugkoppelfase te regelen.

Na een gedetailleerde karakterisering van de lasers met dubbele golflengte en, in het bijzonder, een bevestiging dat deze inderdaad succesvol opereerden bij twee verschillende golflengten, hebben we vervolgens het effect van de fasegestuurde optische feedback op de laseremissie onderzocht. Zo konden we bevestigen dat de voorgestelde techniek consistent kon worden gebruikt om elke modus volledig te onderdrukken met verhoudingen zo hoog als 50 dB. Ondanks verschillende prestaties op de verschillende apparaten, bleek de omschakeling bijzonder robuust ten opzichte van de meeste experimentele variabelen. Bovendien hebben we schakeltijden vastgelegd onder de 4 ns, die meestal beperkt bleken te zijn door de eigen reactietijd van de fasemodulator en die mogelijk zouden kunnen worden teruggebracht tot een tijdschaal onder de nanoseconde, waardoor het een van de snelste schakeltechnieken is die momenteel beschikbaar zijn.

Vervolgens hebben we de beperkingen van zowel de laser met dubbele golflengte als de besturingstechniek onderzocht. Door gebruik te maken van het groot aantal metingen uitgevoerd op verschillende PICs en lasers, in combinatie met een grondige numerieke verkenning van de parameterruimte, konden we verschillende onderzoeksrichtingen identificeren voor verdere optimalisatie. Verbeteringen van de DBRs zouden kunnen leiden tot een verbeterde golflengteafstemming die ondersteund wordt door de externe trilholte, terwijl de laser en de externe trilholtestructuur mogelijk zouden kunnen worden geoptimaliseerd om een hoger uitgangsvermogen, een hogere onderdrukkingsverhouding in de zijmodus en een compacter ontwerp te bereiken. Tenslotte suggereren de huidige resultaten sterk dat overgaan van tweevoudige naar meervoudige ($\geqslant 3$) golflengtelasers realistisch overwogen zou kunnen worden zonder significante conceptuele veranderingen.

Als conclusie stellen we in dit proefschrift een nieuwe oplossing voor om lasers met dubbele golflengte te besturen via een zeer compacte en efficiënte externe structuur die het mogelijk maakt om de golflengte-emissie naar believen te balanceren of te schakelen met behulp van een enkele regelparameter: de optische terugkoppelfase.

## ZUSAMMENFASSUNG

Laser mit der Fähigkeit gleichzeitig auf zwei Wellenlängen zu emittieren sind in verschiedenen Anwendungen, ausgehend von der Datenkommunikation über das Gebiet der THz Generierung bis hin zu optischen Messeinrichtungen äußerst attraktiv, ihre Herstellung erweist sich jedoch als schwierig. Aktuelle Lösungen lassen sich in zwei Gruppen unterteilen. Einerseits kann externes triggern verwendet werden, um einen multi-modalen Laser auf nur zwei Wellenlängen emittieren zu lassen. Diese Lösungen sind äußerst vielseitig und flexibel, benötigen jedoch in der Regel ausreichend Platz und resultieren in komplexen Aufbauten. Andererseits scheinen Laserstrukturen mit intrinsischer Wellenlängenselektion robuster zu sein, jedoch mangelt es ihnen an externer Kontrolle und Flexibilität, da sie nicht feinabgestimmt werden können. In dieser Doktorarbeit wird eine einfache Methode zur Steuerung der Ausgangsleistung von Lasern mit zwei Wellenlängen vorgeschlagen, implementiert sowie experimentell demonstriert. Dabei wird eine kompakte externe Kavität verwendet, die monolithisch mit dem Laser integriert werden kann.

Dieser neue Ansatz basiert auf dem Fabry-Perot-Effekt einer phasen-gesteuerten externen Rückkopplung. Resonante Moden werden durch die externe Kavität bevorzugt, während die anti-resonanten Moden erhöhte Verluste erleiden. Die Phasensteuerung ermöglicht dann die Auswahl der resonanten Moden. Durch justieren der Kavitätslänge kann sichergestellt werden, dass die zwei von dem Laser emittierten Wellenlängen nach einem Durchlauf der externen Kavität phasenverschoben sind und entweder die eine oder die andere Wellenlänge bei Bedarf selektiv bevorzugt oder unterdrückt werden kann.

Um die Machbarkeit und Relevanz des Ansatzes zu demonstrieren, werden zunächst Laser mit zwei Wellenlängen auf einem optischen integrierten Schaltkreis unter Verwendung einer generischen Plattform entworfen und implementiert. Die vorgeschlagene Steuerungsmethode hat den Vorteil besonders kompakt zu sein, um auch Kompaktheit für die Laser zu erreichen, werden Bragg-Reflektoren als wellenlängenselektive Elemente genutzt. Verschiedene Laser wurden unter der Verwendung dieser Reflektoren entwickelt, die entweder sequentiell oder parallel angeordnet sind, um eine Emission auf zwei Wellenlängen in Kombination mit einem Breitbandreflektor oder einem dritten Bragg-Reflektor zu erzielen. Diese Laser wurden dann mit individuell angepassten externen Kavitäten gekoppelt, einschließlich eines elektrooptischen Phasenmodulators und eines optischen Halbleiterverstärkers, um sowohl die Rückkopplungsstärke als auch die Rückkopplungsphase zu steuern.

Nach einer detaillierten Charakterisierung der Laser und insbesondere einer Bestätigung, dass diese tatsächlich auf zwei unterschiedlichen Wellenlängen emittieren, wurde der Effekt der phasengesteuerten optischen Rückkopplung auf die Laseremission untersucht. Auf diese Weise konnte die vorgeschlagene Methode in unterschiedlichen Lasern experimentell demonstriert werden, um eine vollständige Unterdrückung der Wellenlängen mit Unterdrückungsverhältnissen von bis zu 50 dB zu erreichen. Trotz unterschiedlicher Leistungen der verschiedenen Laser war das Schalten gegenüber den meisten experimentellen Variablen robust. Darüber hinaus konnten Schaltzeiten von unter 4 ns demonstriert werden, die größtenteils durch die eigene Reaktionszeit des Phasenmodulators begrenzt zu sein scheinen und die möglicherweise unter die Nanosekunden-Zeitskala reduziert werden könnten, was ihn zu einer der schnellsten derzeit verfügbaren Schalttechniken macht. Als nächstes wurden die Einschränkungen sowohl des Zweiwellenlängenlasers als auch der Steuerungsmethode untersucht. Dank einer Vielzahl von Messungen, die an mehreren optischen integrierten Schaltkreisen und Lasern durchgeführt wurden, sowie einer theoretischen Untersuchung des Parameterraums, konnten unterschiedliche Aspekte für weitere Optimierungen identifiziert werden. Verbesserungen der Bragg-Reflektoren könnten zu einer besseren Abstimmbarkeit der Wellenlängen führen, die die externen Kavität kompensieren könnte, während die Laser- und externe Kavität optimiert werden könnten um eine höhere Ausgangsleistung, ein höheres Unterdrückungsverhältnis für die Seitenmoden und ein kompakteres Design zu erzielen. Zuletzt deuten die aktuellen Ergebnisse darauf hin, dass der Übergang von Lasern mit zwei zu mehreren Wellenlängen ($\geqslant 3$) ohne wesentliche konzeptionelle Änderungen in Betracht gezogen werden könnte.

Zusammenfassend wird in dieser Arbeit eine neue Methode zur Steuerung von Lasern mit zwei Wellenlängen durch eine kompakte und effiziente externe Kavität vorgeschlagen, die es ermöglicht die Wellenlängenemission nach Belieben mithilfe eines einzigen Steuerparameters auszugleichen oder umzuschalten: der optischen Rückkopplungsphase.

# CONTENTS


1 INTRODUCTION ON DUAL-WAVELENGTH LASERS 1
- 1.1 Semiconductor lasers 2
- 1.2 Need for dual-wavelength lasers 5
- 1.3 Achieving dual-wavelength emission 6
- 1.4 Generic foundry platform as a user 9
- 1.5 Influence of optical feedback on lasers 12
- 1.6 Objectives and outline of this work 15

2 CONTROL APPROACH FOR DUAL-WAVELENGTH EMISSION 17
- 2.1 Control approach 18
- 2.2 Simulation model 20
- 2.3 Phase dependency of switching performance 23
- 2.4 Conclusion 33

3 INTEGRATED DUAL-WAVELENGTH LASERS 35
- 3.1 Solitary laser layouts 36
- 3.2 Implementation on first PIC 40
- 3.3 Optimization of dual-wavelength concepts 44
- 3.4 Experimental setup 48
- 3.5 Characterisation of dual-wavelength lasers 50
- 3.6 Conclusion 56

4 AMPLITUDE CONTROL VIA PHASE-CONTROLLED OPTICAL FEEDBACK 57
- 4.1 Feedback cavity design on PIC 58
- 4.2 Impact of tuning the optical feedback delay 60
- 4.3 Exploring the parameter space 64
- 4.4 Switching speed 68
- 4.5 Conclusion 71

5 LIMITATIONS OF PERFORMANCES 73
- 5.1 Robustness against relative phase shift variations 74
- 5.2 Limitations observed 80
- 5.3 Improvements on lasers and feedback section 85
- 5.4 Conclusion 88

6 CONCLUSION 89

6.1 Main achievements 90
6.2 Perspectives for future work 93

LIST OF PUBLICATIONS 95

BIBLIOGRAPHY 97

CURRICULUM VITAE 107

# 1 INTRODUCTION ON DUAL-WAVELENGTH LASERS

In this first chapter, the framework of this PhD thesis will be introduced and all necessary fundamentals will be discussed to give the reader the necessary context and means to follow the upcoming chapters. First, general basics on the laser emission in semiconductor lasers will be introduced in section 1.1. Then the need for multi-wavelengths lasers will be discussed in section 1.2 together with an overview on how a multi-wavelength emission can be achieved in section 1.3. Then, a brief introduction onto multi-project-waver platforms will be given in section 1.4 and the impact of optical feedback onto a laser will be discussed in section 1.5. Finally, the objectives of this thesis will be outlined in the last section 1.6.

## 1.1 SEMICONDUCTOR LASERS

The first step towards the development of a laser was made by Albert Einstein with his prediction of stimulated emission in 1917 [1]. Basically three different events can occur in an two-level energy system occupied by an electron: absorption, spontaneous emission or stimulated emission as shown in Fig. 1.1. An incident photon with the correct energy will interact with an electron occupying the lower energy level and lift it into the higher energy state while being absorbed in the process (a). The electron will relax at some point to reach thermal equilibrium by sending out a photon, releasing the energy in a process called spontaneous emission (b). However, if another incident photon interacts with the excited system, the photon will trigger the emission of another photon, identical in wavelength, polarisation and orientation, this is called stimulated emission and is the fundamental basis of every laser (c).

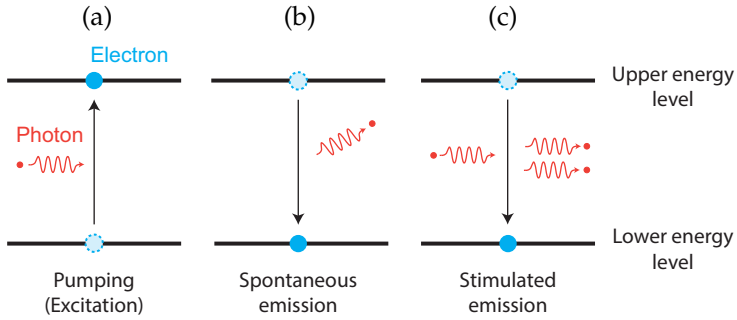


Figure 1.1: Two level energy system showing: (a) An incoming photon lifts an electron to a higher energy level while being absorbed in the process. (b) Spontaneous emission of a photon into a random direction with the electron relaxing to the lower energy state. (c) Stimulated emission with an incoming photon triggering the emission of an identical second photon.

To achieve a continuous-wave emission in a laser, the electron occupation in the upper energy level needs to be higher than in the lower energy level, i.e. a population inversion is required. This is crucial so that stimulated emission dominates the spontaneous emission. Achieving a population inversion in a two-level energy system with pumping is however impossible. The electrons of an atom in a thermal equilibrium mostly occupy the lower energy state. Incident radiation with the correct energy can only achieve a population of 50 % per energy level, no population inversion. A higher population of the upper energy level would otherwise be depleted by stimulated emission. Hence, three and four energy level systems were considered to overcome this limitation. In these systems, two energy levels serve as a radiative transitions with a long carrier lifetime for the upper energy level and a very short carrier lifetime for the lower energy level to maximize the population inversion. The other energy levels serve as pumping levels to refill the radiative energy levels as fast as possible with short carrier lifetimes.

With the development of semiconductor lasers, electrons could be injected right into the upper energy levels to achieve the desired population inversion. Doping the semiconductor material improves its conductivity and allows the transport of the carriers to the area where the two materials are connected, the depletion zone. A p-doping improves

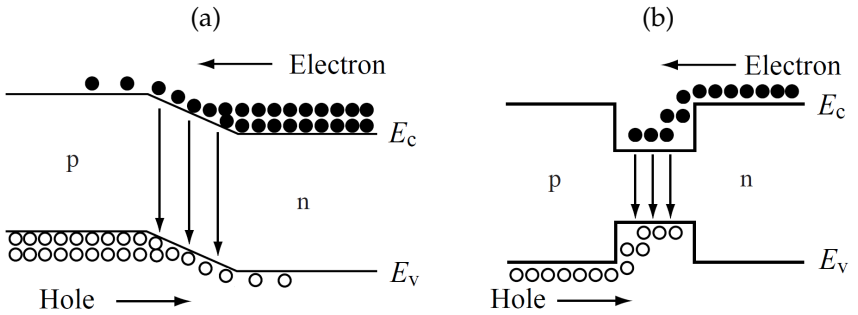


Figure 1.2: In (a), a pn-junction showing the lack of carrier confinement which results in a low carrier population. In (b), a double-hetero-junction with three materials varying in their band gaps confine the carriers in a small region, leading to better performances [2].

the conductivity for the holes while n-doping improves the conductivity for the electrons. In the depletion zone, the recombination process between the carriers occurs and photons are emitted in the process as shown in Fig. 1.2 (a). However, the confinement of these transitions is poor and results in bad efficiencies and even requires pulsed operation due to heat dissipation. Single- and later double-hetero-structures were proposed to overcome these issues and spatially confine the electrons and photons to the same region in order to lower the threshold currents and is shown in Fig. 1.2 (b). This improved the efficiency and lead to continuous-wave operation with high powers at room temperature [3], [4].

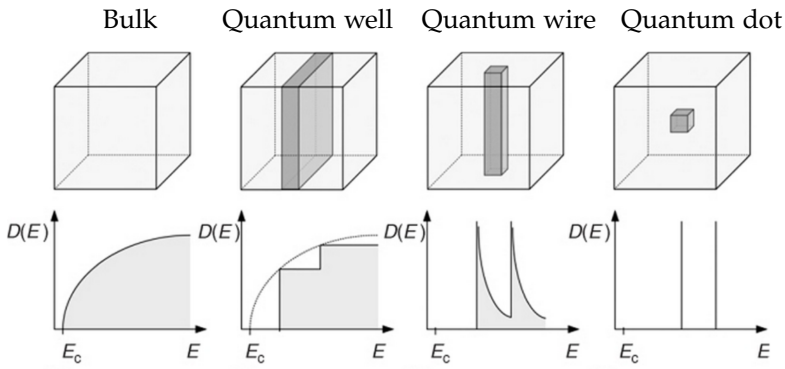


Figure 1.3: Energy confinement of the material structure: Bulk material with a continuous energy states. Confining the material in one direction results in a Quantum-well structure with stepwise energy states. Confining the material in two directions results in Quantum-wires with a sawtooth like energy states. A confinement in three directions results in Quantum-dots with discrete energy states. [5]

Further extensive developments aimed to improve the carrier localisation to specific energy states to achieve even higher efficiencies with higher output powers and lower laser thresholds. The dimensions of the active material was changed in the process as shown in Fig. 1.3. The p-n-junction of the first lasers correspond to the bulk material shown on

the left. This structure has a density-of-states which results in a distributed carrier population, spread out over a lot of different energy states. Reducing the dimension by one leads to so called Quantum-well structures which improve the carrier population of the lowest energy state due to its step function. This improves the confinement of the carriers to a specific energy state and consequently to lower thresholds and higher optical output powers. Quantum-wires have an even higher carrier confinement, but require additional manufacturing steps and are therefore not first choice. Quantum-dots allow to constrain the electrons to discrete energy states resulting from their small dot-sizes and allow for discrete radiative transitions. The lowest three energy levels are called the ground-state, the excited-state and the second-excited-state. Emission either on the ground state or the excited state are most common in quantum-dot lasers. Achieving simultaneous emission on both states has first been shown in [6] and simultaneous emission on all three states has been demonstrated in [7]. However, the dots vary in size as they are grown by a self assembling process which results in varying dot sizes and consequently varying energy states which usually results in a multi-mode emission for each energy state.

## 1.2 NEED FOR DUAL-WAVELENGTH LASERS

Dual-wavelength lasers, or in general multi-wavelength lasers, are relevant for variety of applications. The following application fields show the diversity in which multiple wavelengths could be advantageous. These applications use at least two different wavelength to transmit or obtain more information than single wavelength laser would allow for:

- Telecommunication applications are the major driving force for the integration of multi-wavelength laser sources [8], [9], [10], [11]. To increase the data transmission rates, multiple-wavelength are used to transport large amount of information through a single fibre using wavelength division multiplexing. Increasing the number of wavelengths allows to transmit even more information which leads to the constant development in this direction.

- Dual-wavelength laser in particular are interesting for THz based applications like tomographic imaging [12] or spectroscopy [13]. THz sources usually require two distinct wavelengths superimposed in an active medium to generate a beat frequency, the electrons follow this beat frequency and subsequently emit THz radiation [14], [15], [16], [17].

- For spectroscopy applications, multiple wavelengths can be used to measure different absorption regions at once, or measure a reference at the same time to eliminate environmental background effects. A multi-wavelength laser, covering different absorption regions could therefore be very attractive [18], [19], [20].

- For sensing applications, e.g. structural health monitoring [21], [22], optical fibres with inscribed Fibre-Bragg-Gratings are used to detect strain and temperature variations. A cost-effective method is to sequentially read out one sensor after the other using a tunable single-wavelength laser. However, multi-wavelength lasers could address multiple sensors at once and could even allow for a continuous measurement process of each sensor.

- Dual wavelength lasers are also of interesting in Lidar systems. They have been used to improve the measurement techniques for forest mappings to distinguish between the canopy and the forest ground [23] or to distinguish between leafs and the stem for high accuracy measurements [24]. Dual wavelength lasers have also been used for velocimetry to measure the speed of a moving object [25]. Optical feedback of the two wavelength has been used to determine the objects velocity based on the resulting beat-frequency in the gain medium.

Generating multi-wavelength emission is however not straightforward, especially when compactness, robustness and energy efficiency is desired. Another challenge is also their control to precisely achieve the emission properties required in the applications mentioned. In the following, we give an introduction on the generation of two wavelengths and point out the challenges.

## 1.3 ACHIEVING DUAL-WAVELENGTH EMISSION

Laser emission can be achieved by considering a Fabry-Perot resonator where the optical wave is travelling forth and back while being amplified by stimulated emission in the process. For a stable resonance, the amplitude as well as the phase have to match the initial condition after a full cavity round trip of two times the laser lengths L. If the amplitude condition is met, it follows for the gain $g$, that $g = \alpha + \frac{1}{2L} \ln\left(\frac{1}{r_l \cdot r_r}\right)$, with the losses $\alpha$ and reflectivities $r_r$ & $r_l$ of the right and left mirror, respectively. Laser emission can be achieved if the gain exceeds the losses and it holds $(g - \alpha) > 0$. The reflectivities of the resonator mirrors play a crucial role as they define the optical output power. In semiconductor lasers, these mirrors are usually formed by the edges of the laser chip when cleaving a wafer into individual lasers. Additional higher- and lower-reflection coatings can be applied to modify the reflectivities to increase the optical output power. To achieve a standing wave inside the laser cavity, the phase condition has to be met as well and only modes with multiples of $\lambda/2$ can resonate in a laser. However, due to the width of the gain spectrum, this condition is satisfied for a large number of different wavelengths. The resonator provides a broadband feedback which can result in a multi-mode emission for all modes satisfying the amplitude condition of $(g - \alpha) > 0$ [4]. To restrict the emission to a single mode, different ways can be followed.

A broadband mirror can be used to apply an external feedback to the laser. Adjusting the feedback length such that the phase condition is only met for one specific mode in the laser cavity, allows to select and boost this wavelength. Alternatively, the mirror can be exchanged with a diffraction grating as a wavelength selective element to force the laser emission only on one mode. This also comes with the advantage of a wavelength tunability over the whole gain spectrum, but the mechanical and thermal stabilisation requires huge efforts and these lasers are not well suited for mass manufacturing. Integrated solutions are interesting alternatives and the implementation of the laser together with wavelength selective elements onto a single device is desired. One solution is to replace the cavity mirrors with Distributed-Bragg Reflectors (DBRs) to provide a very narrow reflection window with the advantage of a wavelength tunability [26]. A similar solution is the implementation of the periodic grating right into the active region of the laser, i.e. to obtain a distributed feedback laser [27]. These type of lasers tend to be spectrally more stable as the reflections happen continuously along the laser. Overall, implementing Bragg reflectors improves the wavelength selectivity and stability of the single wavelength source and has low manufacturing costs due to the mass manufacturing capabilities.

Achieving an emission simultaneously on two different wavelengths is more challenging and balancing their optical powers can be achieved in multiple ways. Two simple ways are free space solutions, either based on superimposed light beams, optical injection [30] or on laser sources with external optical feedback, e.g. external grating feedback with two mirrors to select two different wavelengths. These are quite versatile approaches as their wavelengths and relative optical powers can be controlled separately [31], [32], [33]. However, as already discussed, they result in bulky setups and pose a challenge in their alignment as well as in their mechanical and thermal stabilization, hence, full integration is desired. Implementing separate discrete laser sources and

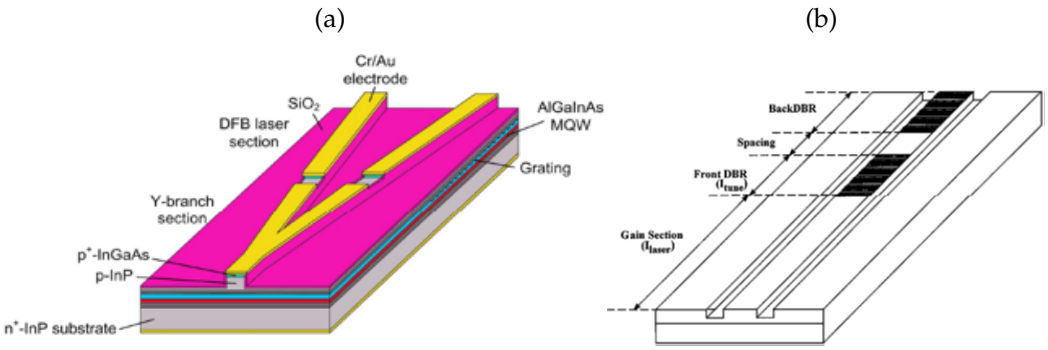


Figure 1.4: Discrete dual wavelength lasers: (a) Two parallel arranged distributed feedback lasers with a Y-junction to merge their beams [28]. (b) Two sequentially arranged DBRs to achieve the emission on two different wavelengths [29].

merging their beams on the chip overcomes some of these disadvantages. In [34], [35] and [28], discrete laser sources were implemented in parallel and their beams were merged using a Y-shaped combiner as shown in Fig. 1.4 (a). In [36], two sequentially arranged sources were implemented in a vertical-cavity surface-emitting laser. These sources are very promising but are individual lasers with separated carrier reservoirs. Hence, they are unsuited for applications where the carrier coupling is crucial, e.g. for THz or mmWave generation. Laser sources with a single gain section and two identical DBRs were proposed to overcome this limitation [37], [29] as shown in Fig. 1.4 (b). The DBRs were arranged sequentially and provide single-mode emission when no DBR is biased. Detuning one of the DBRs, results in a tunable wavelength separation between 0.3 nm and 6.9 nm. A similar design was proposed in [38] with detuned DBRs right away.

Another way to achieve a dual-wavelength emission is to restrict the possible energy transitions directly in the gain material, e.g. semiconductor lasers with intrinsic multi-wavelength selection like edge-emitting quantum-dot lasers [39]. These lasers can emit simultaneously from two different energy levels at the same time, but usually require specific operating conditions. For two-section lasers, asymmetrically biasing allows to tune the optical losses in the absorber section and has proven to achieve dual-wavelength emission [40], [41], [42]. A similar approach to control the emission was achieved by connecting the absorber section to ground over a tunable resistor [43]. Tuning the resistor tuned the losses in the cavity and allowed to either switch between the individual states or to achieve a simultaneous emission on both states simultaneously. Quantum-dot lasers have shown to be highly temperature dependent, tuning the temperature allows to either select specific states or to achieve a simultaneous emission [44], [45]. Another issue of these lasers is their Fabry-Perot cavity which leads to an emission on multiple-modes within each state [46]. Similar solutions to limit the number of emitting modes have already been discussed above for single-wavelength lasers. In [47], a phase sensitive broadband optical feedback was applied and the length of the external feedback cavity was tuned in a sub µm range. This lead to a recurring, but limited exchange in optical power between the two states. Further studies revealed the emergence of multiple longitudinal modes within each state to show energy exchanges between each other,

being the limiting factor for a full control of both states [48]. External grating feedback was applied to limit the number of modes per state in other experiments [25], [48], [45]. More sophisticated solutions embedded distributed feedback gratings into their lasers to achieve a single mode emission [42]. The grating was coupled only to the excited-state of the laser while the ground-state emitted on multiple modes. Asymmetrically biasing the two sections also allowed for a single-mode emission on the ground-state.

Besides these huge efforts to control the laser emission, another challenge is the replication of quantum-dot lasers. As their properties are highly dependent on the dot size, achieving a reliable manufacturing process is challenging. Even the embedded gratings appeared to be insufficient to gain complete control over the dual-wavelength emission. Achieving stable and controllable dual-wavelength laser emission is a challenge, and it seems particularly hard to overcome all current limitations with a single device. Smart schemes therefore seem to be required to achieve dual-wavelength emission with a relatively simple structure. In this context, the design and manufacturing of Photonic Integrated Circuits through a generic foundry platform and Multi-Project-Wafer runs appears as a practical and convenient solution and will be introduced in the next section.

## 1.4 GENERIC FOUNDRY PLATFORM AS A USER

Generic foundry platforms offer an easy and affordable access to a mass manufacturing process to build customized Photonic-Integrated-Circuits (PICs). The Multi-Project-Wafer (MPW) approach allows different participants to share a wafer and thus, to reduce the costs. Different platforms are available: Silicon , TriPleX and Indium-Phosphide. The Silicon and TriPleX platforms focus on passive components with low propagation losses and CMOS integration. This makes these platforms very attractive for hybrid integration together with other platforms as lasers can not be directly manufactured using this technology. Indium Phosphide (InP) targets the telecom wavelengths around 1550 nm. Two foundries offer a participation with similar performances, the Fraunhofer Heinrich Hertz Institute (HHI) located in Berlin, Germany and SMART Photonics located in Eindhoven, The Netherlands. For this thesis, SMART Photonics has been chosen as a foundry due to earlier participations, the well known processes and the lower costs which allow for more development cycles in the course of a PhD. Each participant has an predefined area for a custom design and several copies of this design are distributed over the wafer and diced into individual PICs after manufacturing. Although identical in design, they might perform differently due to their location on the wafer. Multiple active and passive elements can be implemented onto such a PIC to achieve a high density of components. To ease the use and to allow an easy access to these platforms also for non-experts, a library with predefined building blocks is provided by the foundry. A thorough overview over the development of the photonic integration technology is given in [49], [50], [51], [52] and [53]. Only the most important aspects for each component are given in the following to be able to understand the laser concepts presented in this thesis.

- **SOA:** The semiconductor-optical-amplifier (SOA) is based on a Quantum-well structure and is mainly used for light amplification. At threshold, the center frequency of the gain spectrum is around 1550 nm. With increasing gain current the gain dominantly increases for shorter wavelengths up to a total width of about 150-200 nm [49]. The length is the only parameter which can be adapted in the design process.
- **Waveguide:** The waveguides are used to direct the light on the chip and can be implemented with two different etching depths for strong and weak confinement of the light. Shallowly etched waveguides allow to guide the light with lower losses, however, result in low bending radii because of the low refractive index contrast. Deeply etched waveguides have slightly higher losses, but allow for much smaller bending radii which is beneficial wherever compactness is crucial. Several predefined shapes are provided, usually the length and radius, as well as offset in case of S-bend waveguides, can be adapted.
- **Isolation section:** These components are required to avoid cross talk between different active components. They are based on waveguides but with the conductive top cladding removed to avoid current leakage. The length can be adapted and determines the resistance of the component.
- **MMI splitter:** Multimode-Interference (MMI) splitters are used wherever a signal has to be split or merged. Different numbers of input and output ports are available.

1x1 MMI splitters can be used to remove higher order transversal modes. 1x2 MMI splitters are used to split up or merge a signal with a ratio of 3 dB. 2x2 MMI splitters can also provide a splitting ratio of 3 dB as well as odd splitting ratios. In the laser concepts presented in this thesis, splitting ratios of 85:15 are used.

- **MIR:** Multimode-Interference-Reflectors (MIRs) are broadband mirrors, available with a single or a double input port. The 1-port version acts as a normal mirror while the 2-port version can be used to split light with a 50:50 ratio when light is send in via one channel. These 2-port MIRs are ideal as a outcoupling mirror for laser cavities.
- **EOPM:** The Electro-optical-phase-modulator (EOPM) allows to change the phase of the light when a negative voltage is applied. The electro optic effect changes the refractive index and subsequently the optical path length. The EOPM can only be adapted in length, a voltage of 8 V allows for a phase shift of $\pi$ for a 1 mm long EOPM section.
- **Transition section:** Various building blocks are available in different etching depths, depending if low losses or compactness is desired. However, some building blocks like SOAs are only available in shallow etching. To be able to connect different etching depths, transition sections are provided.
- **DBR:** Distributed-Bragg-Reflectors (DBRs) are narrow bandwidth mirrors. Due to the material choices made by the foundry, their coupling coefficient is fixed to 50 $cm^{-1}$ and only the length and the pitch can be adapted. The maximal DBR length is 500 µm with a reflectivity of 97 %. The pitch can be adapted to achieve the desired central DBR wavelength. The fixed coupling coefficient results in a fixed relation between the DBR length, its spectral bandwidth and the reflectivity.
- **Metal track:** The metal track is used to route electrical connections across the PIC and can cross waveguides. It can be adapted in length and width to adapt for the required current of a component.

Implementing a custom design using this set of building blocks also requires the compliance to safety margins between different components. This can make fitting a dense design onto a PIC challenging and time consuming. Each active component has a metal contact and can either be probed by a needle or routed to the edge of the PIC using the metal tracks for packaging. Packaging solutions are provided by independent companies and ease the use of the PICs for electrical and optical connectivity.

Different multi-wavelength lasers emitting around 1550 nm have already been implemented using such platforms. In Fig. 1.5 (a), multiple lasers were combined using an arrayed waveguide grating to achieve a 16-channel laser source with spectral separations of 0.8 nm [54]. A similar laser has been demonstrated in [57] with 8 channels. The arrayed waveguide grating allows to merge the beams of the 16 different laser sources into one single beam for outcoupling and also serves as a intracavity wavelength selective element. The laser itself is a Fabry-Perot resonator formed by the edges of the PIC, selection of a specific wavelength is achieved by biasing the corresponding SOA channel. In (b), a four-channel Fabry-Perot laser, spectrally separated by 3.2 nm, was demonstrated [55]. Here, the arrayed waveguide grating is used to apply a wavelength selective

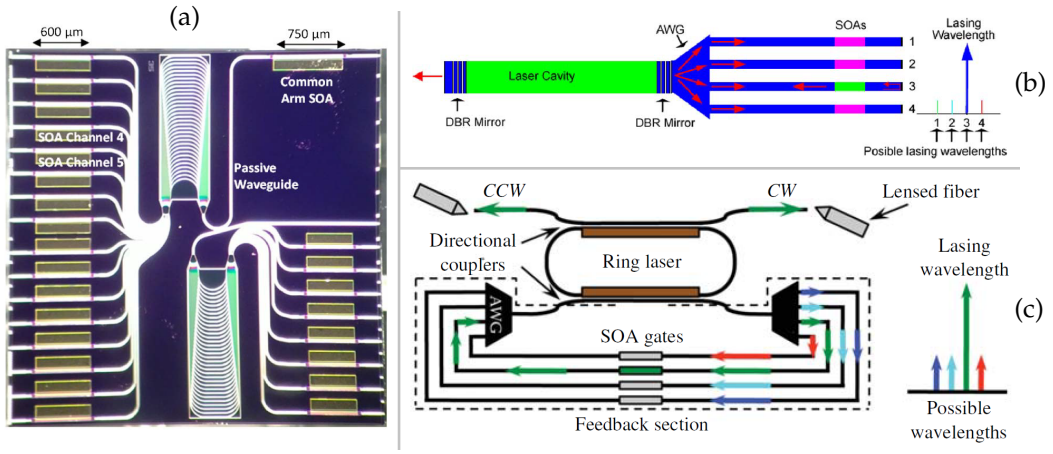


Figure 1.5: Multi-wavelength lasers integrated onto PICs: In (a), a 16-channel laser with an arrayed-waveguide-gratings as the wavelength selective elements, wavelength selection is achieved by biasing the SOA channels [54]. In (b) and (c), a Fabry-Perot laser and a ring-laser, with a four channel external feedback loop. Depending on the biased SOA gate, the laser is forced to emit on the corresponding wavelength [55] and [56], respectively.

optical feedback, the laser is forced to emit on a particular wavelength, depending on which SOA is biased. In (c), a four-channel ring laser with 1.336 nm spectral separation was demonstrated [56]. Also here, an integrated external feedback loop based on two arrayed waveguide gratings is used as a control mechanism to force emission on specific wavelengths. All three lasers are based on arrayed-waveguide-gratings, which itself already poses a challenge to design and another drawback is a large footprint on the PIC. Furthermore, these lasers can emit on a variety of different wavelengths, but lack in ease of use due to multiple gain sections and control currents. Each wavelength is controlled individually by an SOA, which requires a lot of control efforts, especially when simultaneous emission on two wavelengths is desired. The control approach presented in this thesis will be discussed in chapter 2 and aims to reduce the number of control parameters. Ideally only one parameter is envisioned for dual-wavelength lasers.

## 1.5 INFLUENCE OF OPTICAL FEEDBACK ON LASERS

Semiconductor lasers have very high conversion efficiencies from electricity to light by up to 73 % [58], hence, laser oscillation is achieved even for low facet reflectivities. Semiconductor lasers with cleaved facets have reflectivities of about 30 % and to improve efficiency, highly reflective coatings are applied to the back facet and low reflective coatings are applied to the front facet [59]. This leads to the fact that semiconductor lasers are easily affected by back reflections from any optical component and usually optical isolators are used. The optical feedback can have various effects, it can be used to select modes, to suppress side modes, to stabilise the laser emission and can also lead to dynamical behaviour.

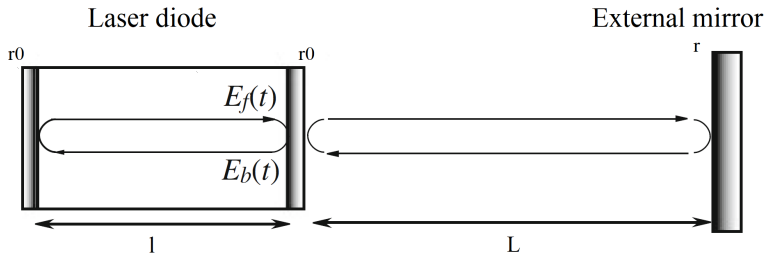


Figure 1.6: Scheme of a laser diode with external feedback. The laser cavity has a length of l, parts of the light are coupled out of the laser depending on the reflectivity $r_0$. A feedback mirror with reflectivity r is placed at distance L and reflects the light back towards the laser cavity [59].

The influence of the feedback onto the laser is connected to three parameters, the amount of feedback coupled back into the laser cavity, i.e. the feedback strength, the time delay, i.e. the external feedback length, and third, the phase of the optical feedback. The feedback strength is based on the reflectivities of the laser resonator and the external feedback mirror as shown in Fig. 1.6 and can be expressed by $\kappa = \left(1 - r_0^2\right) \frac{r}{r_0}$ with identical reflectivities $r_0$ for the front and back facet for simplicity. Both a lower reflectivity $r_0$ and a higher reflectivity r results in a larger feedback strength coupled back into the laser cavity. Together with the time delay, five different parameter regions exhibiting different behaviours have been distinguished and are shown in Fig. 1.7 (a) [60]:

- Region I: For very small feedback strengths of less than 0.001 % and short feedback length, a stable laser response is obtained. Effects like narrowing or broadening of the linewidth are observed, depending on the feedback phase.
- Region II: For feedback strengths of less than 0.005 % and longer feedback length, instabilities like mode hopping can occur.
- Region III: Narrow feedback region between 0.005 and 0.01 % with restabilisation of the laser emission and a narrowing of the laser linewidth.
- Region IV: Feedback strengths between 0.01 and 10 %, dynamical behaviour ranging from linewidth broadening up to a coherence collapse.

- Region V: Large feedback strengths beyond 10 %, extended cavity regime with the laser operating as a long cavity laser with a short active region. Usually an anti-reflection coating is required to reach this region.

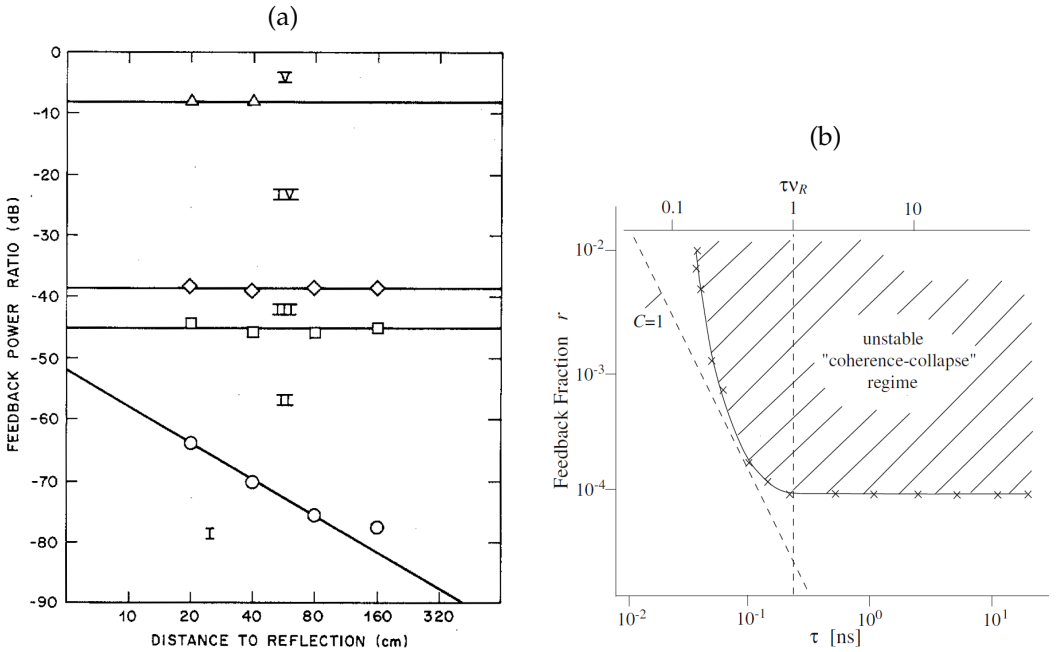


Figure 1.7: In (a), five different regions describe stable to unstable laser behaviour, depending on the feedback strength and feedback delay [60]. In (b), for the short cavity regime (vertical dotted line) and for C < 1, stable emission can be achieved even for high feedback strengths [61].

However, the behaviours in these regions have been observed for long time delays, i.e. when the delay is longer than the period of the relaxation oscillation frequency of the laser. In Fig. 1.7 (b), the stability of a laser with a short feedback cavity is shown. The feedback cavity round trip time corresponding to the relaxation frequency is indicated by the vertical dotted line at $\tau\nu_r$. For all lengths longer than this, unstable regions are found as discussed above. However, for shorter feedback lengths below the relaxation oscillation frequency, even high feedback strengths do not destabilize the laser. Therefore, the short cavity regime is considered to be more stable than the long cavity regime. This stability information has been expressed with the C-parameter as a first approximation for stability. It takes the feedback strength and feedback length of the laser into account and reads as follows: $C = \frac{\kappa\tau}{\tau_{in}}\sqrt{1+\alpha^2}$. $\tau$ and $\tau_{in}$ are the external and internal round trip times, respectively, and $\alpha$ the linewidth enhancement factor. As visible in Fig. 1.7 (b), values of $C < 1$ are a first indication of a stable laser operation under optical feedback.

Besides the feedback strength and length, also the feedback phase can have a crucial impact on the laser emission. Tuning the feedback phase for single wavelength lasers usually tunes the outcoupling losses and results in changes of the output power or can result in a narrowed or broadened linewidth as mentioned for feedback region I. How-

ever, when considering two modes, also two different feedback phases have to be taken into account.

Each mode can have a different feedback phase when coupled back into the laser cavity and two extreme cases can occur. Either both of these feedback phases are are identical, i.e. they are in phase, or they are out of phase. While the former results in modulations of the output power like in the single-mode case, the latter has a much more complex influence on the laser and has been studied in [47] and [48]. In these works, changes of

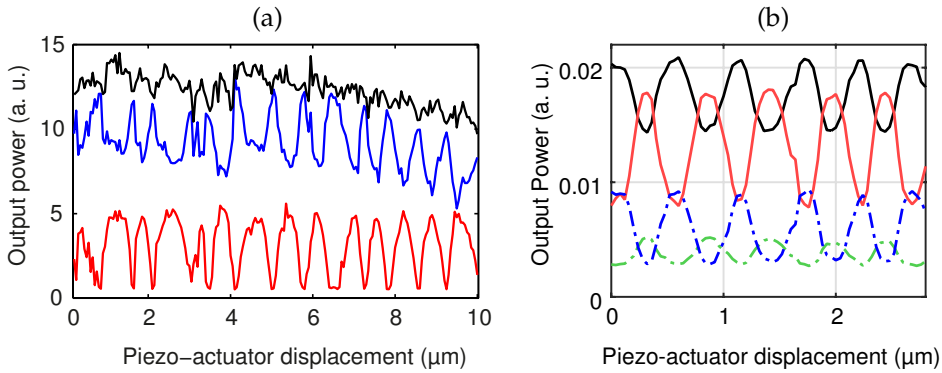


Figure 1.8: In (a), changing the optical feedback length resulted in limited power exchanges between the ground- and excited-state of a quantum-dot laser in red and blue, respectively, while the total output power in black remained the same. In (b), a detailed analysis showed four different modes emitting within the ground-state. Tuning the feedback length resulted in undesired power exchanged and limited the suppression ratio for this laser.

the optical feedback phase on a dual-wavelength emission have been investigated, using quantum-dot lasers emitting simultaneously on two different wavelengths. A broadband mirror was used to apply the feedback and was fine-delay tuned with a piezo actuator to tune the feedback phase, the results are shown in Fig. 1.8 (a). Initially, the mirror was placed such, that one of the wavelength is in resonance and receives a boost while the other one is anti-resonant and experiences additional losses. Fine-delay tuning the external mirror resulted in the selection of the other wavelength and recurring power exchanges for larger displacements. However, in this experiment only a partial switch could be obtained. Further studies revealed multiple modes for each wavelength region to be a limiting factor [48]. In particular, four longitudinal modes have been observed to emit within the excited state and are shown in Fig. 1.8 (b). By tuning the feedback delay, a power exchange between these modes is found and was considered to be the origin of the limited performance in (a). This work suggests that an involvement of fewer modes, ideally only two, could improve the control approach and lead to higher suppression ratios. These findings have therefore been the starting point for the control approach presented in this thesis and will be explained in detail in the following chapter 2.

## 1.6 OBJECTIVES AND OUTLINE OF THIS WORK

In this PhD thesis we aim at gaining a full control over dual-wavelength semiconductor lasers using optical feedback. In particular, the goal is to enable fine tuning of the optical output powers between two wavelengths, ideally by only tuning a single parameter, which is the optical feedback phase. The main objectives are:

- First, identify the critical parameters for this control approach using theoretical investigations. Then, determine optimal parameters for the optical feedback cavity to achieve the most efficient switching. Then, evaluate the control capability of the dual-wavelength emission by only changing the feedback parameters. Finally, address the effect of the feedback phase onto the switching capabilities as well as onto the robustness and limitations when changing their values.
- Second, demonstrate the control approach with on-chip devices including an integrated optical feedback cavity. Using an MPW approach, we aim to design different dual-wavelength lasers and implement them together with our proposed control approach onto a PIC.
- Using this demonstrator, we aim to achieve significant insights on the dual-wavelength switching properties, in particular the extinction ratios and switching speeds. As our lasers are designed to only emit on two distinct modes, we expect to achieve high extinction ratios of at least 20 dB, exceeding previous demonstrations [47]. Moreover, as the phase modulator allows for very fast modulations, we also expect to obtain switching times in the low nano-second range [62].
- Finally, using an independent laser system with a variable external feedback, we aim to evaluate the switching potential and degree of extinction for different feedback delays and different feedback strengths. This will allow us to identify the limitations of this control approach and possibly propose improvements for future designs.

This thesis is structured as follows:

In chapter 2, we present the proposed control approach. The general idea is based on a relative phase shift between the involved modes as we will highlight in detail. We will use a numerical model to study the peculiarities of the phase sensitive optical feedback to better understand the behaviour when the feedback parameters are changed. We will then use these simulations to determine the ideal operating conditions for our lasers and will also use them to determine the required external cavity length and feedback strength to achieve optimal performances.

In chapter 3, we present the design of customized dual-wavelength lasers. First, we present different laser concepts as well as simulations to determine the exact emitting wavelengths for each laser. Then we discuss the experimental setup and characteristics for each laser together with a DBR and temperature analysis.

In chapter 4, we discuss the implementation of our lasers and the feedback cavity onto a PIC. First, we design tailored feedback cavities using the wavelengths determined in

the simulations in chapter 3, and implement them onto the PIC. Then, we present experimental results when tuning the feedback phase and discuss the operating range under varying laser and feedback conditions. Last but not least, we present results on the switching speed.

In chapter 5, we highlight the limitations of our lasers as well as the control approach. First, we adapt the control approach to two discrete devices, a quantum-dot laser and a external cavity diode laser to study the performance under varying feedback delays and spectral separations. Then, we will discuss the limitations on the DBR performances and propose improvements for different laser concepts as well as for the feedback cavity.

In chapter 6, we will summarize the contributions of this work and outline future research topics to further advance this control technique towards an implementations for future applications.

# 2 CONTROL APPROACH FOR DUAL-WAVELENGTH EMISSION

In this chapter, we propose a novel control approach for dual-wavelength lasers based on a phase sensitive optical feedback and study it by simulations. In the first section 2.1, we will introduce the concept of this approach in detail. Then, we will use a theoretical model to describe the two electric fields with their individual feedback phases in section 2.2. Using the two feedback phases, we will map all possible relative phase shifts between them and study varying laser and feedback parameters to identify the most efficient control performance in section 2.3. We will then reduce the parameter space to the parameters addressable in the experiment and study the requirements on the feedback strength to achieve an equal optical output power between the wavelengths. Then, we further reduce the parameter space to only two points in the phase space exhibiting the best switching capabilities. With this, we will be able to study variations of the injection current and feedback strength onto different intrinsic laser parameters. Finally, we will study the switching speed to identify the best operating points for a fast switch.

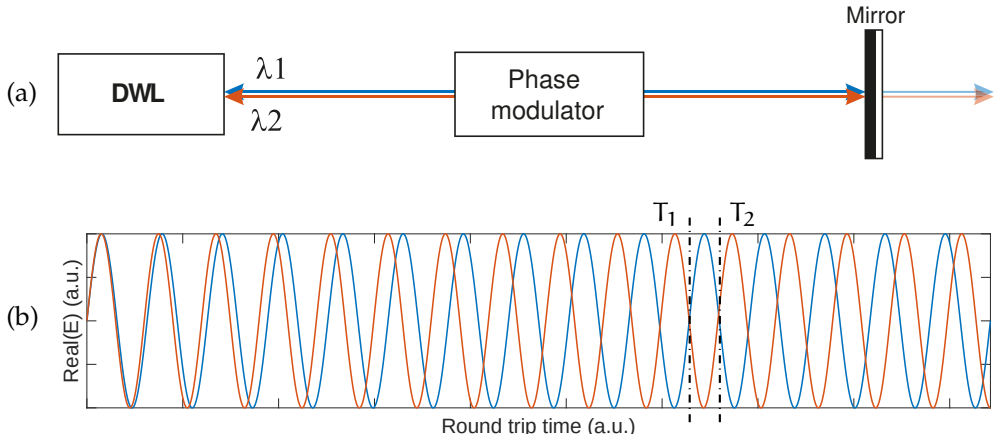


Figure 2.1: In (a), a schematic representation of the proposed control approach is shown, the dual-wavelength laser emits on $\lambda_1$ & $\lambda_2$. The laser facet and the mirror form the external feedback cavity consisting of a phase modulator. In (b), the spectral evolution of $\lambda_1$ & $\lambda_2$ into the feedback cavity is shown, exhibiting a relative phase shift of $\pi$ around the points $T_1$ & $T_2$. With the mirror positioned such that ($T_1$) is resonant to the lasing mode after a full cavity round trip, a boost for $\lambda_1$ achieved while $\lambda_2$ experiences extra losses. The phase modulator allows to tune the optical path length towards a resonance of $\lambda_2$ indicated by ($T_2$).

## 2.1 CONTROL APPROACH

The fundamental idea of the control approach proposed in this thesis exploits the Fabry-Perot effect in the optical feedback cavity. The schematic of a dual-wavelength laser with an external feedback cavity is considered in Fig. 2.1 (a). If a wavelength emitted by the laser resonates in the external feedback cavity, it will receive a boost in gain. If the wavelength is anti-resonant, it will experience additional losses and is disfavoured. For two different wavelengths, the ideal case would be to achieve resonance for one wavelength and anti-resonance for the other. This way, the resonant wavelength is boosted while the second wavelength is disfavoured. To achieve this condition, the evolution of two different wavelengths into a feedback cavity is considered in Fig. 2.1 (b). The two wavelengths evolve differently into the feedback cavity with an increasing relative phase shift between them. For resonance of one wavelength and anti-resonance for the other, ideally a relative phase-shift of $\pi$ has to be achieved after a full round trip in the feedback cavity as indicated with ($T_1$). Changing the emission in favour of the suppressed wavelength can be done by changing the optical path length, i.e. changing the cavity round trip time, to achieve resonance for the second mode indicated with ($T_2$). In a free-space setup, changing the optical path length can be achieved by fine-delay tuning the external mirror using a piezoelectric-actuator. However, for improved stability, speed and precision, a monolithic solution should be preferred by using a phase modulator as shown in (a). The phase modulator uses for instance the electro-optic effect to change the refractive index and subsequently the optical path length when a voltage is tuned. If the two wavelengths are spectrally close to each other, they will experience the same refractive index changes and the Fabry-Perot effect can be tuned in favour of the second mode ($T_2$). The

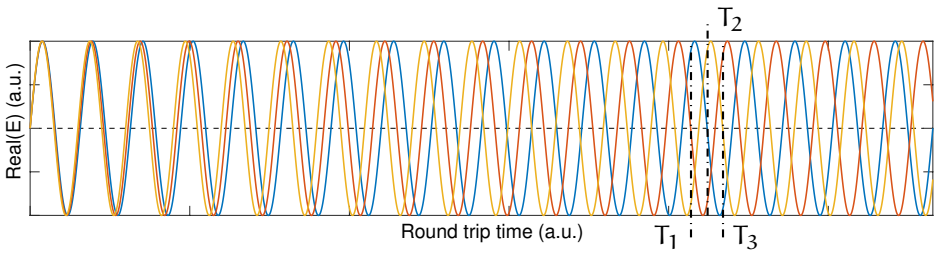


Figure 2.2: Evolution of three spectrally equidistant modes. The ideal relative phase shifts for their control is $2\pi/3$. $T_1$, $T_2$ & $T_3$ correspond to the ideal feedback cavity round trip for them to be resonant and favoured for emission. The cavity length to achieve this relative phase shift depends on the number of modes and differs for the cavity length shown in Fig. 2.1.

position of the points ($T_1$) & ($T_2$) depend on the spectral separation of the wavelengths, hence, the round trip time has to be adapted for each individual dual-wavelength laser.

This control approach is not limited to just two wavelengths but can be extended to $n$ wavelengths. For this, an equidistant distribution of the phase shifts $\Delta\phi$ between the wavelengths has to be achieved, meeting the condition $\Delta\phi = 2\pi/n$. For two modes a phase shift of $\pi$ is ideal while for three modes a relative phase shift of $2\pi/3$ is optimal and is shown in Fig. 2.2. The ideal round trip times to select a specific wavelength are indicated with $T_1$, $T_2$ & $T_3$ and can be addressed using a phase modulator. The maximal number of wavelengths which can be controlled using a single feedback section has yet to be determined. In this PhD thesis, we aim to demonstrate the feasibility of this control approach using only two wavelengths to study its peculiarities, demonstrate the approach experimentally and determine its limits. These insights could then be used to further develop this approach towards a multi-wavelength control in the future.

The performance of the control approach is dependent on two types of parameters that we classify as intrinsic versus addressable parametersand will be introduced in the following section 2.2. The intrinsic parameters are laser based parameters like the gain difference between the two wavelengths and the mode coupling. As the control approach is based on modulating the gain in the laser cavity, an identical gain for both wavelengths is desired. If the gain difference is too large or the carrier coupling too weak, a compensation might not be possible or only a partial switch might be achieved. Both of these parameters can not be controlled and are device dependent. However addressable parameters like the optical feedback strength or the injection current can be controlled and allow to compensate for suboptimal intrinsic parameters. To assess the degree in which this is possible, we perform numerical simulations to study the parameter dependencies in the following.

## 2.2 SIMULATION MODEL

For the theoretical studies on the laser behaviour, we used the multi-mode extension of the single-mode Lang-Kobayashi equations introduced and studied in [63]. In particular, we used the model B which takes two carrier reservoirs into account to describe two free-carrier density gratings burned into the laser cavity. These two carrier gratings are spatially burned by the standing wave pattern of the two considered modes and are connected via a cross-saturation parameter $\beta$. Each wavelength burns carriers from one pool, a value of $\beta = 0$ describes two decoupled carrier pools whereas $\beta = 1$ corresponds to one single carrier pool for both wavelength. Studying values between $0 < \beta < 1$ allows us to evaluate the potential of our control approach to obtain a full control over the laser emission. Throughout all simulations, we assume that the coupling between the carrier reservoirs is symmetrical. Two equations describe the electrical fields $E_1$ and $E_2$ of two longitudinal modes with varying feedback delays $e^{-i\phi_1}$ and $e^{-i\phi_2}$. They are coupled to two equation for the free-carrier density $N_1$ and $N_2$ as follows:

$$\frac{dE_1}{dt} = \frac{1}{2}(1+i\alpha)(g_1 N_1 - \gamma_1) E_1 + \kappa E_1(t-\tau)\cdot e^{-i\phi_1} \tag{2.1}$$

$$\frac{dE_2}{dt} = \frac{1}{2}(1+i\alpha)(g_2 N_2 - \gamma_2) E_2 + \kappa E_2(t-\tau)\cdot e^{-i\phi_2} \tag{2.2}$$

$$\frac{dN_1}{dt} = J - \frac{N_1}{\tau_s} - N_1\left(g_1 |E_1|^2 + g_2\beta |E_2|^2\right) \tag{2.3}$$

$$\frac{dN_2}{dt} = J - \frac{N_2}{\tau_s} - N_2\left(g_1\beta |E_1|^2 + g_2 |E_2|^2\right) \tag{2.4}$$

If not stated otherwise, we used a linewidth enhancement factor of $\alpha = 3$ and a feedback delay of $\tau = 50$, normalized by the photon lifetime $\tau_p$. We added a low noise term to reach steady state solution quicker as well as to avoid unstable solutions. We introduced a noise term of $1e-10$ for the amplitude and phase by $\sqrt{\beta \cdot g_{1/2} \cdot (E_1 + E_2 - 1)} \cdot rand$ with $rand$ being a Gaussian random number with zero mean and unit variance. This term is added to every mode after each calculation step when computing the time series. This noise term is only included to ensure that our simulations do not remain stuck on unstable steady-states, it does not to qualitatively reproduce the effect of a real spontaneous emission noise. We will indicate the injection current J with the pump parameter $P = J/J_{th} - 1$, with J and $J_{th}$ being the current and the threshold current, respectively. To study the impact of the optical feedback phase onto the laser emission, we will vary the feedback strength $\kappa$, the gain for each of the modes $g_1$ & $g_2$ and the coupling coefficient $\beta$ in the following simulations. The equation is then solved using a 4-th order Runge Kutta method to obtain the time traces for each of the wavelengths.

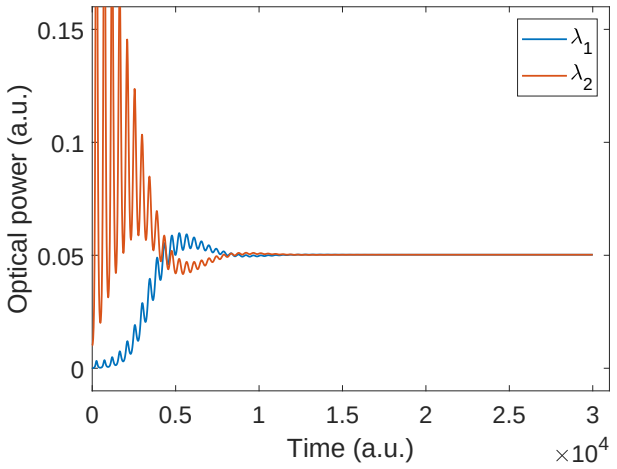


Figure 2.3: Time traces of $\lambda_1$ in blue and $\lambda_2$ in red. Different initial conditions lead to a transient behaviour, evolving into an equal optical power for each of the wavelength due to their equal gain.

### 2.2.1 *Defining a figure of merit*

In a first step, we consider a symmetric system with a pump parameter of $P = 0.1$, a coupling coefficient of $\beta = 0.99$ and an equal gain for both modes of $g_1 = g_2 = 1$. Without any feedback applied to the system we obtain the free running laser emission shown in Fig. 2.3. Due to the identical gain, both wavelength exhibit the same optical power after the transient behaviour. In a next step, we apply an optical feedback of $\kappa = 1 \cdot 10^{-3}$ to this system which allows us to control their optical powers. For the first case, the feedback phases $(\phi_1, \phi_2)$ of the electrical fields will be set to $(0, \pi)$ to obtain the desired relative phase shift of $\pi$. The resulting time traces are shown in Fig. 2.4 (a). After the transient behaviour, the wavelength $\lambda_1$ in blue is dominating while $\lambda_2$ in red is suppressed. When setting the feedback phases to identical values of $\phi_1 = \phi_2$, none of the modes is favoured or disfavoured and an equal optical power, similar to the case without optical feedback, is achieved and shown in (b). Feedback phases of $(\phi_1, \phi_2) = (\pi, 0)$ result in an emission on $\lambda_2$ while $\lambda_1$ is suppressed as shown in (c). Following Fig. 2.1, these three cases represent the transition from a resonant mode $\lambda_1$ indicated by $(T_1)$ to a resonant mode $\lambda_2$ indicated by $(T_2)$ and exhibiting an equal optical power point for an identical feedback phase in between $(T_1)$ & $(T_2)$. Hence, using the optical feedback phase allows us to control the optical powers of the wavelengths at will.

To evaluate the power ratio between the two wavelengths, we define a figure of merit as follows:

$$R = \tanh\left(\frac{P_1}{P_2} - \frac{P_2}{P_1}\right) \tag{2.5}$$

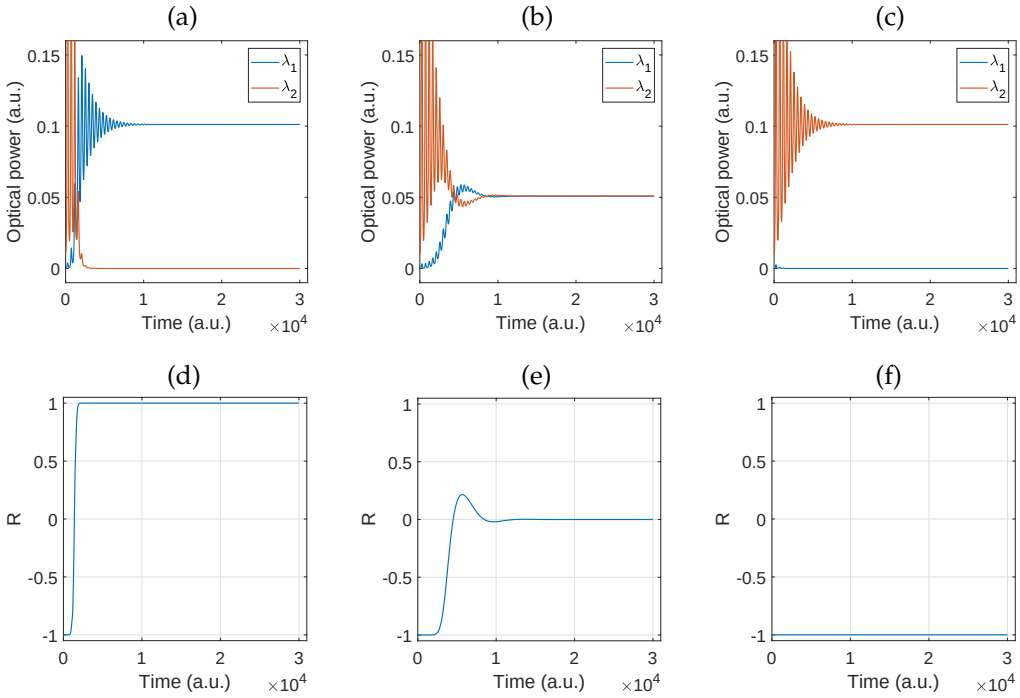


Figure 2.4: Temporal evolution for $\lambda_1$ & $\lambda_2$ for different feedback phases in (a) - (c). In (a), the phases have been set to $(\phi_1, \phi_2) = (0, \pi)$, in (b) to identical phases of $\phi_1 = \phi_2$ and in (c) to $(\phi_1, \phi_2) = (\pi, 0)$. In (d) - (f), the R values are plotted, quantifying the power ratios between the wavelengths with values of -1 to +1, representing emission on $\lambda_2$ and $\lambda_1$, respectively, values of 0 represent equal optical powers.

with the optical powers $P_1$ & $P_2$ for the wavelengths $\lambda_1$ & $\lambda_2$, respectively. This approach allows us to specify the outcome of the simulation by one single parameter and simplifies the analysis in the following studies. The $\tanh$ allows for a figure of merit with values between +1 and -1, a +1 represents the sole emission on $\lambda_1$ with $\lambda_2$ suppressed, a value of 0 corresponds to an equal emission on both wavelengths and a -1 represents the sole emission on $\lambda_2$ while $\lambda_1$ is suppressed. In Fig. 2.4 (d) - (f), the evolution of R has been calculated for each case of (a) - (c), respectively. In (a), the emission starts on $\lambda_2$ due to the initial starting conditions and evolves towards a sole emission on $\lambda_1$. This corresponds to an evolution from -1 to +1 in panel (d). For the equal phases in (b), an evolution from $\lambda_2$ to an equal power of both wavelengths is achieved, corresponding to a transition from -1 to 0 in panel (e). In (c), the emission on $\lambda_2$ is persisting at all times, corresponding to a constant value of -1 in panel (f). Hence, R allows to evaluate the system behaviour by only one parameter. In the rest of this work, we will only consider the value of R taken when the system reaches a steady-state, i.e. we discard transient and dynamical behaviours.

## 2.3 PHASE DEPENDENCY OF SWITCHING PERFORMANCE

To analyse the laser behaviour for all possible relative phase shifts, we vary the optical feedback phases $\phi_1$ & $\phi_2$ in a range from 0 to $2\pi$. Taking the steady-state solutions of R for each of the simulation outcome allows us to achieve mappings of the entire phase space as shown in Fig. 2.5 (a) - (d). By varying specific parameters we can study the impact on different relative phase shifts.

The first mapping Fig. 2.5 (a) represents an ideal set of parameters as a reference point. We assumed an identical gain of $g_1 = g_2 = 1$ together with a coupling coefficient of $\beta = 0.99$ and a feedback strength of $\kappa = 3{\cdot}10^{-4}$. This set of parameters leads to a mapping with two dominant areas, the large blue and red region correspond to the sole emission of $\lambda_1$ & $\lambda_2$, respectively. The extreme cases for these two areas $(\phi_1, \phi_2) = (0, \pi)$ for the blue region and $(\pi, 0)$ for the red region, modulo $2\pi$, correspond to the steady state solutions in panel (a) & (c) of Fig. 2.4. The identical gain for both wavelengths leads to this symmetrical case with equal power points along the lines of equal phases $\phi_1 = 2\pi \pm \phi_2$ in green. An ideal coupling coefficient of $\beta = 1$ would lead to a complete redirection of the carriers to the favoured wavelength. The two areas would have values of either +1 or -1, with sharp edges separating them along the diagonal lines and without equal optical power points. However, as this is an behaviour unlikely to be observed in an experiment, we refrain from studying this extreme case. Starting from this reference point, we either reduced the coupling which lead to panel (b), or we reduced the gain of one mode which lead to panel (c).

When reducing the coupling as shown in Fig. 2.5 (b), we observed a much smoother transition between the wavelengths. For this, we assumed a value of $\beta = 0.98$ which hampers the carrier redistribution and only leads to a partial switch with values of up to $R = \pm 0.6$.

When assuming different values of gain, one mode is expected to show a dominant behaviour and is shown in panel (c). We assumed gain values of $g_1 = 0.999$ & $g_2 = 1$, whereas the coupling coefficient and feedback strength was kept to $\beta = 0.99$ and $\kappa = 3{\cdot}10^{-4}$. As visible in panel (c), the blue region is much larger, i.e. $\lambda_1$ is dominant for large range of relative phase shifts due to the higher gain. Only for a very small region around $(\phi_1, \phi_2) = (\pi, 0)$, a partial switch up to a point of an equal power with $R = 0.2$ is obtained.

In practice, a real laser source could possibly exhibit both effects at once. A lowered mode coupling could originate from limited carrier exchanges in the gain medium and depending on the shape of the gain profile, the gain for each mode could be different. Therefore, both, the reduced coupling coefficient of $\beta = 0.98$ as well as the asymmetric gains of $g_1 = 0.999$ & $g_2 = 1$ are assumed in (d), combining the cases (b) and (c). The transitions between the different areas are very smooth and only a small modulation in their power ratio of about $R = \pm 0.1$ is achieved. Increasing the optical feedback strength allows for a much better control, hence, we increased the optical feedback strength to a value of $\kappa = 9{\cdot}10^{-4}$ to achieve the mapping shown in Fig. 2.6. This increase in feedback strength is sufficient to regain the full control over the laser emission and to achieve a full switch between the wavelengths. Furthermore, the increase in feedback strength reveals an asymmetry for the different areas. This could results in different slopes for the transitions from $(\phi_1, \phi_2) = (0, \pi)$ to $(\pi, 2\pi)$ compared to the transition from $(\pi, 0)$ to

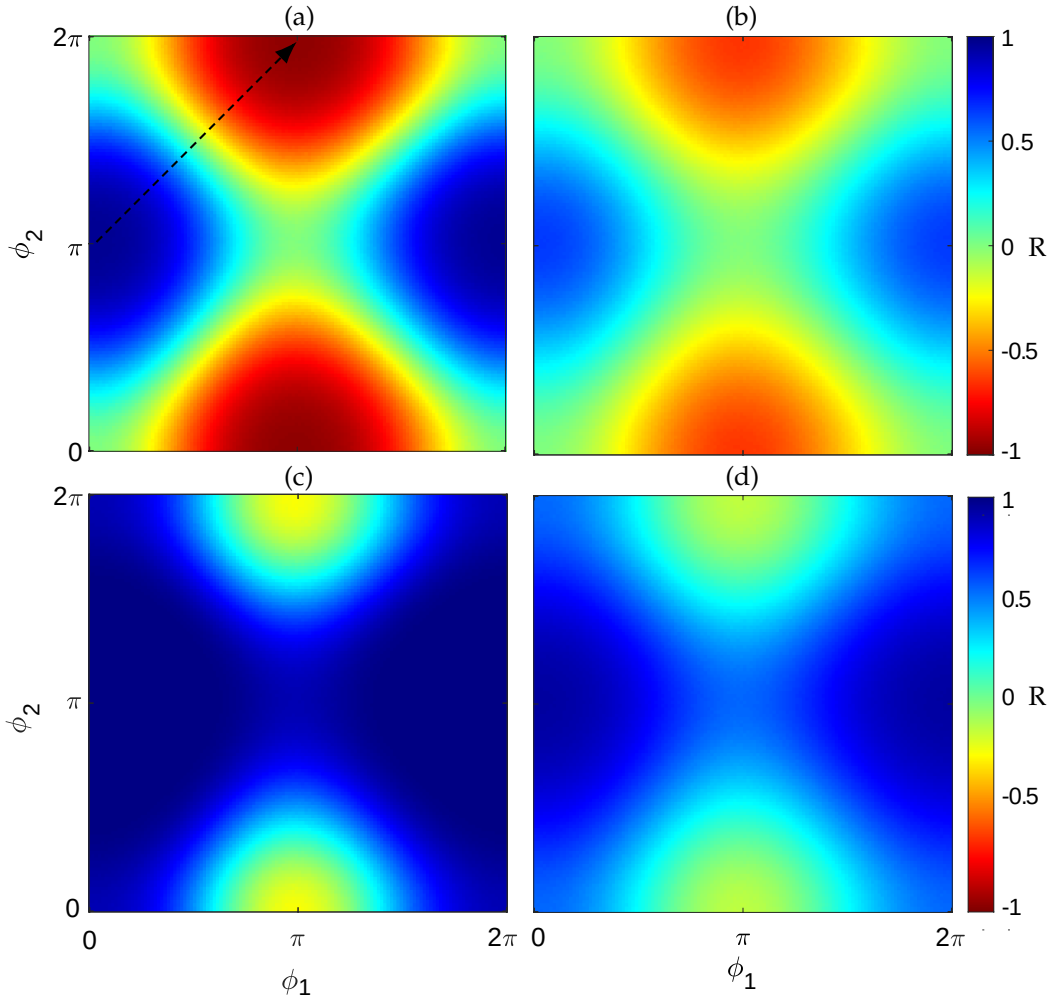


Figure 2.5: Phase space with all possible relative feedback phases for $\lambda_1$ & $\lambda_2$. Blue and red regions correspond to the sole emission of $\lambda_1$ and $\lambda_2$, respectively, while green regions represent equal optical powers. In (a), ideal conditions are assumed with equal gain $g_1 = g_2 = 1$ and a coupling coefficient of $\beta = 0.99$. In (b), only the coupling is reduced to $\beta = 0.98$ and $g_1 = g_2 = 1$, in (c) only the gain $g_1 = 0.999$ with $\beta = 0.99$ and in (d), both, $\beta = 0.98$ and $g_1 = 0.999$ are assumed.

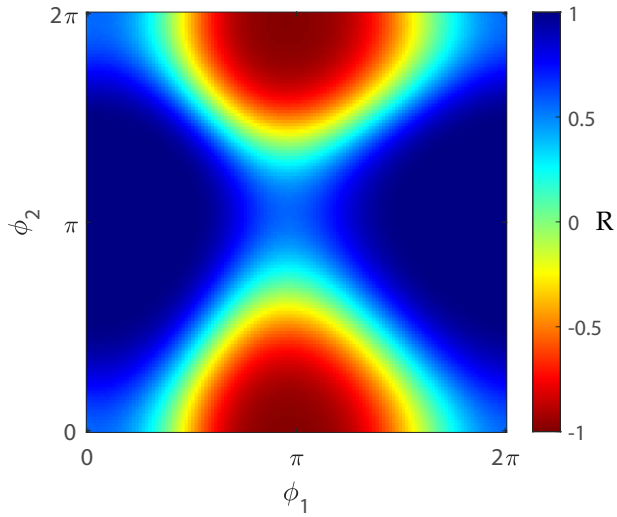


Figure 2.6: Phase mapping with $\beta = 0.98$, $g_1 = 0.999$ and $g_2 = 1$ together with an increased feedback strength of $\kappa = 9{\cdot}10^{-4}$ to compensate for the low performance shown in Fig. 2.5 (d).

$(2\pi, \pi)$. However, the impact of this effect is very low and is not expect to have a major influence onto our control approach.
To put the applied feedback strengths into perspective, to gain full control over the emission shown in Fig. 2.5 (b), a feedback strengths of $\kappa = 5 \cdot 10^{-4}$ would be sufficient and for the case shown in panel (c), a feedback strength of $\kappa = 6 \cdot 10^{-4}$ would be required. As we consider the combined parameters in panel (d), a higher feedback strength of $\kappa = 9 \cdot 10^{-4}$ is required to compensate for both of them. We only observed dynamical behaviour at feedback strengths beyond $\kappa > 22 \cdot 10^{-4}$ for this set of parameters, providing additional margins for even lower carrier coupling or gain differences. Moreover, the feedback strength does not only allow to achieve a full switch, but it also allows to control the size of the regions, i.e. the amount of possible relative phase shifts leading to a full switch. Consequently, suboptimal relative phase shifts, which are very likely to occur in a manufactured device, can still lead to a full switch when the optical feedback strength is adapted properly.

These simulations reveal that the optical feedback strength is an effective control parameter to compensate for potentially suboptimal intrinsic laser parameters. Together with a phase modulator, full control over the power ratio of the two wavelengths can be gained, allowing to transition between the desired points of interest in the phase space. However, considering a physical feedback cavity, both wavelengths experience the same phase shift which corresponds to diagonal lines in these phase mappings. The ideal transition therefore results from $(\phi_1, \phi_2) = (0, \pi)$ to $(\pi, 2\pi)$, corresponding to points $(T_1)$ and $(T_2)$ in Fig. 2.1 and is indicated with the black arrow in Fig. 2.5 (a). Another aspect of higher feedback strength results in steeper transition between the areas. In case an equal optical power is desired, this steep transition might require a very precise setting for the feedback phase and will be discussed in the following.

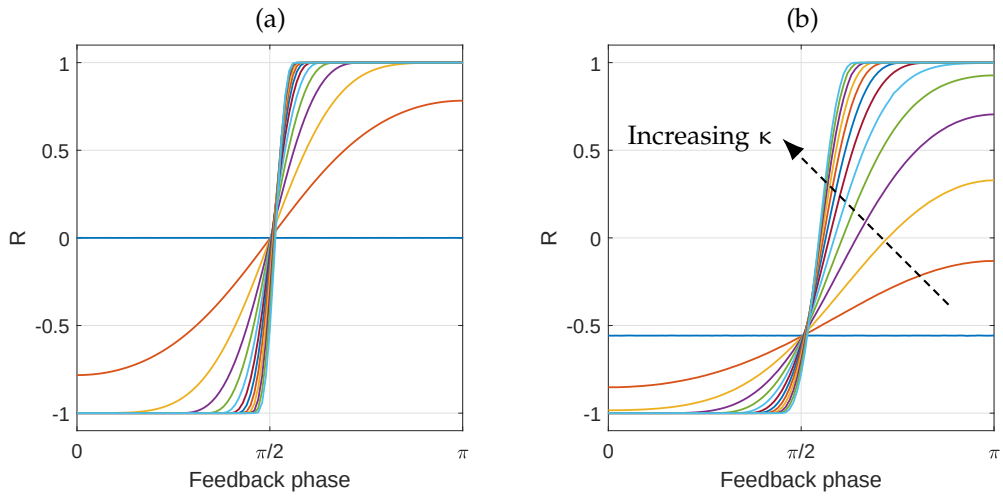


Figure 2.7: Transition from $(\phi_1, \phi_2) = (0, \pi)$ to $(\pi, 2\pi)$, i.e. transitioning along the arrow in Fig. 2.5 (a). Shown are solutions for different feedback strengths in the range of $\kappa = 0$ to $22 \cdot 10^{-4}$ in steps of $2 \cdot 10^{-4}$. The transition in (a) corresponds to the parameters used for Fig. 2.5 (a) while (b) corresponds to the parameters used in for Fig. 2.5 (d). Partial switches are achieved around $\kappa \approx 2.5 \cdot 10^{-4}$ and full switches beyond $\kappa \approx 9 \cdot 10^{-4}$.

### 2.3.1 *Achieving a balanced optical power*

In this section, we focus on achieving an equal optical power between the wavelengths and study the dependency of the optical feedback strength under different parameters. For a detailed analysis, we reduce the phase space to the transition between the points of $(\phi_1, \phi_2) = (0, \pi)$ and $(\pi, 2\pi)$ along the arrow shown in Fig. 2.5 (a). This corresponds to an optimal transition induced by the phase modulator as desired in our experiments.

We study two sets of parameters to compare their impact on the capability of the system to reach an equal output power for the two wavelengths. First, we use the same operation point than already discussed for Fig. 2.5 (a) with $\beta = 0.99$ and $g_1 = g_2 = 1$ and vary the feedback strength in a range between $\kappa = 0$ to $22 \cdot 10^{-4}$ in steps of $2 \cdot 10^{-4}$. With this, we obtain the results shown in Fig. 2.7 (a). With the symmetrical gain considered and no feedback applied, we expect an equal optical power between the modes and no influence of the feedback phase. This case corresponds to the horizontal blue line. Increasing the feedback strength to $\kappa \approx 2 \cdot 10^{-4}$ allows for a partial switch and with feedback strength beyond $\kappa \approx 3 \cdot 10^{-4}$ a full control over the laser emission is achieved. However, as the laser will not exhibit this highly symmetrical behaviour in practice, we considered a second set of parameters with asymmetrical parameter settings. We used the same operation point already discussed for Fig. 2.5 (d) with a coupling coefficient of $\beta = 0.98$ and $g_1 = 0.999$ & $g_2 = 1$ together with the same variations in feedback strength of $\kappa = 0$ to $22 \cdot 10^{-4}$ to obtain the results shown in Fig. 2.7 (b). Without optical feedback applied, the emission is in favour of $\lambda_2$ with values of $R \approx -0.5$, represented by the horizontal blue line and is a result from the asymmetric gain of the wavelengths. With increasing feedback strength, an equal optical power can be achieved with feedback strength around $\kappa \approx 2.5 \cdot 10^{-4}$ at a feedback delay of $\pi$. To gain full control over the

laser emission, a feedback of at least $\kappa \approx 9 \cdot 10^{-4}$ is required as already discussed for Fig. 2.5 (d). A further increase of the feedback strength is only required for low coupling coefficients $\beta$, as it flattens the transition, or for large gain differences where a high gain compensation would be required. However, when an equal optical power is desired, large feedback strengths are disadvantageous due to a steeper transition and a higher precision required to set the optimal feedback phase. In practice, a phase-modulator used in the SMART Photonics platform achieves a phase shift of $\pi$ at $\approx 8$ V for a length of 1 mm. Setting an equal power point with a precision of 1 %, translates to a required precision in voltage of about 25 mV for a feedback strength of $2.5 \cdot 10^{-4}$ but 2.5 mV at $20 \cdot 10^{-4}$. Furthermore, the larger the gain differences, the more the transition is shifted towards the disfavoured wavelength, i.e. here to the right. In extreme cases, close to a feedback delay of $\pi$, a high feedback strength has to be applied to achieve a steep transition towards the equal power point.

### 2.3.2 *Exploring the parameter space*

In a final step, we further reduce the parameter space to the two points $(\phi_1, \phi_2) = (0, \pi)$ and $(\pi, 2\pi)$. With this, we are able to study variations of the injection current and feedback strength onto different intrinsic laser parameters. For this, we combine the two points into a single value and define the figure of merit as follows:

$$T = \frac{1}{2} \cdot \mathrm{abs}\left[R(0,\pi) - R(\pi,2\pi)\right] \tag{2.6}$$

$$T = \frac{1}{2} \cdot \mathrm{abs}\left[\tanh\left(\frac{P_1(0,\pi)}{P_2(0,\pi)} - \frac{P_2(0,\pi)}{P_1(0,\pi)}\right) - \tanh\left(\frac{P_1(\pi,2\pi)}{P_2(\pi,2\pi)} - \frac{P_2(\pi,2\pi)}{P_1(\pi,2\pi)}\right)\right] \tag{2.7}$$

This figure of merit results in a scale between 0 and 1, a value of 0 represents no impact of the feedback phase on the laser emission, while a value of 1 represent a full switch when transitioning between the points $(0, \pi)$ and $(\pi, 2\pi)$. Values in between represent partial switches.
Unless stated otherwise, the parameters are set as follows: the pump parameter is set to 0.5, the coupling coefficient is set to $\beta = 0.98$, the normalized feedback delay is set to $\tau = 50$, the feedback strength is set to $\kappa = 3 \cdot 10^{-3}$ and the gain of the wavelengths are to $g_1 = 1$ and $g_2 = 0.995$. With this, the dependencies of two parameters on each other are studied and will be used to determine the operating range leading to a full switch. Moreover, these simulations are also used to identify the optimal feedback length for a later implementation on the PIC.

First, the injection current has been mapped as a function of the feedback strength and is shown in Fig. 2.8 (a). We found a large area exhibiting a full switch, however, at least a feedback strength of $\approx 2 \cdot 10^{-3}$ is required to initiate the switch for low injection currents. At larger injection currents, the feedback strength has to be increased to maintain a full switch.

In (b), the injection current is plotted against the feedback delay. A good switching performance is achieved for a large range of injection currents up to cavity lengths of about

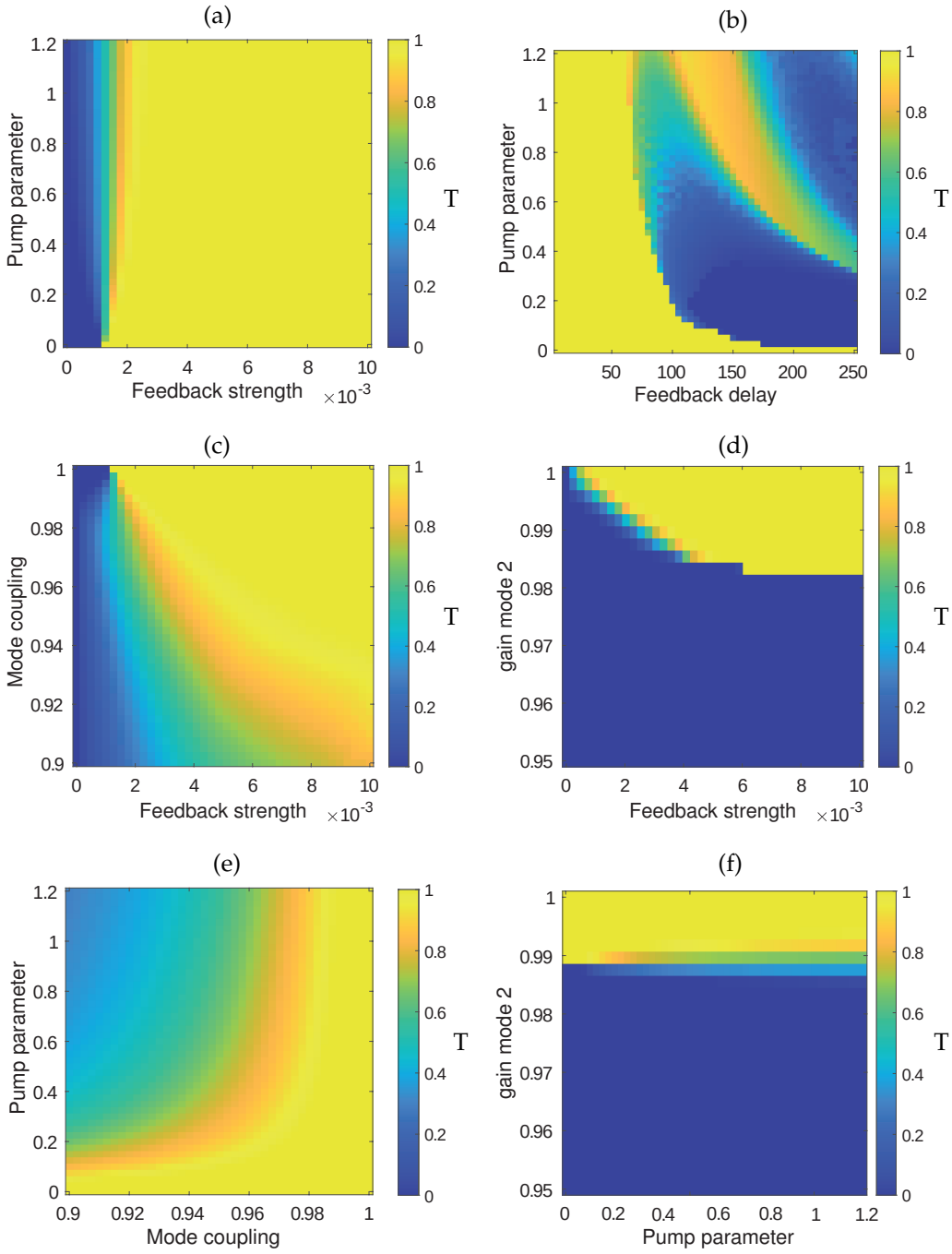


Figure 2.8: Mappings to study parameter dependencies on each other, the yellow regions correspond to full switches, values in green correspond to partial switches while the blue region represent no impact of the feedback phase. In (a) and (b), accessible parameters are studied while in (c) - (f), their impact on laser intrinsic parameters are studied. In general, an increasing optical feedback enables a full control by compensating low intrinsic parameters while the injection current needs to be limited for good operation.

$\tau = 60$. For larger feedback delays however, the injection current has to be limited to still obtain a full switch. This result is particularly interesting for a physical implementation of the feedback cavity onto the PICs. To implement the best performing external cavity length, a very short feedback cavity seems to be suited the best. Assuming a photon lifetime of 1 ps [59] and a refractive index of 3.36 for InP, then a feedback delay of $\tau = 60$ corresponds to a cavity length of about 2.5 mm on the PIC. Longer photon life times allow for even longer feedback cavity lengths.

Then, in the mappings (c) - (f), the impact of the injection current and the feedback strength are are studied on the coupling coefficient $\beta$ and gain differences between the modes. In (c), the coupling coefficient is plotted against the feedback strength. Also here, a certain feedback strength is required to achieve a full switch. Moreover, it is visible that a lower coupling coefficient can be compensated by a higher feedback strength. Dynamical behaviour was only achieved at feedback strengths beyond $\kappa = 2.2 \cdot 10^{-3}$, hence even higher feedback strength could be used to compensate for even lower coupling coefficients. A similar behaviour can also be found in (d), the gain for the first mode is considered to be 1 while the gain for second mode is varied and plotted against the feedback strength. It is visible that the gain for the second mode can also be compensated with increased feedback strengths. However, a clear limitation is visible: below a certain gain asymmetry a stronger feedback simply has no effect at all. In (e), the pump parameter is plotted against the coupling coefficient. For good coupling coefficients above 0.98 and high injection currents, full control over the switch can be achieved. For a reduced coupling, the injection currents needs to be limited to still allow for a full switch. In (f), the gain is plotted against the injection current. The margins to achieve a full control are very small and low currents should be preferred to achieve optimal operation conditions.

Overall it can be summarized that an increase in optical feedback actively enables a better performance. A higher feedback strength compensates for low coupling coefficients and larger gain differences and increases the operation range of the control approach. Increasing the injection current on the other hand might lead to a lower performance and even partial or no switches, hence, needs to be limited to obtain optimal operation conditions.

### 2.3.3 *Switching speed*

Finally, we numerically study the switching speed between the two wavelengths and the dependencies on the feedback strength, the feedback delay and the injection current will be highlighted. These simulations are based on a two-fold time series, after a steady-solution has been reached, an instantaneous phase shift is applied and an extended time series is computed. First, the time series for the feedback phase of $(\phi_1, \phi_2) = (0, \pi)$ is computed and the steady state solution is determined. This solution serves as the starting parameters for the extended time series. The feedback phases are then set to $(\phi_1, \phi_2) = (\pi, 2\pi)$ and the extended time series are computed. Such an approach is shown in Fig. 2.9 with the initial time series on the left, the switch is indicated with a vertical dotted line and the system is then evolving towards a new steady state solution on the right. For an estimation of the switching times, a photon-lifetime of $\tau_p = 1$ ps has been assumed to calculate the time scale [59]. The switching time is determined by

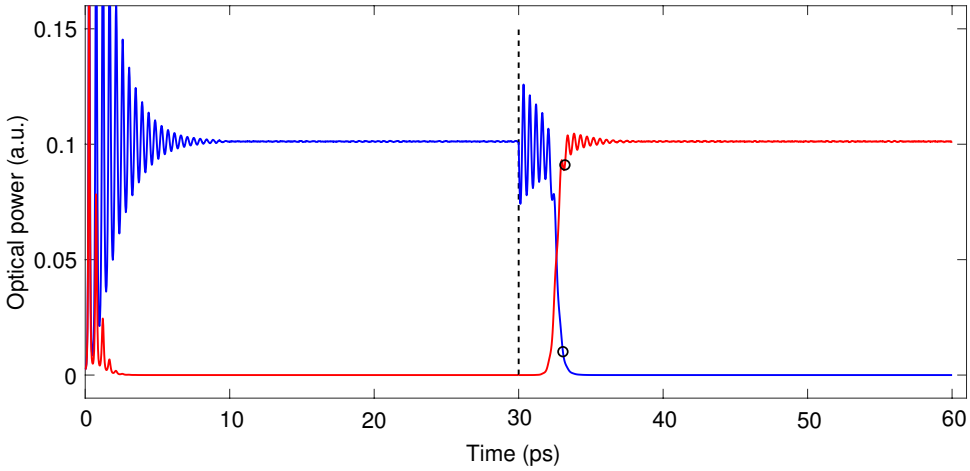


Figure 2.9: Temporal evolution of $\lambda_1$ & $\lambda_2$ with two different phase conditions to study the switching times. A photon lifetime of $\tau_p = 1$ ps has been assumed to calculate the time scale. On the left, the time traces for the phase conditions of $(\phi_1, \phi_2) = (0, \pi)$ are calculated. At the dashed line a switch to $(\phi_1, \phi_2) = (\pi, 2\pi)$ is initiated and the wavelengths evolve to a new steady state solution. The circles indicate the switching points of 10 % and 90 % for the wavelength being switched off and on, respectively.

taking the time between the trigger and the point where all values are below a 10 % or above a 90 % threshold, depending if the mode is turned off or on, respectively, and are indicated by circles.

In these simulations, only the injection current, the feedback strength and the feedback delay showed a significant impact on the switching times and are discussed in the following. Parameters like the gain difference or the carrier coupling showed no influence or dependency on any of these parameters and are therefore not shown.

The injection current is mapped as a function of the feedback strength in Fig. 2.10 (a) & (b), with the mode being switched off and on, respectively. For the mode being switched off in (a), almost no impact can be found on the injection current. Only a very small effect of the feedback strength is visible at low injection currents and switching times of about 1 ns are achieved across the whole mapping. The mode being switched on in (b) shows also only a very low influence by the optical feedback strength whereas the injection current shows to have a much more significant impact. Higher injection currents lead to faster switching times, improving from 8 ns at low currents to 2 ns at high injection currents. In Fig. 2.10 (c) & (d), the injection current is mapped as a function of the feedback delay. For the mode being turned off in (c), almost no impact is visible for variations of the injection current whereas a shorter feedback delay reduces the switching times from 2 ns to 1 ns. However, this is expected as longer cavity lengths lead to longer response times. For the mode being turned on in (d), faster switching times are observed for higher injection currents as well as for shorter cavity delays, improving the switching times from 7 ns down to 1 ns.
Hence, faster switching times seem to be achievable at higher injection currents and

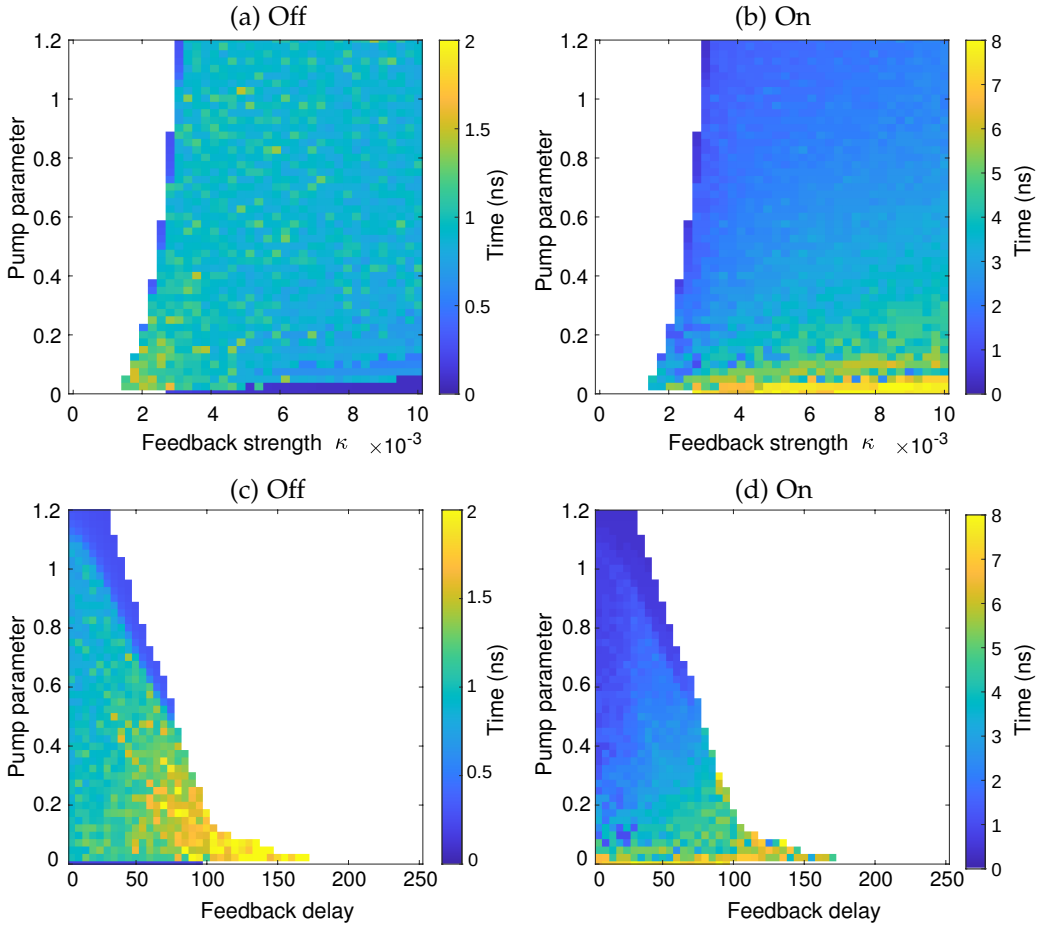


Figure 2.10: Mapping of the switching times in dependence of the gain current, feedback strength and feedback delay calculated with a photon lifetime of $\tau_p = 1$ ps, note the different scales. White regions represent areas without switches. The feedback strength seems to have a rather small impact on the switching times, visible in (a) & (b) for the modes being turned off and on, respectively. A higher injection current is only improving the switching times for the mode being turned on in (b). Similar behaviour is observed for cases (c) & (d) where a higher injection current only favours case (d). A shorter feedback delay is improving the switching times for both modes being switched off and on on (b) & (d), respectively.

shorter feedback delays, whereas the feedback strength does not seem to be a crucial parameter. We have seen that the feedback strength allows to gain a full control over the laser emission in previous sections. Finding a low influence of the feedback strength on the switching times is particularly interesting as it allows to achieve a full laser control without influencing the switching times. To put the switching times into perspective, other simulations performed on dual-wavelength switching have been conducted in [55], [62], [64] and [65] and have been discussed for in Fig. 1.5 (b) & (c). Their simulations are based the same model and switching times of down to 1 ns have been obtained. However, the major difference in their approach is the use of SOAs to induce a switch, hence, a higher feedback strength leads to better switching times. Experimental switching times of 31 ns have been reported in [62] with a wavelength transition time of 5 ns. Hence, our approach could lead to significantly faster switching times than other solutions.

## 2.4 CONCLUSION

To conclude this chapter, we first proposed a novel control approach based on a phase sensitive optical feedback loop to control the power ratio between two modes. First, we introduced a simulation model to determine and study the most crucial parameters leading to the best performances. We mapped all possible relative phase shifts between the two wavelengths and found large regions exhibiting a full switch. Using the optical feedback strength as an active control allowed us to obtain a full switch even for suboptimal relative phase shifts. This finding might be crucial in case manufacturing tolerances lead to slight deviations in the spectral separation, i.e. to an imperfect relative phase shift, which could impede the control approach. We then focused on achieving an equal optical power between the wavelengths by using the feedback strength as a control mechanism. We found that increasing the feedback strength allows to compensate large gain differences and low carrier couplings. However, these increased feedback strengths require a precise setting of the feedback phase to obtain an equal optical power. In a last step we focused on exploring the parameter space to find good laser operation points which can be used as indicators for later experimental work. Moreover, we also found an optimal parameter region for the implementation of feedback cavity on the PIC. We identified two major points: first, a larger feedback strength enables a better control whereas the injection current has to be limited to obtain a better switching performance. This is a good indicator when aiming for a full emission control in a later experiment. Second, we found a shorter feedback cavity to be beneficial for the best switching performance as well as fastest switching times.

In the next chapter, we will discuss the design and optimization process of our dual-wavelength lasers. The goal is to determine the exact emitting wavelengths already in the design stage to implement corresponding feedback cavities to achieve the optimal relative phase shift of $\pi$ in chapter 4.

# 3 INTEGRATED DUAL-WAVELENGTH LASERS

In this chapter, we design different dual-wavelength lasers, that will then be used later on, to demonstrate our control approach. Four different laser concepts, capable of emitting simultaneously on two different wavelengths, will be presented. We aim to determine the precise emitting wavelengths of our lasers by simulations to implement corresponding optical feedback-sections in a next step as will be discussed in chapter 4. We use a circuit simulator as an optimisation tool, but also to determine the precise wavelengths each laser will emit on. These wavelengths are then basis for the implementation of corresponding optical feedback-sections in chapter 4. In the first section 3.1, the different dual-wavelength laser concepts will be presented and the characteristics and limitations of each concept will be discussed. In the second section 3.2, the experimental results of a first MPW participation will be presented and are the basis for the optimisation process of each laser discussed in section 3.3 which were then implemented onto a second MWP run. The experimental setup and practical aspects of operating the PIC will be discussed in section 3.4. Their characterisation will be presented in section 3.5, together with the impact a change in current or temperature has on the DBR structures.

## 3.1 SOLITARY LASER LAYOUTS

In the first section of this chapter, we discuss the design process for the dual-wavelength lasers. The general idea is to implement the design together with other components for potential applications onto a single PIC. Hence, a very compact design is desired which allows to free as much space as possible on the PIC for these applications. Ideally the operation should also be as easy as possible, i.e. have as few control parameters as possible. Furthermore, as our control approach is based on modulating the gain using the optical feedback phase, a single gain section with a common carrier reservoir is required. Therefore the use of the multi-wavelength lasers such as those already discussed in chapter 2 is not suitable. They either use different gain sections to select the emitting wavelengths [54] or are already based on optical feedback to select the wavelength [55], [56]. Moreover, all of these solution use arrayed-waveguide-gratings which occupy a large amount of space on the PIC and are therefore not the first choice.

As no other laser sources were available, we designed our own custom lasers. For a wavelength selection, DBRs have been favoured over arrayed-waveguide-gratings for compactness and simplicity in their design. As an orientation for their arrangements, the discrete devices with parallel [28] and sequential [29] DBR arrangements, already discussed in section 1.3 and shown in Fig. 1.4, have been considered. Following this, we implemented a single gain section with two narrow bandwidth DBRs in a similar way, but with detuned wavelengths right away.

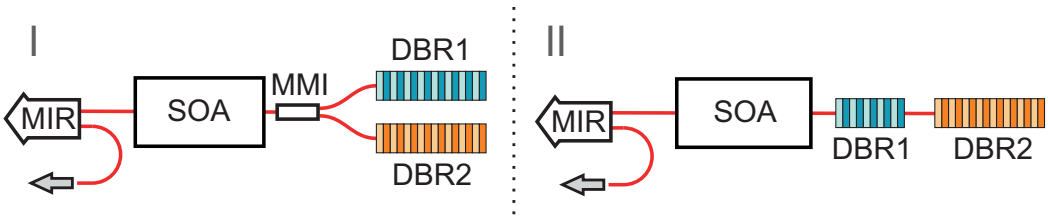


Figure 3.1: Dual wavelength laser concepts: In I, two DBRs are arranged in parallel and connected via an MMI splitter to form a laser cavity with an MIR. In II, two sequential DBRs are arranged to form a laser cavity with an MIR. Not shown are transition sections from shallow/deep etching and isolation sections.

A DBR arrangement in parallel is the simplest approach due to the symmetry and the low design efforts and is shown in Fig. 3.1, concept I. A sequential DBR arrangement requires a much higher design effort as the DBR lengths have to optimized for equal optical output powers for both wavelengths and is shown in Fig. 3.1, concept II. Both concepts use a broadband 2-port Multimode Interference Reflector (MIR) to form the laser cavity and to serve as the outcoupling mirror. The general design of the two concepts are described in the following. However, the exact parameters, e.g. lengths, reflectivities etc. for the components are left for section 3.3 as they result from simulations introduced later.

**Concept I:** Two DBRs with maximum lengths can be implemented to provide the highest reflectivities and consequently the lowest losses. The maximum length the foundry provides are 500 µm with a reflectivity of 97 %. To connect the DBRs to the gain section,

bend waveguides are used to connect them via an MMI splitter to the SOA. Another waveguide then connects the SOA to one port of the MIR with a reflectivity of $\approx 50$ % to form the laser cavity. The second port is used to couple light out of the laser. This approach results in a long laser cavity as the DBRs need to be spatially separated for manufacturing. The bending radius for the waveguides connecting the DBRs to the MMI splitter is however limited, hence, long waveguides have to be implemented. However, a long cavity results in a small longitudinal mode separation which can lead to a multi-mode emission if the reflection bandwidth of the DBR is too large. Hence, the selectivity of the DBRs need to be sufficiently high to select individual modes. As the coupling coefficient for the DBRs is fixed by the foundry, the DBR lengths have to be reduced to improve their selectivity. Shorter DBRs have a curved top instead of a flat top which increases the wavelength dependency. However, this would increase the losses and has therefore been avoided. Instead, the longitudinal mode separation has been improved by minimizing the cavity length. For that, deeply etched waveguides with small bending radii have been used to achieve the shortest cavity length possible. To avoid transition sections between different etching depths, as they increases the cavity length and also add additional losses, every component should ideally be implemented deeply etched to achieve the most compact design. However, SOAs are only available in shallow etching which makes transition sections unavoidable. This result in a trade-off between maximal compactness to achieve a large longitudinal wavelength separation and a longer cavity length with less components and lower losses but a smaller wavelength separation. As a dual-wavelength emission on two single modes is crucial, the compactness of the design is favoured. Hence, every component has been implemented in deep etching, except the SOA which required two transition sections on either side. Furthermore, mode-filters to avoid emission on higher order transversal modes have not been included to reduce the cavity length. Nevertheless, a major drawback of this approach is the transparency of the DBRs at each others wavelength. This results in optical output at three different points and in undesired losses. To overcome this issue, the laser cavity should not be transparent and consequently suggests a sequential arrangement of the DBRs. This way, the transmitted light by one DBR is confined to the laser cavity by the second DBR as will be discussed in the following.

**Concept II:** For this concept, two DBRs are arranged sequentially to improve output power, reduce the cavity length and subsequently increase the longitudinal wavelength separation. However, these benefits come with a much higher design effort to optimize the DBRs for an equal optical output power for both wavelengths. The sequential DBR arrangement avoids the mutual transparencies of the DBRs, therefore results in reduced losses which consequently lowers the laser threshold and improves the optical output power. To minimize losses, the DBR lengths should be as long as possible to provide highest reflectivities. However, this leads to a very long cavity length formed by $DBR_2$ and could potentially lead to a multi-mode emission. Hence, also for this concept, a trade-off between high reflectivities for low losses and short DBRs for high selectivities and single-mode emission has to be considered. Moreover, this consideration also has to include the correct lengths for an equal output power of both wavelengths. To find the best set of parameters, simulations will be used in section 3.3. For this layout, no MMI splitter or s-bend waveguides are required, allowing for the implementation of the DBRs

in shallow etching. Hence, only one transition section is required to connect the MIR in the most compact way possible. Due to the much more compact layout, we implemented a mode-filter to avoid higher order transversal modes. The DBRs are connected to the mode filter and then to the SOA and also each active components is separated by a short isolation section to avoid any cross talks.

Due to the wide bandwidth of the MIR, the desired wavelengths for the DBRs can be set anywhere within the gain bandwidth, allowing for a variable spectral separation. However, to avoid interference between the DBRs and the potential emission of undesired modes, their reflectivities should be well separated. Hence, using this approach is limited to larger wavelength separations. Another limitation is the lack in amplitude control for each wavelength. In case variances in the DBR reflectivities occur due to manufacturing tolerances, one wavelength might dominate and lead to different optical powers or a single wavelength emission. Although a DBR tuning allows for a limited degree of control, as will be discussed in section 3.12, it is far from being a convenient solution. To overcome both of these limitations, all DBR based laser concepts are used to bridge the gap towards smaller spectral separations and also to allow an active control over the individual amplitudes of each wavelength as will be presented in the following.

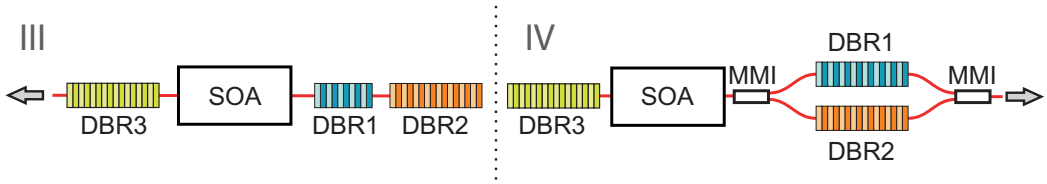


Figure 3.2: Dual wavelength laser concepts: In III, two sequentially arranged DBRs define the emitting wavelengths and form a laser cavity with another spectrally broader DBR. In IV, two parallel arranged DBRs define the emitting wavelengths and are connected via MMI splitter to form a laser cavity with another spectrally broader DBR. The transparency of the DBRs to each others wavelengths has been used to form the optical output using another MMI splitter. Not shown are isolation sections and a mode filter.

For these concepts, we have replaced the MIR with a third DBR to form the laser cavity. The three DBRs are detuned in such a way, that their reflection spectra are overlapping intentionally to achieve two reflection windows for each wavelength. In particular, the concept is based on a wide bandwidth for $DBR_3$, which reflects at both wavelengths generated by the narrow-bandwidths of $DBR_1$ & $DBR_2$. The required spectral overlap limits the wavelength splitting to about 1 nm. However, due to the tuning capabilities of the DBRs, this concept allows for a control of the individual wavelengths by detuning their spectral overlap.

**Concept III:** This concepts is based on three sequentially arranged DBRs as shown in Fig. 3.2, concept III. This arrangement minimizes the losses and is the shortest of our laser cavities as the $DBR_3$ acts as the outcoupling mirror. This avoids the need for a bend waveguide and the DBR can be positioned close to the SOA. Therefore, the whole laser can be implemented in shallow etching and no transition sections are required, lowering the footprint to a minimum. A mode-filter has been added to avoid higher

order transversal modes and isolation sections have been implemented between each active component.

**Concept IV:** Although we identified the parallel laser arrangement to have higher losses due to their transparency to each other, we aimed to exploit this peculiarity in this concept. We therefore combined the outputs of $DBR_1$ & $DBR_2$ via an MMI and merged their beams to serve as an optical output to improve the optical output power as shown in Fig. 3.2, concept IV. For compactness of the laser cavity, deep etching has been used for both MMIs and $DBR_1$ & $DBR_2$. This approach is not directly comparable to the other laser concepts as the transparency of the DBRs to each other also allows the optical feedback to easily enter the laser cavity. This approach therefore represents an ambitious attempt to achieve controllable dual-wavelength laser with a maximum output power for a wavelength separation around 1 nm.

## 3.2 IMPLEMENTATION ON FIRST PIC

For our first MPW participation, we shared one PIC together with another project to get first insights on the performance of our laser concepts. Due to the limited space and the early design stage, we only implemented the laser concepts I & II. However, the designs implemented for the shared project allowed to study two DBR lasers which were part of their design. Both will be discussed in the following. We then used the experimental results obtained to further develop and optimise our concepts for a second MPW run, discussed in section 3.3.

### 3.2.1 *Dual-wavelength lasers*

This first MPW participation was in an early stage of this PhD and allowed to share about 50 % of the space on a PIC with another project. With this opportunity, we got first experiences on the design process, how to handle PICs and set up a characterisation bench. At this stage, we had not yet established the simulation tools necessary to optimise each laser concept. We therefore implemented first designs with a short laser cavity for a large longitudinal wavelength separations to achieve single-mode emission for each wavelength. In total, we implemented four dual-wavelength lasers and two DBR lasers, which were part of the other project, onto the PIC, we manufactured two PICs and also packaged both of them. Unfortunately, the implemented lasers did not meet our expectations and performed poorly. Out of the 8 different lasers (2 PICs, each with 4 lasers), only one showed laser emission, and only emitted on one of the two wavelengths whereas both DBR lasers performed well.

On a positive note, we successfully identified the root cause of this poor results: an incorrect offset between straight and curved waveguides has been used. In a straight waveguide, the mode travels in the center whereas it travels off axis in a curved waveguides. To optimize the coupling efficiency between them, an offset has to be implemented. The waveguide has a width of 2 μm and an optimal offset for deeply etched waveguides transitioning from a straight into a 90° bend waveguide is 32 nm. However, we introduced a value of 400 nm, originating from a wrong simulation. This introduces losses of about 2 dB each time the wave passes the gap, accumulating to 8 dB for a full round trip in the laser cavity and has been implemented for all dual-wavelength lasers. Additional losses of about 12 dB were introduced between the laser and the outcoupling facet of the PIC. In later MPW runs, the offsets were automatically taken into account and do not require any actions since then. For the laser concept I, the accumulation of these losses together with the transparency of the DBRs to each other could not be compensated by the 300 μm short SOA. None of the four implemented lasers showed any lasing emission.

Only one of the lasers for concept II showed lasing, the LI curve is shown in Fig. 3.3 (a) and the optical spectrum is shown in (b). The laser emission only occurred on one wavelength with a seemingly low optical output power of 70 μW, to be compared with a power in the mW range measured for the DBR lasers on the same chip. Changes of the injection current, the temperature or a DBR tuning were not sufficient to trigger the emission on the shorter wavelength.

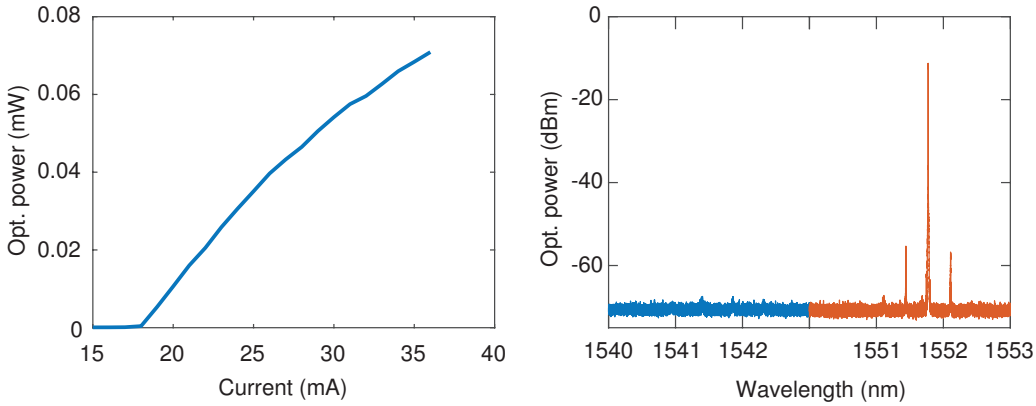


Figure 3.3: LI curve of the laser concept II for first PIC generation. Optical spectrum for the laser concept II at a gain current of 36 mA, emission could only be achieved at the longer wavelengths with a single mode emission at 1551.8 nm and a SMSR of about 45 dB. The lower wavelength could not be triggered by any means.

The origin for this is not clear, however, two possible issues could be identified: high losses due to the wrongly implemented offsets or unbalanced DBRs. For this laser, DBR lengths of $DBR_1$ = 200µm and $DBR_2$ = 370µm have been implemented with wavelengths of 1540 nm & 1550 nm, respectively. Possibly a shortening of $DBR_1$ or an increase of the $DBR_2$ length could lead to simultaneous dual-wavelength emission. To improve our designs and overcome this issue, we will perform simulation work for the second generation of dual-wavelength lasers to optimize the DBR lengths in section 3.3.

### 3.2.2 *Single-wavelength DBR laser*


Figure 3.4: Schematic of DBR laser, implemented with two different SOA lengths of 500 µm and 1500 µm with identical central DBR wavelength for each laser individually.

Studying the DBR lasers allowed us to have a reference point in terms of optical output power and spectral tuning capabilities for our dual-wavelength lasers. The DBR laser consists of a SOA section and two spectrally identical DBRs illustrated in Fig. 3.4. The DBR lasers have an SOA lengths of 500 µm and 1500 µm and have been implemented with the parameters detailed in Tab. 3.1. $DBR_1$ on the left, serves as a highly reflective mirror, while the $DBR_1$ on the right was kept short to serve as an outcoupling mirror. We expected single mode emission for the shorter DBR laser and multi-mode emission for the longer DBR laser due to its long laser cavity.
The LI curve for the 500 µm long DBR laser without any DBR currents applied is shown in Fig. 3.5 (a) and exhibits a maximum optical output power of 2.2 mW at 100 mA. The

Table 3.1: Design parameters for DBR lasers.

| SOA length (μm) | 500 | 1500 |
|---|---|---|
| $DBR_1$ | Length = 250 μm<br>R = 0.72 | Length = 440 μm<br>R = 0.95 |
| $DBR_2$ | Length = 125 μm<br>R = 0.31 | Length = 125 μm<br>R = 0.31 |
| DBR wavelength (nm) | 1550.8 | 1540 |
| Cavity length (μm) | 1044 | 1961 |
| Longitunidal mode separation (nm) | 0.34 | 0.18 |

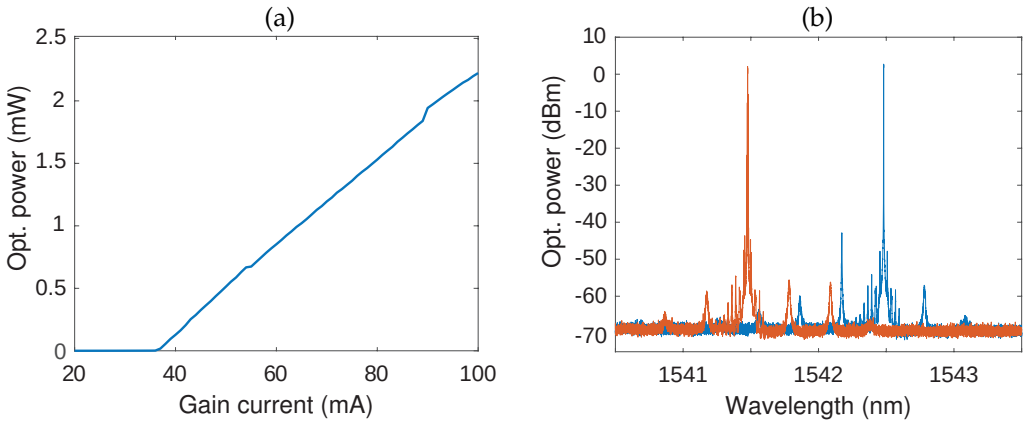


Figure 3.5: Experimental results for the 500 μm long DBR laser, in (a) the optical output power and in (b) the optical spectrum at a gain current of 100 mA. In blue and red the spectra without and with DBR tuning, respectively.

optical spectrum displayed in (b) in blue, shows that this high optical power originates from a single mode. The side modes are well separated with a longitudinal mode spacing of 0.31 nm and are suppressed by 45 dB. Detuning the DBRs allows to shift the spectrum to shorter wavelengths while maintaining single-mode as shown in red.

The results for the 1500 μm long DBR laser are shown in Fig. 3.6. In (a), the LI curve with an maximum optical power of 1.3 mW at 100 mA is shown. Although injection currents of up to 300 mA would have been possible, we refrained from increasing the gain current to avoid possible damages to the PIC. The optical spectrum without any DBR currents applied is shown in (b) in blue. The high optical power also originates from a single mode with the side modes are suppressed by 42 dB and the longitudinal modes are separated by about 0.16 nm. In this laser, a detuning of the DBRs triggers multiple modes as shown in red.

Both DBR lasers showed good results with high optical output powers and single-mode emission. First of all, these results confirm that our under-performing dual-wavelength

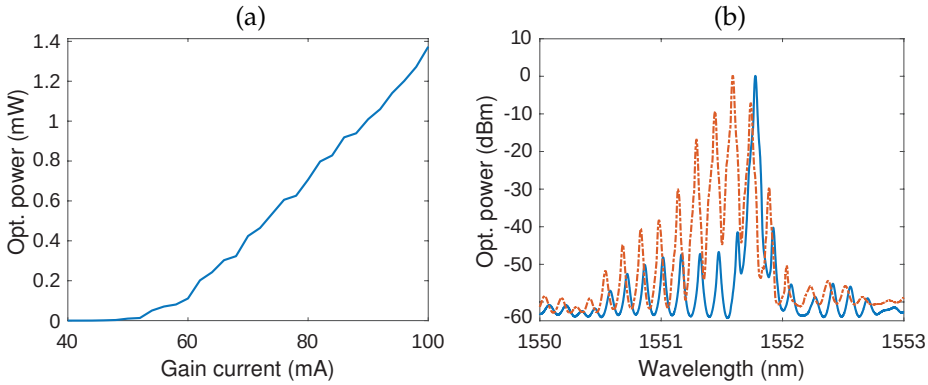


Figure 3.6: Experimental results for the 1500 µm long DBR laser, in (a) the optical output power and in (b) the optical spectrum at a gain current of 100 mA. In blue and red the spectra without and with DBR tuning, respectively.(Lowered spectral resolution of the OSA of 0.02 nm.)

lasers are in fact the result of a failure in our implementation process. This is evident when comparing the optical power levels of both DBR lasers with up to 2.2 mW to the dual-wavelength laser layout II, only emitting with 0.07 mW. Clearly high losses are the origin of this limited performance. Following these results, we implemented 500 µm long SOAs in our next generation of dual-wavelength lasers. The lengths of our dual-wavelength laser cavities are in the same range than the ones of the 500 µm long DBR laser, hence, single-mode emission with a high optical output powers can also be expected for our laser concepts.

## 3.3 OPTIMIZATION OF DUAL-WAVELENGTH CONCEPTS

With the insights gained from our first MPW run, we aimed to improve each laser concept for a second MPW participation. In this section, we determine the ideal DBR parameters to ensure the best performance as well as to determine the expected wavelength differences the lasers will emit on. These wavelengths will then be the starting point to design customized optical feedback cavities for each laser concept in chapter 4. With the results obtained from the DBR lasers, we fixed the SOA lengths of all laser concepts to 500 µm. In a next step, the DBR lengths will be determined using the circuit solver Lumerical Interconnect. The software solution provides a set of building blocks which can be adapted to the specific platform used. At the development stage of the software, no dedicated library for the foundry platform was available. We therefore adapted each component in compliance with the foundry manual to achieve the best starting conditions possible. The foundry provided refractive indices, dimensions of waveguides, mirror reflectivities as well as the coupling coefficient for the DBRs. For the gain curve, no experimental data could be implemented, we therefore used a standard Lorentzian line shape to model it. An example of an implementation into the simulator is shown in Fig. 3.7 and represents the laser concept I, shown in Fig. 3.1.

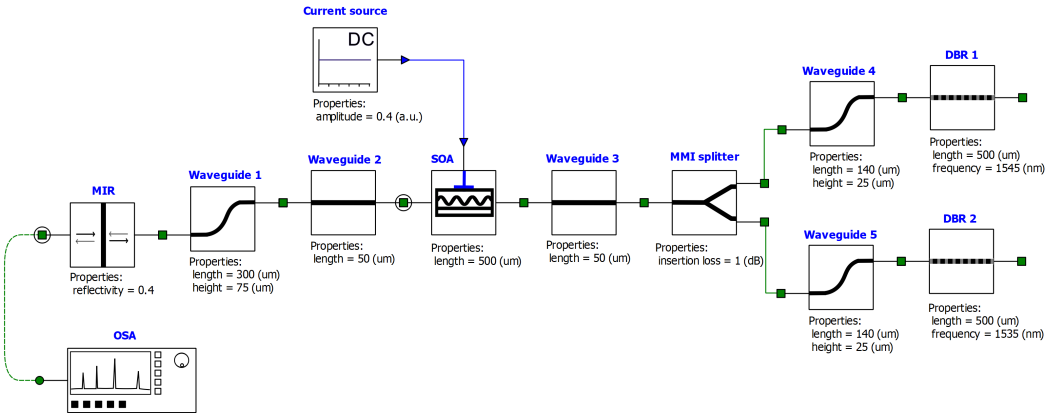


Figure 3.7: Example layout for a circuit simulation of laser concept I using the software solution Lumerical Interconnect. Each component corresponds to a counterpart, implemented in the physical laser layout.

To model the behaviour of this laser, we have implemented two DBRs on the right hand side, with the coupling coefficient being fixed to a value of 50 $cm^{-1}$ according to the foundry specifications. Each DBR is connected to the MMI splitter via an s-shaped waveguide which is then connected to the SOA via a short waveguide. On the other side of the SOA, another short waveguide connects the SOA with an s-shaped waveguide to the MIR. This s-shaped waveguide is the best solution to achieve a short laser cavity and to couple light out. The short waveguide sections on both sides of the SOA are implemented to compensate for the lengths of components like modefilters and transition- and isolation-sections used in the physical implementation of the PIC. These waveguides are adapted for each laser design individually and allows us to model the physical implementation on the PIC as close as possible.

In the first step of the optimization, each laser layout was implemented into the PIC design software Optodesigner in the most compact way possible and the resulting length of each component was determined. In the second step, these layouts were then transferred to the circuit simulator including the lengths of each component. In a last step, the DBR lengths were varied to find the best operation point meeting the following conditions: Firstly, both wavelengths should exhibit an equal optical output power, and secondly, the SMSR should be maximized to prevent a potential emission on multiple modes.

To ensure a good robustness of the emission properties for each laser, the gain current as well as the DBR lengths were varied in a small range around the optimal parameters to verify that the desired features were kept. However, additional factors had to be taken into account when designing the DBRs: As the coupling coefficient is fixed, the length, bandwidth and reflectivity are related to each other. Long DBRs with high reflectivities reduce the losses of the laser and lead to a lower thresholds. However, this also limits the optical power which can be coupled out of the laser via the DBR. Moreover, it also reduces the selectivity of the DBRs and leads to long cavity lengths which can potentially result in a multi-mode emission due to the small longitudinal mode separation. Hence, to increase the optical output power and selectivity, shorter DBRs can be beneficial. They have a lower bandwidth and improve the selectivity together with the larger longitudinal mode separation due to the resulting shorter cavity. However, if chosen too short, high losses and low output powers could be the result and might even pose a risk of not reaching laser threshold. We therefore aimed for an optimal trade-off between optical output power and a spectral selectivity. In particular, for cases where two DBRs are arranged sequentially (concept I & III), we made the first DBR ($DBR_1$) significantly shorter than the second one to be sure that single-mode emission would be obtained for both wavelengths.

The simulation results achieved for laser concepts I & II are shown in Fig. 3.8 (I) & (II), respectively. We achieved an equal output power for both, with multiple side modes appearing in the spectrum. In particular for concept II, we were not able to achieve a higher suppression ratio than 10 dB for the side mode. However, as the even longer cavity length of the 1500 µm long DBR laser also exhibited single mode emission, we also expected to achieve single mode emission for this laser. The simulation results for laser concepts III & IV are shown in Fig. 3.8 (III) & (IV), respectively. In both concept, we were able to achieve two dominant modes, exhibiting an equal optical power with high side mode suppression ratios. The simulations were particularly important for these concepts as the emission is not expected at the central DBR wavelengths, but instead at the intersection point of the overlapping DBR spectra. Hence, the first expected wavelength is between the central wavelengths of $DBR_1$ & $DBR_3$ and the second wavelength between $DBR_2$ & $DBR_3$.

All design parameters are summarized in Tab. 3.2, together with the resulting laser cavity lengths as well as the expected emitting wavelengths. The laser cavity lengths were calculated by adding the length of each component together with the effective DBR lengths calculated by $L_{eff} = \frac{1}{2\kappa} \cdot \tanh(\kappa \cdot L_g)$ [66] with $\kappa$ being the coupling coefficient of 50 $cm^{-1}$. Furthermore, as the detuning of the the $DBR_1$ & $DBR_2$ in concept III & IV allows for some control of the optical powers, we implemented them with a wavelength shift of +0.3 nm onto the manufactured PIC. This requires a tuning of the DBRs to achieve the optimal operation wavelength, but allows to achieve a larger spectral separations for

studying purposes. These results are the basis for the implementation of corresponding feedback cavities in the next chapter 4.

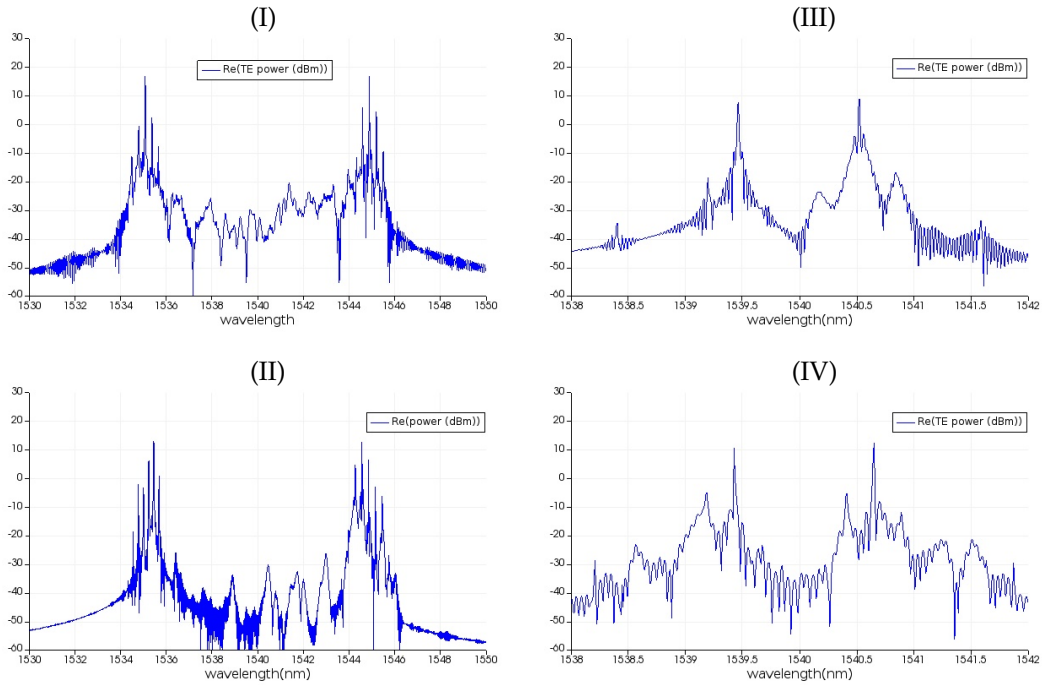


Figure 3.8: Simulation results for laser concept I to IV, denoted with (I) to (IV), respectively. In (I) & (II), a spectral separation of 10 nm and in (III) & (IV) a 1 nm spectral separation is achieved. We aimed for an equal optical power and high side mode suppression in all concepts.

Table 3.2: Implemented DBR parameter for different laser layouts together with the resulting laser cavity length and the expected emitting wavelengths. The feedback cavity parameter are given here for simplicity and overview but will be discussed in chapter 4.

| Concept | I | II | III | IV |
|---|---|---|---|---|
| $\Delta\lambda$ (nm) | 10 | 10 | 1 | 1 |
| DBR wavelength (nm) | $\lambda_1 = 1535$<br>$\lambda_2 = 1545$ | $\lambda_1 = 1545$<br>$\lambda_2 = 1535$ | $\lambda_1 = 1541^*$<br>$\lambda_2 = 1539^*$<br>$\lambda_3 = 1540$ | $\lambda_1 = 1541^*$<br>$\lambda_2 = 1539^*$<br>$\lambda_3 = 1540$ |
| DBR length ($\mu$m) | $DBR_1 = 500$<br>$DBR_2 = 500$ | $DBR_1 = 250$<br>$DBR_2 = 500$ | $DBR_1 = 200$<br>$DBR_2 = 350$<br>$DBR_3 = 250$ | $DBR_1 = 450$<br>$DBR_2 = 450$<br>$DBR_3 = 350$ |
| R | 0.97<br>0.97 | 0.72<br>0.97 | 0.58<br>0.89<br>0.72 | 0.96<br>0.96<br>0.97 |
| DBR bandwidth (nm) | 1.08<br>1.08 | 1.47<br>1.08 | 1.72<br>1.23<br>1.47 | 1.11<br>1.11<br>1.09 |
| Expected wavelength (nm) | $\lambda_1 = 1535.07$<br>$\lambda_2 = 1544.88$ | $\lambda_1 = 1544.55$<br>$\lambda_2 = 1535.44$ | $\lambda_1 = 1540.52$<br>$\lambda_2 = 1539.45$ | $\lambda_1 = 1540.65$<br>$\lambda_2 = 1539.42$ |
| Cavity length ($\mu$m) | 1253.80 | 1082.4<br>1396.3 | 881.0<br>1149.0 | 1129.9 |
| Longitudinal mode spacing (nm) | 0.28 | 0.33<br>0.25 | 0.40<br>0.31 | 0.31 |
| Feedback SOA length ($\mu$m) | 300 | 300 | 300 | 300 |
| EOPM length ($\mu$m) | 1200 | 1200 | 1200 | 1200 |
| Feedback length ($\mu$m) | 2500 | 2500<br>4850 | 2400 | 2800 |

*DBR wavelength has been implemented onto the PIC with +0.3 nm longer wavelength

## 3.4 EXPERIMENTAL SETUP

In Fig. 3.9 (a), the design layout for our second PIC is shown and a close up of the manufactured PIC is shown in (b). In panel (a), thin horizontal blue lines correspond to waveguides, while the more visible green connections are the metal tracks connecting the active components to the bond pads located at the edges of the PIC. The different lasers are distributed all over the PIC to utilize the available space, with their optical outputs routed to the right edge of the PIC via waveguides. The layout for laser concept II is exemplary highlighted in the inset. To electrically connect the active components, either probes or a packaging can be used. Besides the mechanical stress probing can have on the PIC, the amount of probes is also limited by the available space which can be arranged around the chip. Our lasers have up to 6 active components and a packaging solution has therefore been favoured [67]. Therefore, the metal tracks from each active component are routed to the edges of the PIC with varying widths to adapt for the different required currents of each element. On the edges of the PIC, bond wires are then used to connect the metal tracks to an external circuit board. The bond wires are visible in the manufactured PIC in (b) with the close up of the laser concept II in the inset. The electrical circuit board together with a metal housing is shown in (c). The packaging also provides an integrated thermal control solution and allows an easy electrical connection via a 40-wires ribbon cable. A lensed optical fibre is used to couple the light out of the PIC for measurements and has not been packaged for flexibility as a total of 22 optical outputs have been implemented. Instead, the packaged PIC is mounted to allow alignment of the lensed optical fibre to one of the optical outputs using a microscope, show in (d). The currents have been controlled via an Pro8000 system (ITC8022 & TED8020) and the measurements for the optical spectra have been obtained using an APEX 2083A with a resolution down to 5 MHz/40 fm. If not mentioned otherwise, a resolutions of 1.2 pm has been used throughout this thesis. A higher resolution has been avoided as it increases the measurement times without practical benefits.

Although the packaging allows for an easy usage of the PIC, practical issues on the mechanical stability still remain to be improved. As visible in (c), the distance between the PIC and the optical fibre mount is relatively large and is prone to vibrations and air drafts which can result in fluctuations for some measurements. Shielding and stabilisation of the fibre allowed for a temporary solution, a long term solution should aim for a redesign of the packaging or the fibre holder.

In total, 15 PICs were manufactured across three different wafers in two different runs. 8 PICs were considered mechanical grade and can be used for testing purposed. 7 PICs were considered as good cells of which 5 have been packaged. The PICs are listed in Tab. 3.3 and denoted with A - E, including their wafer identification and their position on the wafer. Each of these PICs contains the concepts I - IV, however, for concept II variations in the feedback length have been included as stated in Tab. 3.2. Throughout the thesis, different lasers from different PICs will be used, either to demonstrate the best performances achieved or to discuss specific limitations observed. To identify the individual lasers in the thesis, we will indicate the concept together with the corresponding PIC used in each section, in case of concept II, the feedback length will be stated as well.

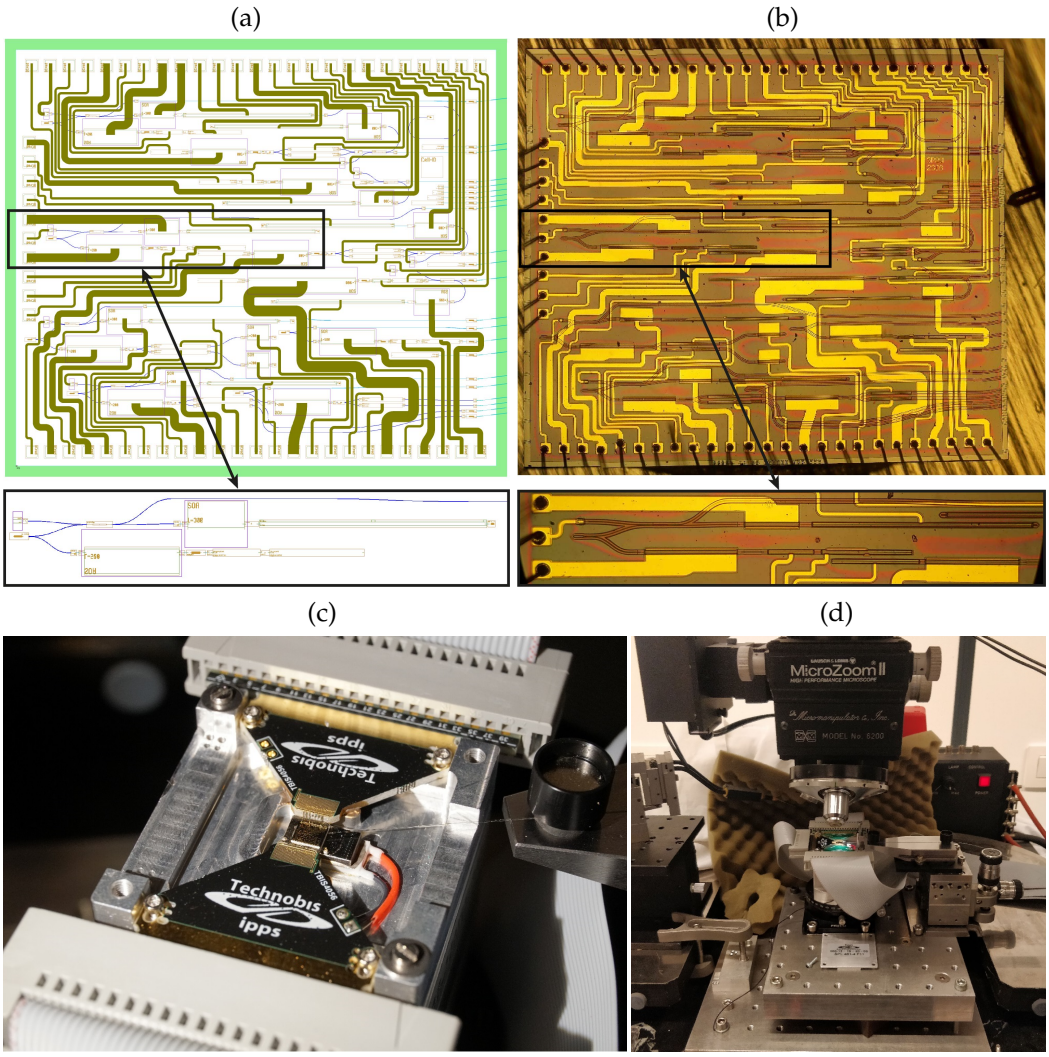


Figure 3.9: In (a), the design layout of the second MPW run, the horizontal blue lines are waveguides and the green connections are metal tracks for electrical routing. In (b), the manufactured PIC and in the insets of (a) & (b) a close up of laser concept II. In (c), the packaged PIC with a metal mount including a build in temperature control (black & red cables), the electrical 40-pin cables (top and bottom) and the optical fibre on the right. In (d), the mounted PIC together with a microscope to align the optical fibre to couple light out of the PIC.

Table 3.3: PIC identification used throughout this thesis.

| PIC | A | B | C | D | E |
|---|---|---|---|---|---|
| Wafer | SPL 553-5 | SPL 553-6 | SPL 553-5 | SPL 553-6 | SPL 461-4 |
| Position on wafer | J8 | J8 | B8 | B8 | F11 |

## 3.5 CHARACTERISATION OF DUAL-WAVELENGTH LASERS

In the following, we study the performance of each solitary laser and discuss their peculiarities. We aim to identify the best operation points for each laser exhibiting a dual-wavelength emission. With this, we are then able to apply an optical feedback to control their emission in chapter 4.

### 3.5.1 *Achieving dual-wavelength emission*

All measurements presented were obtained at a temperature of 20 °C. Key results for each concept are given in Table 3.4 with the spectral separation $\Delta\lambda$ and the wavelengths acquired experimentally together with the best values found for the optical power, the side-mode suppression-ratio (SMSR) and the longitudinal mode separation. Typical LI curves and optical spectra for every concept are shown in Fig. 3.10.

Laser concept I showed large variations in the performance. Unfortunately, most of these lasers showed a single mode emission across different PICs and different wafers.A deviating splitting ratio of the MMI splitters, deviations in the DBR reflectivities or non negligible optical feedback from the DBRs of the not emitting wavelengths might be the origin. Nevertheless, one laser (PIC C in Tab. 3.3) showed a dual-wavelength emission for a large range of injection currents and is shown in Fig. 3.10 (a). Both wavelengths show a linear increase in optical output power of up to -12 dBm. Each of the wavelengths emits on a single mode as shown in (b). However, at an injection current of 49 mA, a switch to another longitudinal mode within $\lambda_2$ occurs. As will be discussed in sections 3.5.2 and 5.1.3, we observed that applying a small current to $DBR_2$ can suppress this jump to another longitudinal mode when increasing the laser current. The large range of equal optical powers in this laser makes it a potentially versatile laser source, however, the bad reproducibility is a major drawback.

The laser concept II (PIC C) appeared to be much more reliable with better performances. We found reproducible behaviours with a simultaneous dual-wavelengths emission at multiple equal power points across different PICs. This concept is outperforming the concept I in terms of optical output power and reproducibility. This laser shows multiple equal power points when the gain current is tuned, visible in the LI curve shown in (c), the optical spectrum at an injection current of 85 mA exhibiting an equal power of -8.5 dBm is shown in (d). The longitudinal wavelength separation for the cavity formed by $DBR_2$ is lower than for concept I which resulted in multiple side modes to appear when tuning the injection current. To suppress these undesired modes, we applied a current of 5 mA for $DBR_1$ and 4 mA for $DBR_2$ to tune the DBR spectra such that no mode appeared within the whole range of laser injection currents. This concept seems to be the best option for variable wavelength separations, i.e. for a spectral separation of 10 nm. To bridge the gap to smaller wavelength separation, we implemented all DBR based concepts with a 1 nm separation.

Laser concept III (PIC C) also showed to have a reproducible behaviour across different PICs, however, exhibits a sudden switch from one wavelength to the other as shown in (e) and also showed a hysteresis cycle. This seems to be a peculiarity of this concept as we found the same behaviour in all of our PICs. As the DBRs were implemented with

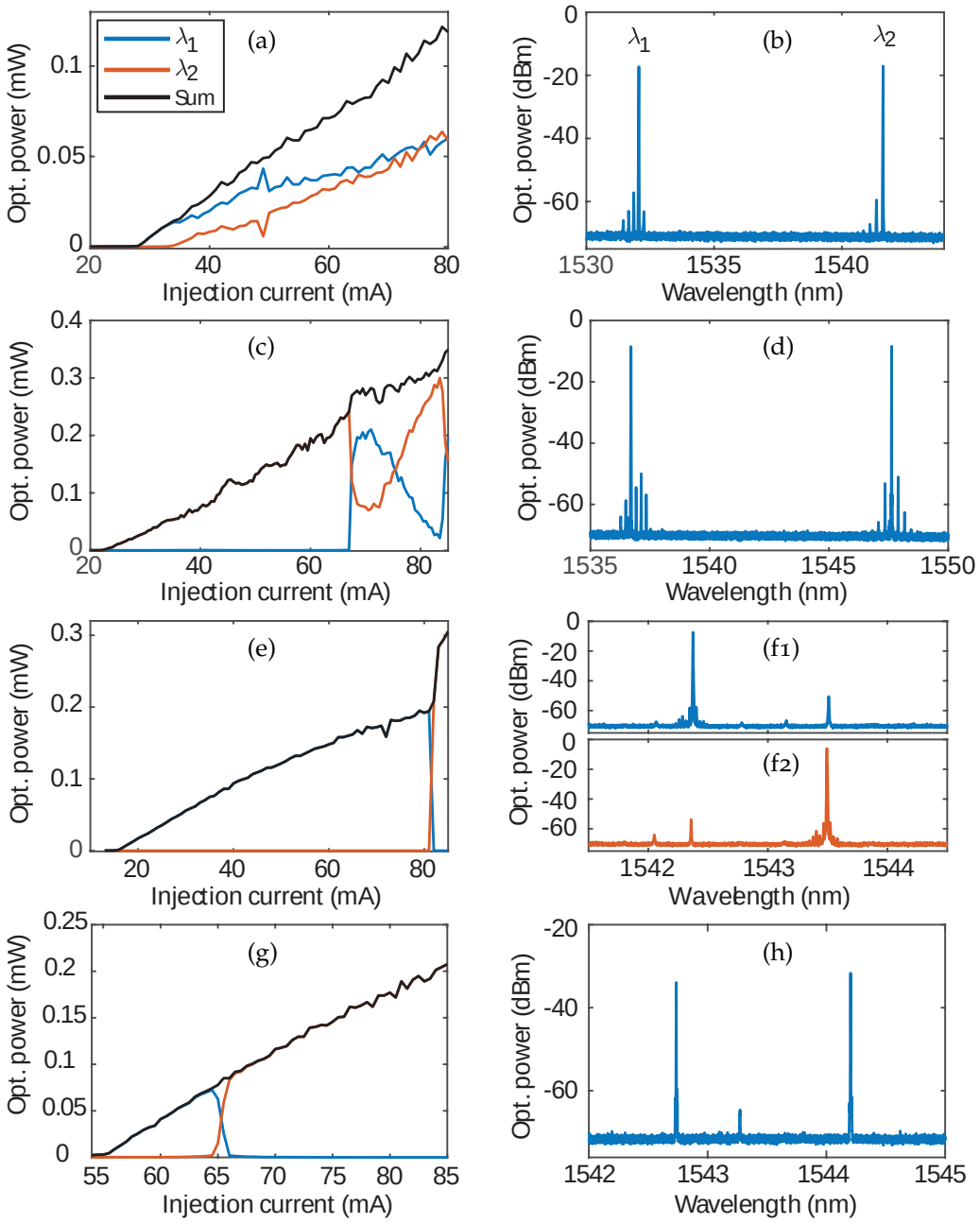


Figure 3.10: LI curves and optical spectra for each laser concept: Concept I: (a) & (b), exhibiting large current ranges with equal powers, the optical spectrum plotted at 80 mA. Concept II: (c) & (d), exhibiting multiple equal power points, the optical spectrum plotted at 85 mA. Concept III: (e), (f1) & (f2), exhibiting a sudden switch with the spectrum plotted before (f1, 81 mA) and after (f2, 82 mA) the switch. Concept IV: (g) & (h), exhibiting a smooth transition with a full switch between the wavelengths with an equal power point in between, the optical spectrum plotted at 65 mA.

slightly detuned wavelengths, a DBR current of 1.7 mA to $DBR_3$ has been applied to achieve the presented LI curve. The optical spectra before (81 mA) and after (82 mA) the switch are shown in (f1) and (f2) with optical powers of -7 dBm in single-mode emission and represents an attractive choice for dual-wavelength switching.

Concept IV (PIC E) was designed to improve the optical output power, however failed to meet our expectations. Although this concept also shows reproducible results across all PICs, it exhibits high thresholds and a low optical output powers. In this concept, the imbalance between the two wavelength in concept I, leading to a single-wavelength emission, can be compensated by detuning the DBRs and allowed to achieve similar results across different PICs. Contrary to concept III, this laser showed smooth transitions from one wavelength to the other together with an equal power point at 65 mA as visible in the LI curve shown in (g). However, the optical power is rather limited as can be seen in the optical spectrum in (h) and is with -32 dBm the lowest achieved throughout our concepts. Nevertheless, it turned out to be the most versatile concept as it is the only laser allowing for a simultaneous dual wavelength emission as well as a full wavelength switch by just tuning the laser gain current.

Both concepts, III & IV, allow for an active control over the wavelengths by the relative tuning of the DBRs. Depending on the set of currents for the DBRs, a single wavelength as well as the desired dual wavelength emission is possible.

Table 3.4: Key experimental results for each Layout.

| Layout | $\Delta\lambda$ (nm) | Experimental wavelength (nm) | Fiber coupled optical power (dBm) | SMSR (dB) | long. mode separation (nm) |
|---|---|---|---|---|---|
| I | 10.4 | 1531.8 | -12.3 | 39 | 0.24 |
| | | 1542.2 | -11.8 | 41 | 0.24 |
| II | 10.9 | 1536.7 | -8.5 | 42 | 0.27 |
| | | 1547.6 | -8.4 | 43 | 0.21 |
| III | 1.1 | 1542.4 | -7.4* | 43 | 0.37 |
| | | 1543.5 | -6.1* | 43 | 0.31 |
| IV | 1.5 | 1542.7 | -36.4 | 29 | 0.25 |
| | | 1544.2 | -31.8 | 33.1 | 0.25 |

*Optical power for single-mode emission

Because of the well-known blue shift of the gain spectrum that occurs with increasing currents, we would expect that the longer wavelength reaches its threshold first. This results from the blue shift of the gain spectrum with increasing injection currents. However, only laser concept II exhibits this behaviour while all other lasers started lasing in the reversed order, i.e. on the shorter wavelength first. The origin for this in not clear, but could possibly be connected to local temperature gradients induced by the increased SOA current. Nevertheless, we are able to achieve dual-wavelength emission in all concepts which is the starting points to apply optical feedback for a control.

We found that the laser wavelengths were not very accurately predicted by our simulation (neither the wavelength nor the wavelength splitting): they have been shifted to shorter as well as to longer wavelengths, indicating high variances in the target wavelengths of the DBRs across different wafers. Moreover, the wavelength separation is of major importance, we found severe variations across our lasers with spectral separations of about 10 % in all of our lasers as denoted in Tab. 3.4. A tuning of the DBRs was expected to allow for a match of the experimental- and design-wavelengths in this event. Unfortunately, the DBR tuning lead to a single-wavelength emission instead of a change in the spectral separation. This is caused by a reduction in the DBR reflectivity with increasing DBR current and will be discussed in the following. The impact of the DBR tuning onto an laser simultaneously emitting on two wavelengths and the resulting single-wavelength emission will be discussed in section 5.1.3.

### 3.5.2 *DBR characterisation*

We have seen different impacts of a DBR tuning onto the laser emission in the experiments. By tuning the DBR current, we were able to trigger the second wavelength to achieve a dual-wavelength emission or could limit the number of emitting modes by increasing the DBR current. Here, we focus onto the spectral response of a DBR to understand the origin of these behaviours. We study $DBR_2$ of laser concept II from PIc (C) when subject to a DBR current as a representative example, the same behaviours are found in other DBRs. One side of this DBR has been connected to the laser and the other side has been routed to the edge of the PIC for characterisation. We used an optical circulator to separate the beams coupled into and out of the PIC and used a tunable laser source to measured the reflection spectrum of the DBR via an OSA. The work presented in this section has been achieved in the framework of the master thesis of Robbe de Mey, under supervision of M.Sc. R. Pawlus and Prof. M. Virte [68].
The DBR has a length of 350 µm, is centred at a wavelength of 1535 nm and allows for a maximum current of 21 mA. The resulting reflection spectra are shown in Fig. 3.11 (a). The modulations visible around the maxima result from back-reflections from the edge of the PIC when coupling light onto the waveguide. With increasing DBR current, the reflectivity spectrum shifts to shorter wavelengths while also decreasing in width and in reflectivity. The evolution of the spectral width with increasing current is shown in (b) and results in a decrease of about 0.3 nm. The evolution of the reflectivity is shown in (c) with a reduction in reflectivity of 1.2 dB.

As we have only limited control ability over the lasers, especially for laser layouts I & II, this behaviour could be exploited to our advantage (though overall quite detrimental). As some lasers only show single-wavelength emission, a current can be applied to the DBR of the emitting wavelength to reduce its reflectivity and increase its losses. In some cases, this allowed to trigger the suppressed mode and lead to a dual-wavelength emission. In other cases when the laser was emitting simultaneously on two wavelengths together with multiple undesired side modes, a small DBR current lead to a selection of one particular mode while suppressing the side modes. Thus, leading to an ideal dual-wavelength emission on two modes and might be related to two effects at once, the reduction in spectral bandwidth and the tuning of the wavelength. The narrower

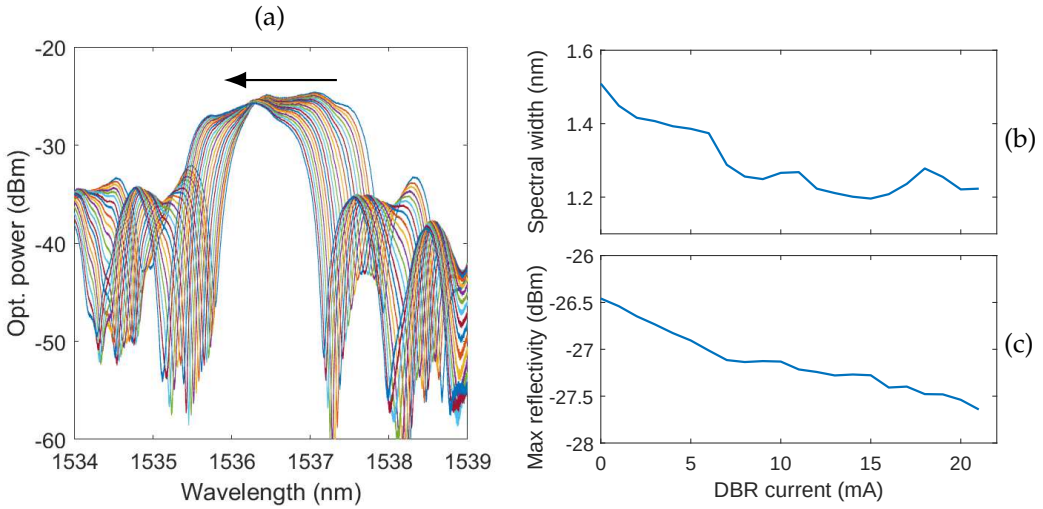


Figure 3.11: The spectral evolution of the DBR is shown in panel (a), the current is tuned from 0 mA to 21 mA, shifting the optical spectrum to shorter wavelengths. In (b), the evolution of the spectral width as a function of the DBR current. In (c), the reduction in reflectivity as a function of the DBR current.

DBR spectrum allows for an easier selection of a particular mode and the shift aligns the central DBR wavelength with the longitudinal mode. Moreover, as this also reduces the reflectivity, a too large DBR current can lead to a complete suppression of one of the wavelength up to a point of a single wavelength emission. This peculiarity will be discussed in detail in section 5.1.3 as it limits the performance of our lasers.

The temperature of the PIC has also a major impact on the DBR performance, as shown for different LI curves ranging in temperature from 15 °C to 35 °C in 5 °C steps in Fig. 3.12 (a). Here, we characterise the laser concept IV as it allowed for a single-wavelength emission to conduct these measurements and a direct access to also characterise the DBR. At a temperature of 15 °C, we find a laser threshold of 38 mA and the threshold shifts to 55 mA at 30 °C, already showing a flattening of the curve. At 35 °C no lasing could be achieved within the current limit of the SOA. We changed the temperature in a range from 15 °C to 25 °C and measured the reflection spectra of $DBR_2$, the results are shown in (b). The DBR has a length is 450 µm and a central wavelength of 1541.3 nm. While changing the temperature, the spectral width and the reflectivity remain unaltered. The deviations in the maximum reflectivity originate from the realignment if the fibre required when the temperature is changed, thus changing the coupled power into and out of the PIC. A shift of 1.2 nm was achieved for the temperature range of 10 °C, e.g. a spectral shift of 0.12 nm/°C. Wavelength shifts ranging from 0.11 nm/°C to 0.19 nm/°C have been observed characterising other DBRs.

Shifting the DBR spectrum with the temperature can be used to set a precise wavelength within the tuning range, however, with the risk of a higher threshold and a lower optical output power. As our dual-wavelength lasers also exhibit a deviation from the design to the experimental wavelengths, we could compensate for it to a certain de-

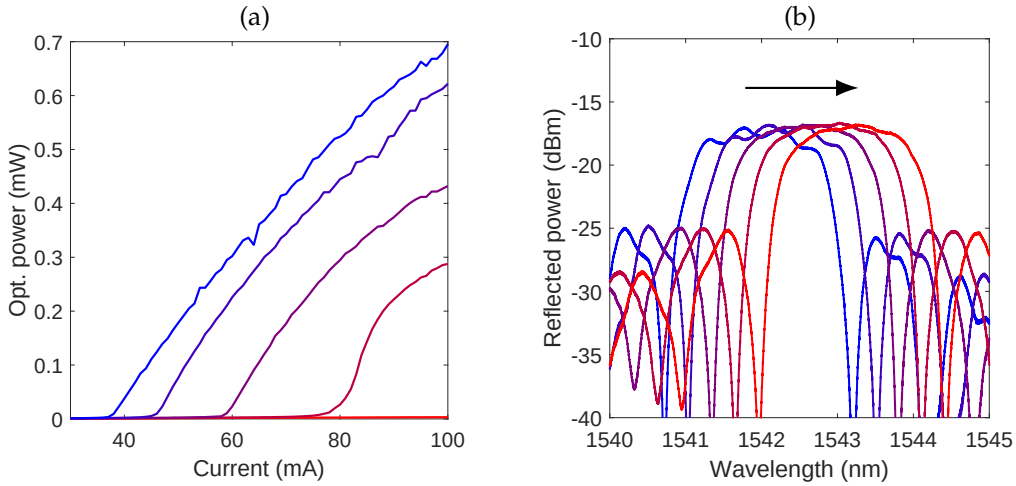


Figure 3.12: In (a), the LI curve for temperature from 15 °C to 35 °C is shown, the threshold shifts to higher currents with increasing temperature. At a temperature of 35 °C, no lasing is achieved. In (b), the spectral evolution of the DBR for a temperature range from 15 °C to 25 °C is shown, an increase in temperature shifts the spectrum to longer wavelengths by 1.2 nm.

gree. However, the crucial parameter for our control approach is the spectral separation between the two wavelengths. This feature turned out to remain constant as both wavelength experience the same wavelength shift. Therefore, lower temperatures seem to be advantageous for higher optical output powers. But, at temperatures around 15 °C condensation is visible on the PIC due to humidity and we therefore set our operating temperature to 20 °C for all our experiments. Furthermore, we also found a shift in the DBR spectrum when a nearby device like an SOA or a neighbouring DBR was operated with high currents. The resulting temperature gradient within the PIC shifted the DBR spectrum to longer wavelengths. Although it would require further investigations to be confirmed, we think that this feature might be, at least in part, at the origin of the spectral evolution opposed to the blue-shift of the gain spectrum that we observed in some of our lasers. Yet, our work does not allow us to confirm it for now.

## 3.6 CONCLUSION

To conclude this chapter, we presented four different dual-wavelength laser concepts and optimized them with the insights gained from a first MPW participation towards a second generation. For the optimization, we used a circuit simulator to determine optimal DBR lengths for dual-wavelength emission, but also to determine the exact wavelength each of the lasers will emit on. We then presented experimental results for each laser and found simultaneous or sequential dual-wavelength emission across all structures and discussed their peculiarities. Layouts II & III showed to be the best performing concepts with high output powers and reproducible results across different PICs and wafers which suggests a good robustness of the designs. Finally, we also presented DBR characteristics under varying currents and temperatures and discussed their impact on the laser emission. With the resulting wavelengths obtained from the simulations, we implemented customized feedback cavities presented in the next chapter. Together with the operation points for dual-wavelength emission determined in this chapter, we will then be able to demonstrate the control capabilities of our feedback approach.

# 4 AMPLITUDE CONTROL VIA PHASE-CONTROLLED OPTICAL FEEDBACK

In this chapter, we use the optical feedback phase to control the laser emission of our dual-wavelength lasers. In the first section 4.1, we discuss the implementation of the optical feedback sections onto the PIC. With the knowledge of the expected wavelength for each laser concept from the simulations, we implement a customized feedback section for each laser. In the second section 4.2, we present the experimental results on the amplitude control for each laser concept, using the operation points for the dual-wavelength lasers determined in the previous chapter. In the next section 4.3, we study the impact of a varying laser and feedback currents to evaluate control potential when deviating from an equal-power point and map the maximal operating range of our control approach. In the last section 4.4, we discuss the switching speed between the different wavelengths which are competitive to other solutions implemented on this MPW platform.

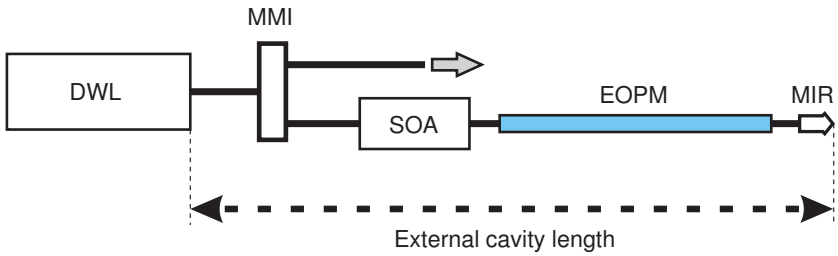


Figure 4.1: Schematic of the implemented feedback section. The emission of the dual-wavelength laser is split into a measurement and feedback path. The light in the feedback section passes an SOA to control the feedback strength, an EOPM to control the feedback phase and is reflected back towards the laser using an MIR.

## 4.1 FEEDBACK CAVITY DESIGN ON PIC

For each laser, an optical feedback section with a specific external cavity length is monolithically integrated, schematically shown in Fig. 4.1. The output from each laser concept, either from the 2-port MMI splitter for concepts I & II or from the DBR output for concepts III & IV, is guided into an 2x2 MMI splitter with a splitting ratio of 85:15. The 15 % are guided to the feedback section, passing an SOA and an EOPM before being reflected back to the laser cavity via an 1-port MIR. The SOA has a length of 300 µm, identical for all lasers, and allows to control the feedback strength. The EOPM has a length of 1200 µm, also identical for all lasers, and allows to achieve a feedback delay of $2\pi$ for a design voltage of 8 V which results from the light passing the EOPM twice. The EOPM sections have a breakdown voltage above 15 V. With the 1200 µm length used here, this upper limit correspond to feedback phase shift of $4\pi$ (two times $2\pi$ for one round trip). Each of these active components is separated by an isolation section, ranging between 30 µm and 75 µm, depending on the neighbouring components, to avoid any cross-talks. Then, a 1-port MIR is used to reflect the light back towards the laser cavity. Accumulating the splitting ratios and reflectivities for all components results to about 1.5 % of the light being send back towards the laser cavity. This is valid when assuming no losses of the light for the round trip and transparency of the SOA. As the reflectivities of the outcoupling mirrors differ for each laser concept, the actual amount of feedback entering the laser cavity varies. With a reflectivity of 50 % for the MIR, about 0.8 % is expected to be coupled back into the laser cavities of concept I & II while about 0.6 % is expected to be coupled back for laser concept III with a $DBR_3$ reflectivity of 58 %. Laser concept IV is rather special because of the DBR transparencies to each others wavelengths. This allows the optical feedback to fully enter the laser cavity via the transparent DBR and to about 4 % via the reflective DBR. Together with the 1x2 MMI splitter to merge the laser beams in this laser, about 0.4 % are expected to be coupled into the laser cavity.

An unknown factor is the required current for the feedback SOA to reach transparency. Due to the gain spectrum of the SOA, this characteristic is wavelength dependent and cannot be easily estimated from our available data. Dedicated test structures need to be implemented in a future design to estimate it. This is, in fact, quite important in our case:

Below transparency, the SOA acts as an attenuator while it amplifies the feedback above transparency.

As each laser is expected to emit on specific wavelengths, their feedback cavities have to be adapted in length individually. To achieve this, the waveguide between the EOPM section and the 1-port MIR is implemented with different lengths. To calculate the corresponding feedback cavity length, the spectral separation of the wavelengths has to be used to calculate the beat length $L_{beat} = \frac{\lambda_1 \cdot \lambda_2}{n \cdot (\lambda_1 - \lambda_2)}$ for $\lambda_1 > \lambda_2$ with $n$ being the refractive index. To obtain the desired relative phase shift of $\pi$ after a full round trip in the feedback cavity, a delay of half the length $L_{beat}$ is required. This length can be extended by a number $m$ of full cycles of the beat length to accommodate for additional components to be placed inside the cavity and it follows:

$$L_{delay} = (m + 0.5) \cdot L_{beat} \tag{4.1}$$

$m$ should be chosen to be minimal to improve robustness against high optical feedback strengths as discussed in section 1.5. To obtain the length of the physical feedback cavity, $L_{delay}$ needs to be divided by a factor of two to obtain the implemented lengths stated in Tab. 3.2 on page 47, ranging from 2400 µm to 4850 µm. For laser II, two identical lasers where implemented together with two different feedback cavity lengths to study the influence of much larger delay lengths. All feedback lengths are expected to be within the short cavity regime, thus, reducing the risk of potential dynamical behaviour to a minimum. The second output of the MMI with a transmission of 85 % is guided to the edge of the PIC to couple the light out for measurements. To avoid reflections from the edge of the PIC, an angled facet of 7 ° is implemented together with an anti-reflection coating to reduce the reflections below -40 dB. This is much lower than the expected feedback strength from our feedback section and should therefore not influence our control approach.

## 4.2 IMPACT OF TUNING THE OPTICAL FEEDBACK DELAY

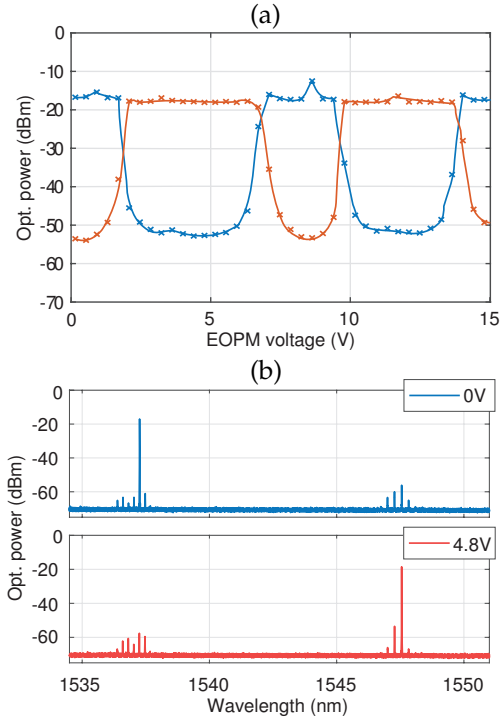


Figure 4.2: Spectral evolution of the wavelengths for laser II when the EOPM voltage is tuned in (a), exhibiting switches and equal power points in the transition. In (b), the optical spectra for 0 V and 4.8 V.

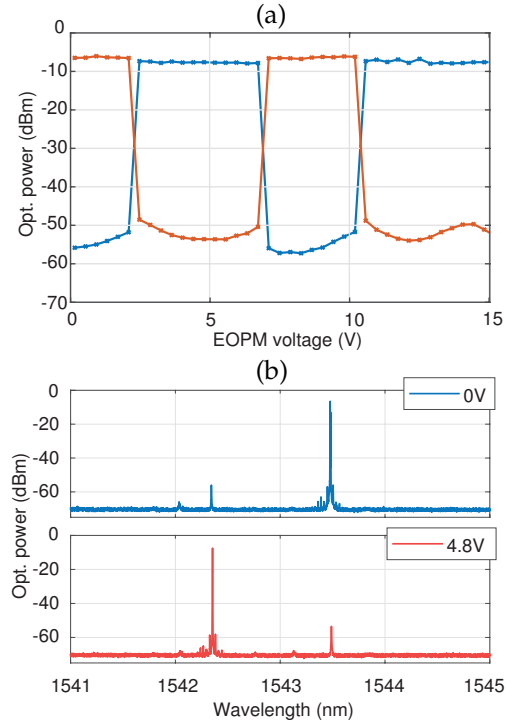


Figure 4.3: Spectral evolution of the wavelengths for laser III when the EOPM voltage is tuned in (a), exhibiting sudden switches. In (b), the optical spectra at 0 V and 4.8 V.

In the following, we apply optical feedback to our lasers at the operating points leading to dual-wavelength emission, identified in chapter 3. For the concept I with the LI curve presented in chapter 3, no feedback could be applied as the EOPM had a short-circuit. However, we implemented an extended version of this concept with additional boosters to achieve a dual-wavelength emission in lasers based on concept I. We will present these results in chapter 5 due to their complex control.

Applying feedback and tuning the EOPM-voltage, i.e. tuning the optical feedback phase, we obtained the spectrally resolved evolution of each wavelength for concept II & III shown in Fig. 4.2 (a) and 4.3 (a), respectively. These lasers exhibited the highest extinction ratios achieved for a 10 nm & 1 nm wavelength separation throughout all PICs. Increasing the EOPM voltage up to 15 V for both lasers leads to repetitive cycles with power exchanges corresponding to a total feedback delay of $4\pi$.

For laser II, the PIC (C) was used as it showed the highest extinction ratios, in some other PICs side modes appeared which limited the extinction ratios. This issue will be

discussed in chapter 5. An extinction ratio of up to 38.6 dB has been achieved as shown in Fig. 4.2 (a). The two wavelengths are shown in panel (b) for 0 V & 4.8 V. Setting the EOPM voltage precisely to the wavelength transition points allows to balance their optical output powers to achieve a simultaneous dual-wavelength emission. To obtain these results, a feedback current of 12 mA has been applied. This laser concept demonstrated to be quite robust and showed similar results across other PICs. However, the overall performance varies as undesired side modes appeared in some cases and limited the performance severely as will be discussed in detail in chapter 5.

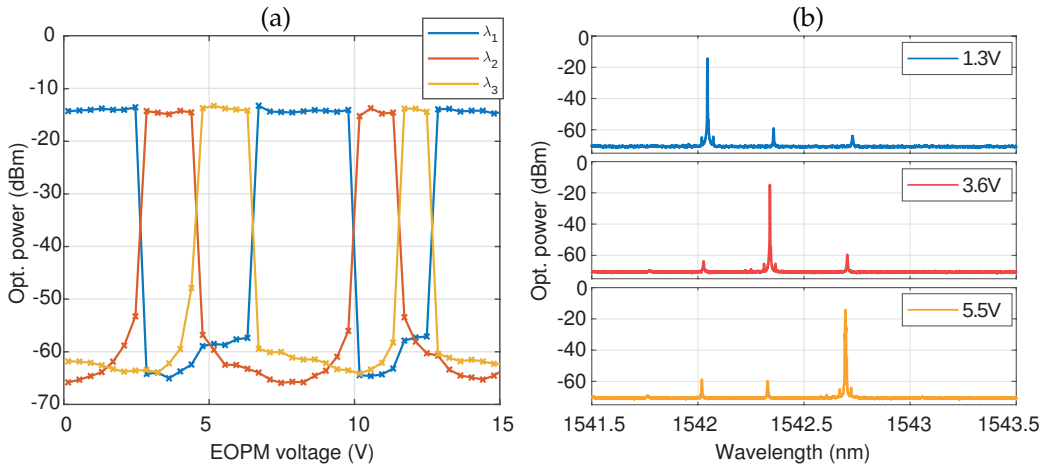


Figure 4.4: In (a), sequential selection of three wavelengths by a tuning of the feedback phase. In (b), the corresponding optical spectra for the individually selected wavelengths.

For laser III, the PIC (C) was used as it exhibited the highest optical power and the highest suppression ratio, however, PIC (A) & (B) showed almost identical results. For this concept, we obtained even higher extinction ration of up to 50.5 dB as displayed in Fig. 4.3 (a). It shows the spectrally resolved evolution for each wavelength, exhibiting multiple sudden switches between the wavelengths. As already observed for the solitary laser, it is not possible to achieve a simultaneous emission on both wavelengths in this laser, even using the phase controlled optical feedback. We also found a hysteresis cycle of about 0.6 V when increasing and decreasing the EOPM voltage. However, the hysteresis as well as the sudden switches are related to the laser itself and not to the feedback control approach. The optical spectra for voltages of 0 V and 4.8 V are shown in (b). Beyond 14 V, we observe a saturation as $\lambda_1$ can not be triggered any more at these high voltages. A feedback current of 6.9 mA has been applied to achieve this result. Furthermore, as the DBRs can be individually tuned, we were also able to identify an operation point exhibiting three distinct modes which can be individually selected by tuning the feedback phase. Their spectral evolution is shown in Fig. 4.4 (a) and exhibits a sequential selection of the three modes when the feedback phase is tuned. The emission of $\lambda_1$, $\lambda_2$ and $\lambda_3$ are shown in (b) in blue, red and yellow, respectively. We found the same behaviour with the possibility to select two or three modes and sequentially select them also in PIC (B), suggesting this behaviour to be a laser specific characteristic. To obtain these results, the

operation point of the laser was changed to an injection current of 60.1 mA, together with a higher feedback current of 10.2 mA and a $DBR_3$ current of 6 mA to detune the DBRs such that three neighbouring modes are involved in the emission.

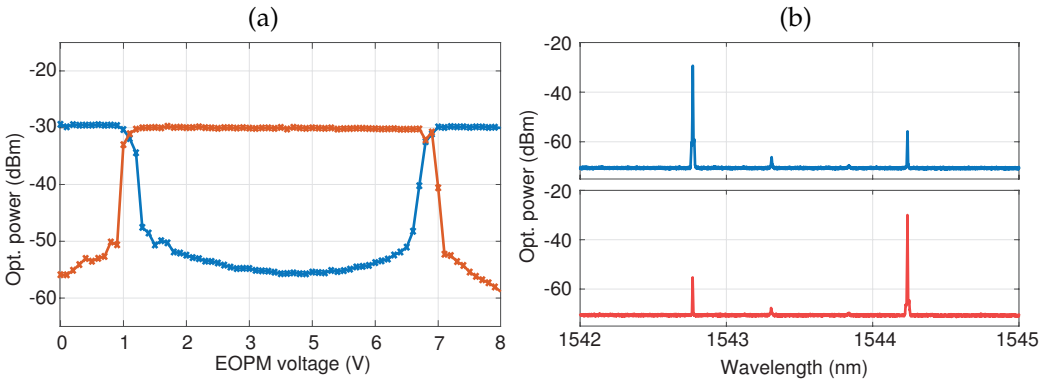


Figure 4.5: Spectral evolution of the wavelength when changing the feedback phase for concept IV in (a). The optical spectra is shown in (d) for 0 V and 5 V.

For Laser IV, the PIC (E) was used, although other lasers showed even higher extinction ratios (about 5 dB), this laser showed to emit only at two wavelengths for any given laser or feedback current. For this reason, it will be used also for further studies in the following section and is therefore presented here. Without optical feedback, the equal-power point is around 65 mA, however, applying feedback to this operating point resulted in the sole emission of one wavelength and a tuning of the optical feedback phase had no impact. Only an increase of the laser current up to 71.5 mA allowed to obtain a switch and is shown in Fig. 4.5 (a) with an extinction ratio of up to 29 dB. The EOPM voltage was limited to 8 V, corresponding to a phase shift of $2\pi$ which allows for a full switching cycle between the wavelengths and avoids excessive load. In (b), the two wavelengths are shown with a spectral separation of 1.5 nm without the appearance of any side modes. The origin of the required increase in injection current to obtain the switch is not fully understood yet. This laser also exhibits a very low output power, but is the only laser exhibiting a full switch between the wavelengths as well as an equal optical power when the injection current and the feedback phase are tuned. Therefore, it will be used to study variations in the laser and injection current in the following sections.

To conclude, we found deviations in the spectral separation of at least 10 % in all of our lasers. Nevertheless, we were able to demonstrate high extinction ratios for the presented concept. This is a good indication of the robustness of the control approach as it shows a relatively low demand on precise relative phase shifts between the wavelengths. In the simulations discussed in chapter 2, we identified a relative phase shift of $\pi$ between two wavelengths to be optimal to transition between the points $(\phi_1, \phi_2) = (0, \pi) \rightarrow (\pi, 0)$. However, also suboptimal relative phase shifts allow for a full switch. They are represented by diagonal transitions, parallel to the arrow shown in Fig. 2.5 on page 24, and result from a mismatch of the spectral separations to the feedback cavity lengths.

Nevertheless, we achieve a good performances for each laser concept despite these deviations in the spectral separations. Furthermore, we found that the EOPM voltage allows for large margins as a particular wavelength is selected for a relatively large range of voltages. It confirms that a precise setting of the feedback phase is not crucial.

To apply the optical feedback for the different concepts, we increased the feedback current until we achieved a full suppression of one wavelength. For laser concepts II & III, the starting point for this suppression was around 5 mA, below this feedback current, no influence on the optical spectra has been found. For laser concept IV, a lower feedback current of 3 mA already showed an impact due to the mutual DBR transparencies. When tuning the EOPM voltage, the concepts II & IV showed smooth transitions between the wavelengths, allowing for an easy adjustment of an equal optical power point while the laser concept III exhibited sudden jumps between the wavelengths as well as a hysteresis cycle. Overall, lasers II & III showed the best performances with the highest extinction ratios and high optical power. For concept III, even a discrete tuning of three modes could be demonstrated. The operation of the solitary lasers I & IV is rather difficult whereas the feedback control also allowed for high extinction ratios in these lasers.

So far, we only applied the control approach to equal optical power points. In the following section, we analyse to which extend a control can be achieved when diverting from this point. We will use laser IV as the smooth and full transition between the wavelengths for the solitary laser as well as the contribution of only two wavelength without any side modes makes this laser an ideal candidate to conduct this experiment.

## 4.3 EXPLORING THE PARAMETER SPACE

All results presented so far have been carefully chosen to show the best performance to show the potential of our control approach. Here we explore the parameter space of the laser- and feedback-currents to study the operation range of the control approach. With this, we are able to evaluate the applicability of our approach to the entire operation range of the laser. The ideal case would be to determine one particular feedback strength which allows us to control the laser emission at any given laser current. In a first step, we fix the feedback strength and only vary the laser current as discussed in the following. In a second step, we will then vary both, the feedback strength and the laser current.

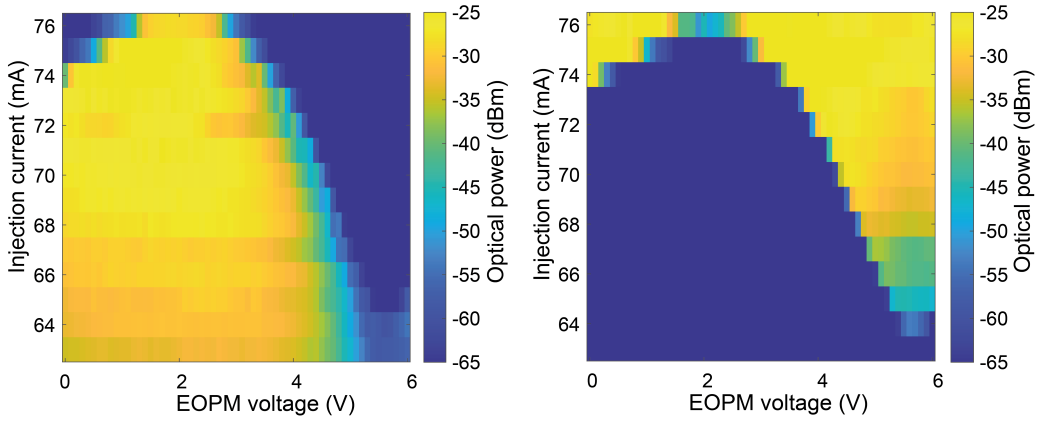


Figure 4.6: Mappings of switches between two wavelengths $\lambda_1$ & $\lambda_2$ in (a) & (b), respectively, as a function of the laser current and the EOPM voltage. The feedback strength if fixed. In (a), $\lambda_1$ is dominant at 63 mA while $\lambda_2$ is dominant at 76 mA for most EOPM voltages. In between, large regions where a switch between the wavelengths can be achieved by changes of the feedback phase.

Here we vary the laser current to study the impact on a fixed feedback strength. The goal is to determine the margins where a full control over the laser emission can still be achieved. Here we study laser IV as it is the only laser showing a smooth and full transition between the wavelengths with increasing laser current. Also only two wavelengths are contributing to the emission without any side modes which makes it an ideal choice for these studies. This work has also been done within the Master thesis of R. de Mey [68]. The experiment is based on the laser PIC (E), already discussed for Fig. 4.5 (b) where an injection current of 71.5 mA was used. Here, we change the current in a range between 63 mA and 76 mA to obtain the mappings shown in Fig. 4.6 (a) & (b), for $\lambda_1$ & $\lambda_2$, respectively. Starting at a laser current of 63 mA, we find a dominant emission of $\lambda_1$ and only at high EOPM voltages a partial switch to $\lambda_2$ occurs. At a laser current of 76 mA, we find $\lambda_2$ to be the dominant mode, emitting for most EOPM voltages. These two currents represent the extreme cases where only partial switches can be achieved, lower or higher laser currents result in the dominant emission of the particular wavelengths. In between these two currents, full switches can be achieved by changes of the EOPM voltage.

In the solitary laser without feedback, the transition between the wavelengths occurs within a range of 2 mA. This result shows, that applying our control approach allows to extend the operation range to a larger laser current range of 13 mA. Furthermore, these results were obtained with a fixed optical feedback strength, however, in the simulations we already discussed that a higher feedback strength can be used to increase the operating range in case partial switches are achieved and will be discussed in the following.

We study the maximal achievable control range over the laser emission by varying the optical feedback strength and the laser current to achieve the mappings shown in Fig. 4.7. The measurements have been obtained by sweeping the EOPM voltage for every combination of laser and feedback current. To present these mapping, we had to reduce the parameter space and merged the EOPM voltages to one figure of merit, describing if a switch has been achieved or not when the EOPM voltage is tuned.

To analyse this, we set two different thresholds, one corresponding to the wavelength being turned on and one for being turned off. To determine if a switch is achieved, each of the wavelengths has to trigger both of the thresholds when the EOPM voltage is tuned, i.e. it is either being turned on or off when the voltage is tuned. This procedure has been done with both wavelengths individually and a switch was only registered when both wavelengths exhibited a switch at the same EOPM voltages. A switch was considered when the wavelengths showed a power exchange of at least 10 dB.

To obtain the experimental results, we used an optical filter to select a wavelength and measured the optical power with a photo diode. This was a fast measurement technique, however, required the sequential measurements of both wavelength individually. Comparing the measurement times to using an OSA for each parameter setting, would have result in a ten-fold measurement time. Nevertheless, we still encountered a drop in the fibre coupled optical power over time, hence, the obtained results do not allow to compare absolute values in amplitude. Due to the use of the photo diode, we also did not obtain any indication on the influence of a multi-mode emission affecting the extinction ratios. Furthermore, we also discard information on which wavelength is emitting at which EOPM voltage and even if dynamical behaviour occurs and only focus on the question if a switch between the wavelengths can be achieved or not.

We mapped the individual operation ranges of laser concept I , II and IV, shown in Fig. 4.7. The results are represented by white and black markers, representing no switches and full switches, repectively.

In (a), the mapping for laser IV, already discussed in section 4.6, is shown. The PIC (E) is used which exhibits only two modes was therefore the ideal choice to perform these measurements. We found that the operation range can be extended until the maximal laser current when the feedback current is also increased. With increasing laser current, the required feedback has also to be increased to maintain a full control. This is connected to the shift of the gain spectrum with increasing laser current. This shows that the feedback strength enables a much larger operation range in which the laser emission can be controlled.

In Fig. 4.7 (b), the mapping for laser I of PIC (C) and in (c) & (d) the mappings for two laser concepts II are shown for PIC (B) & (C), respectively. Large areas exhibiting a full switch are found in all mappings. A minimal amount of feedback has to be applied to achieve switching, ranging from 5 mA to 10 mA. For large laser and feedback currents

areas without switches are also visible where one wavelength is dominant. Different white areas can also correspond to different wavelengths being dominant, in particular above and below the black areas in (a) and (c). For both lasers II with different feedback lengths, we were able to obtain large areas exhibiting full switches.

The areas for large laser and feedback currents in panel (b) & (d) exhibiting alternating results, i.e. multiple switches and no switches next to each other, could be related to a multi modes emission as this severely limits the extinction ratios and might therefore not be sufficiently reduced to trigger the 10 dB detection threshold. However, this is a laser specific characteristic and requires further improvements of the lasers itself. With an improved dual-wavelength laser, the mapping suggests that a full control of the emission could be possible for large laser and feedback currents. This demonstrates that the feedback based control approach is quite versatile and can be adapted to a variety of different laser operation points.

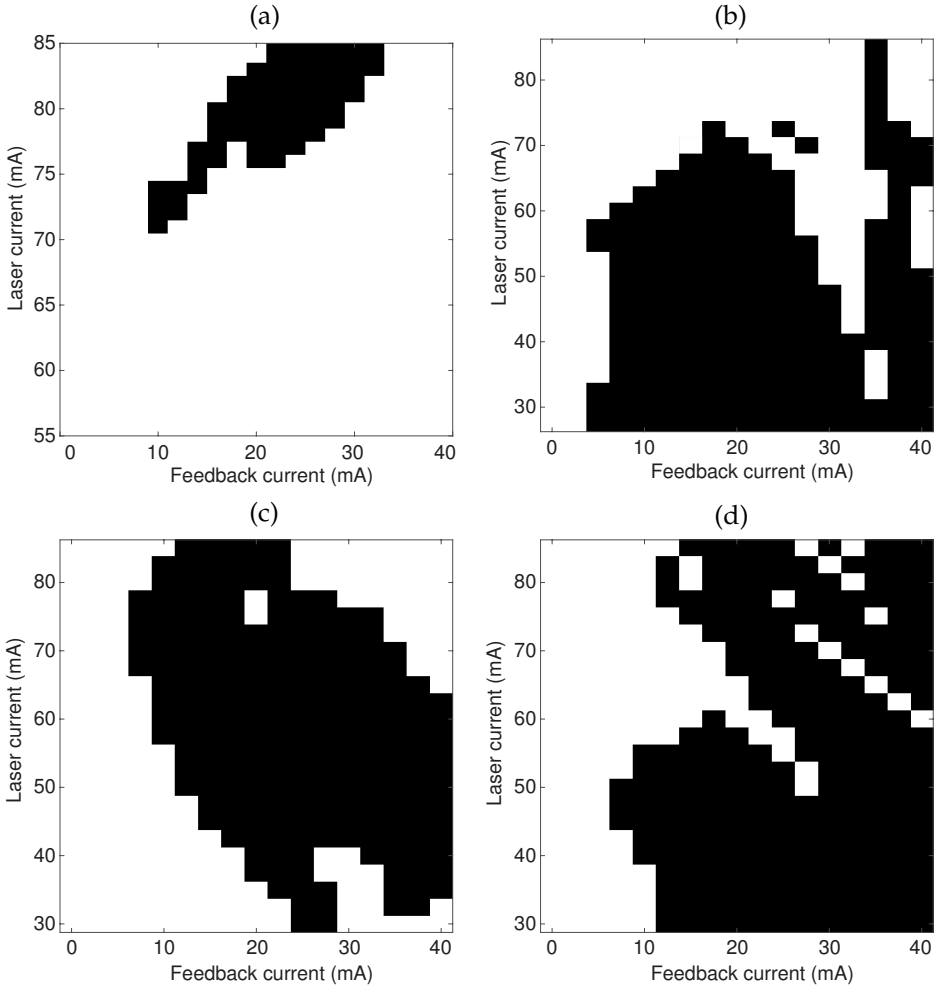


Figure 4.7: Mappings showing the switching potential for varying laser and feedback current. Black markers represent full switches and white marker represent no switches. In (a), laser IV is shown, in (b) laser I and in (c) & (d), laser II is shown. Adapting both parameters allows to achieve a full control over the laser emission for almost all laser currents.

## 4.4 SWITCHING SPEED

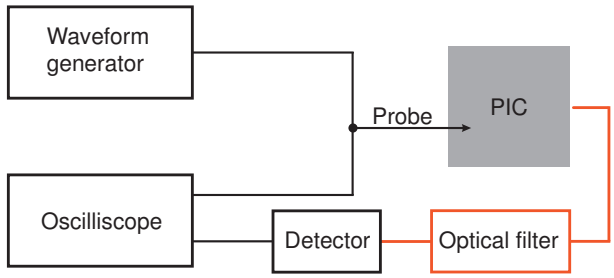


Figure 4.8: Schematic representation of the setup to measure the switching speed. A square wave voltage is applied to the EOPM on the PIC and also serves as the trigger signal for the oscilloscope. The emitted light is coupled into a fibre, one wavelengths is selected at a time using an optical filter and then measured via a detector and the oscilloscope.

To study the switching speed between two wavelengths, we used the experimental setup shown in Fig. 4.8. It consists of an arbitrary-waveform-generator (Tektronix AWG520) to generate a step function with voltages corresponding to the EOPM voltages required to select the specific modes. The implemented EOPM is not optimized for RF operation as no GSG pads have been implemented, we therefore use a standard DC probe to contact the EOPM. The emitted light is coupled into the lensed fibre, indicated by red lines, an optical bandpass filter (EXFO XTM-50) selects a specific wavelength for measurements using an oscilloscope (CSA 7404) with an build in photo-diode. The difference in signal time delay between the trigger and the signal was determined to be 36.95 ns and is corrected in each experimental result.

We used the concept II on PIC (C), already discussed for Fig. 4.2 and applied a step function with a peak-to-peak amplitude of 3.5 V and an offset of 1.75 V to the EOPM. The experimental results are shown in Fig. 4.9 for the rising and falling trigger edge in (a) & (b), respectively. The EOPM signal serves as the trigger signal and is shown in black, the two wavelengths $\lambda_1$ & $\lambda_2$ are shown in red and blue, respectively. We find response times of around 3 - 4 ns after the trigger signal and complete switches around 5 - 7.5 ns. The vertical black dotted line indicates the trigger signal as the reference, and the coloured dotted lines indicate the thresholds of 10 % and 90 % for the wavelengths being turned off and on, respectively. The amplitudes have been normalized to allow an easy comparison of the high EOPM voltage to the low detector signal with a few tens of milli-volts. The shorter wavelength $\lambda_2$ seems to react 1 - 2 ns faster for both, the rising and falling edge. The transition time itself is in the range of 2 - 3 ns and is limited by the transition time of the applied EOPM voltage step itself. Exchanging the arbitrary-waveform-generator with another generator (HP8131A) capable of higher frequencies of up to 500 MHz allowed for an improvement in this limitation. The experimental results achieved are shown in Fig. 4.9 (c) & (d), exhibiting a faster transition time visible for the trigger signal. The rise- and fall-times of the EOPM signal are in a range of 1 ns which also improves the response times of both wavelengths by about 1 ns. The transition times show also an improvement and are with about 3.5 ns, visible for $\lambda_1$ in blue

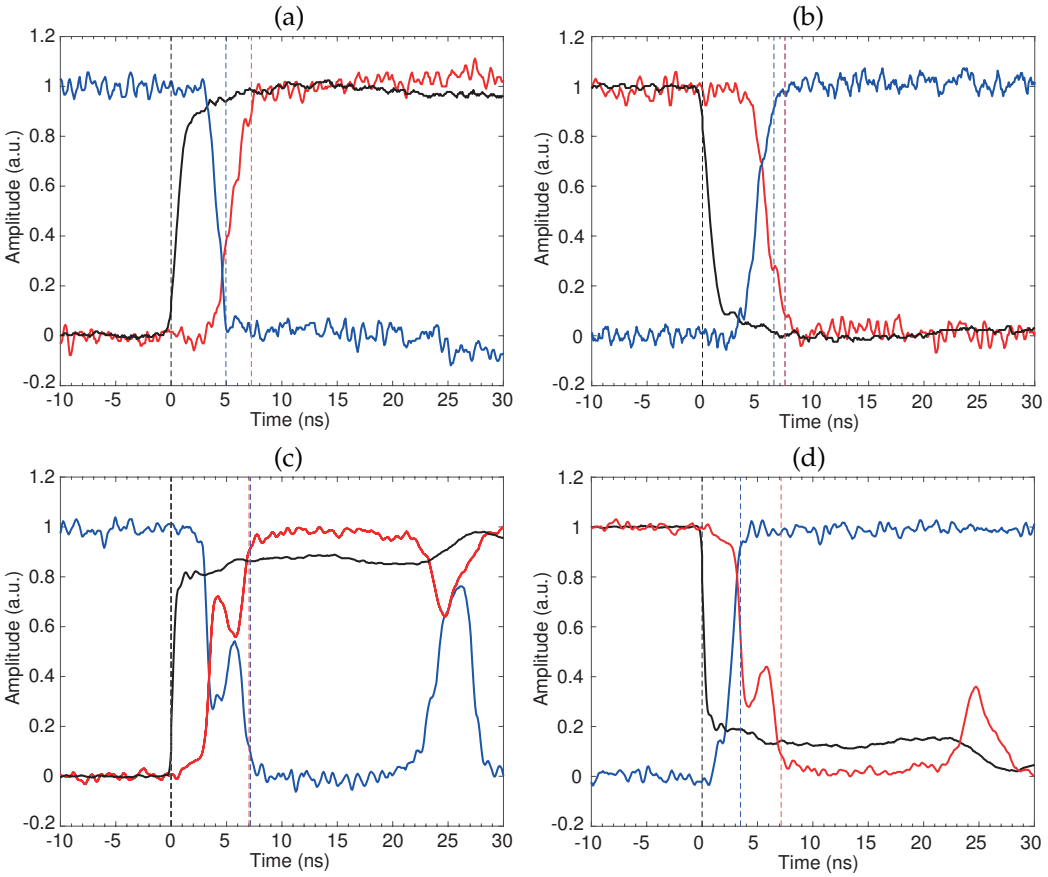


Figure 4.9: Switching speed measurements for laser II. In black the trigger signal serving as a reference, in blue the mode being turned off and in red the mode being turned on. In (a) & (c), for the rising trigger edge and in (b) & (d) the falling trigger edge. In (c) & (d), the laser and operation points are identical to (a) & (b), however with a waveform generator capable of higher frequencies which results in faster response and switching times. However, dynamics appear which show the current limitation of the non optimized setup for RF operation.

in (d), the fastest we obtained. However, the arbitrary-waveform-generator itself showed a transient behaviour and reached its desired amplitude only much later which also introduced a corresponding laser response. The varying EOPM voltage also influences feedback phase and consequently changes the operation voltage which results in undesired power exchanges visible around 6 ns and 25 ns. This represents a current technical limitation and prevents even faster transition times. As the electro-optic effect used in EOPM is capable of much higher frequencies, a dedicated RF-setup with GSG probes could prevent these modulations to achieve maximal performance. Thorough studies on the impact of the laser current or the optical feedback strength on the switching times are currently out of reach as carefully chosen operation points have been used for these measurements. Either undesired modes are triggered or dynamical behaviour appears,

both hampering the performance. This also limits our interpretation with respect to the presented simulations. The limitations and potential improvements on this will be discussed in the following chapter 5.

## 4.5 CONCLUSION

In this chapter, we implemented feedback cavities to every laser with an SOA to control the feedback strength and an EOPM to control the feedback phase. We then applied our control approach to the different lasers operated at the equal power points identified in the laser chapter. We were able to demonstrated switching ratios of up to 50 dB as well as equal power points by only tuning the feedback phase. To investigate the operation range of our control approach, we studied different laser currents. We found that the feedback phase allows to control the laser emission even for laser currents deviating from the equal power points. We explored also parameter space of laser currents and feedback strengths to extend the operation range to a maximum. We found that our control approach can be applied to a large range of laser currents by adapting the feedback strength. This shows the flexibility of our control approach which is not limited to single operation points. Finally, we investigated the switching times between the wavelengths and found values of down to 3.5 ns. While conducting the experiments presented in the last two chapters, we encountered several limitations in the laser operation. This restricted several experiments and did not allow to study important details. In the following chapter, we will discuss these issues in detail, point out weaknesses in the laser designs and propose improved structures for a next MPW participation.

# 5 LIMITATIONS OF PERFORMANCES

In this chapter, we will highlight the current limitations of our lasers as well as the control approach and propose improvements. In particular, we identified a limited tuning of the spectral wavelength separation or a low wavelength selectivity of the DBRs to possibly result in a multi-mode emission which limits the flexibility of our lasers. This hinders our study of the control approach and restricts the operation points to only a few sets of parameters. Hence, we were not able to answer two major questions to assess the robustness of the control approach so far: First, how the extinction ratio behaves with varying relative-phase shifts and, second, how the maximal achievable extinction ratio scales for different spectral separations. We followed three different approaches to gain further insights into this issue. As the implemented feedback section on our PICs are fixed, we used two external setups, either using a quantum-dot laser or an external cavity diode laser, together with a freely tunable external feedback delay. The third approach is based on a DBR tuning to change the spectral separation on PIC. Unfortunately, different hurdles and limitation lead to a limited outcome in all three experiments as will be discussed in the first section 5.1. In the next section 5.2, we will discuss the variability of our results from different wafers and PICs. After this, we will discuss the poor performance of concept I and present an extended version of the laser to overcome the present limitations. Then, we discuss the impact of a multi-mode emission on the extinction ratio as well as the transient behaviour when switching between two wavelengths. Next, we highlight potential improvements for our integrated laser concepts. The second generation of our PIC design showed convincing results for most of our laser concepts. However, besides the best lasers with good results presented in the chapter 4, it also revealed drawbacks and design flaws which we will addressed in section 5.3. Our goal is to identify the most crucial parameters which can lead to substantial improvements in their performance and to a successful third PIC generation.

## 5.1 ROBUSTNESS AGAINST RELATIVE PHASE SHIFT VARIATIONS

Although convincing performances were achieved in our PICs, the fixed wavelengths and fixed feedback cavities prevent us from studying the robustness of the control approach against variations in the spectral separation and against varying phase-shifts. Hence, two major questions remain to be answered:

- Firstly, how does the suppression ratio scale when the wavelength separation is changed. Extinction ratios of up to 50 dB were achieved for a 1 nm wavelength separation but only 35 dB for a 10 nm separation. Studying the extinction ratios with varying wavelength separations could reveal potential limitations and could allow to draw connections between the wavelength separation and the mode coupling.
- The second open question is, how the suppression ratio scales for different relative-phase shifts between the two wavelengths. The lower extinction ratios for larger wavelength separation could also originate from unsuitable feedback cavity lengths. A larger wavelength separation results in a higher beat frequency and consequently to a shorter distance between two nodes of the beat signal. Hence, the margins for an implementation for an ideal feedback length are quite small and might lead to suboptimal relative phase shifts. This could hamper the gain modulation and lead to lower extinction ratios.

To gain more insights, we considered the use of either a quantum-dot laser and an external cavity laser to achieve the required level of flexibility in terms of wavelength separation and feedback delay. The quantum-dot laser used, was expected to emit simultaneously on two wavelength, separated by 70 nm and exhibiting single-mode emission. The fixed wavelengths would have allowed us to study varying feedback delays and the impact on the extinction ratios. Unfortunately, the available laser source showed no dual-state laser emission and prevented detailed studies. Nevertheless, two individual modes could be identified which showed a very limited extinction ratio when the feedback phase was tuned as will be presented in the following. Another approach uses an external cavity diode laser allowing to individually tune both, the wavelength separation as well as the feedback delay. However, the freedom in tunability comes with mechanical and thermal instabilities and were too demanding to control. Each adjustment only allowed for single measurements at a time before losing the alignment and prevented thorough studies with this setup. However, when encapsulated in a thermal and mechanical stabilized environment, this setup might offer promising control and tuning capabilities as high extinction ratios have been obtained. A third approach is based on a detuning of the spectral separation between the wavelengths of our dual-wavelength lasers. Tuning the wavelength separation also tunes the beat-frequency which results in a different feedback phase and could have allowed to study the impact on the extinction ratio. Unfortunately, limited DBR tuning capabilities prevented these measurements.

### 5.1.1 *Discrete devices: Quantum-Dot laser*

Quantum-dot lasers are capable of emitting simultaneously from two different energy states due to their spatial confinement of the active region. We have studied a 1 mm

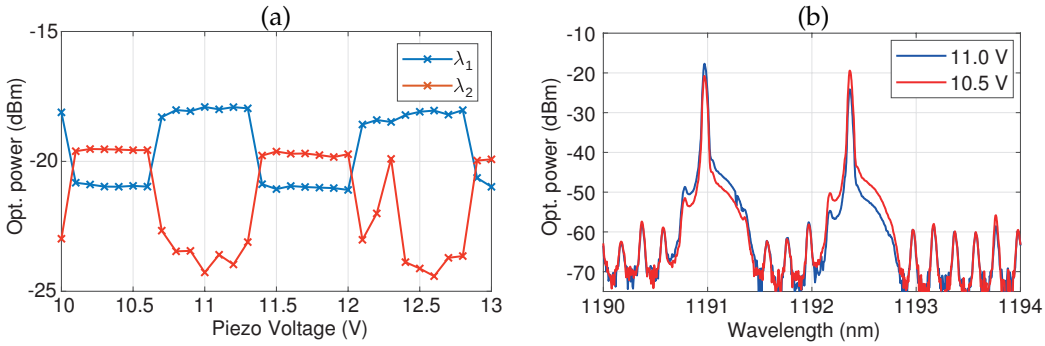


Figure 5.1: Experimental results using an quantum-dot laser with external broadband feedback. In (a), power exchanges between the spectrally resolved modes when the piezo-mirror, i.e. the feedback phase, is tuned. In (b), the optical spectra showing the low changes in amplitude for 10.5 V and 11 V.

long two-section quantum-dot distributed feedback laser shown to emit simultaneously on two different wavelengths around 1200 nm with a 70 nm separation in [42]. The grating is coupled to the excited-state of the laser and provides a single-mode emission. Via an asymmetric bias of the two sections, also single mode emission on the ground-state could be demonstrated. This would have been the ideal candidate to conduct our studies, unfortunately, the laser degraded to a state where only excited-state emission was achieved. Neither external broadband feedback, a wavelength selective grating feedback nor asymmetric biasing was sufficient to force laser emission on the ground-state. Also low temperatures down to -15 °C, which have shown to trigger the ground-state emission before [69], failed to achieve the desired dual-wavelength emission.

Nevertheless, we were able to identify two wavelengths within the excited-state, spectrally separated by 1.5 nm at a temperature of 20 °C. Applying a broadband optical feedback and tuning the feedback phase with a piezoelectric actuator allowed to achieve limited power exchange of 3-4 dB. The spectral evolution as a function of the piezo-voltage for each mode are shown in Fig. 5.1 (a). The corresponding spectra for a piezo-voltage of 10 V and 11.5 V are shown in (b). The optical feedback was adjusted by applying a sinusoidal modulation to the piezo actuator which results in a repetitive tuning of the losses and subsequently in a power modulation of the laser which allowed to optimize the alignment towards the highest modulations. However, the broadband optical feedback trigged multiple undesired side modes, which required a limitation of the feedback strength to about 0.1 % in front of the laser facet and possibly prevented higher extinction ratios. A quantum-dot laser with a double-layer Bragg grating embedded into the laser as proposed in [38] could be a promising solution to trigger an emission on both states simultaneously. However, due to the limitations of this laser and the lack in availability of other dual-state emitting quantum-dot lasers, we did not further follow up these investigations and left them for future work. This work was done in collaboration with the group of Priv. Doz. Stefan Breuer at the Technische Universität Darmstadt, Germany.

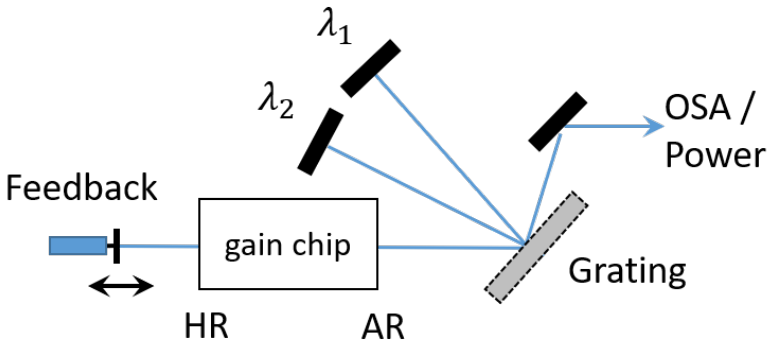


Figure 5.2: Schematic representation of the external cavity diode laser. The laser cavity is formed by the high-reflective coated side of the gain chip together with the two mirrors for the wavelength selection. A grating splits up the spectrum where the zeroth order is used for measurements. The optical feedback is applied at the high-reflective coated side of the gain chip.

### 5.1.2 *External cavity diode laser*

An external cavity diode laser, as schematically shown in Fig. 5.2, allows to control each wavelength individually to achieve any desired wavelength separation. Together with a variable feedback delay, the dependency of the extinction ratios at different spectral separation as well as for different relative phase shifts can be studied. To set up the laser system, we used a double Littmann-Metcalf configuration, comprising of a grating to split up the spectrum and two mirrors to individually control each wavelength. All components are commercially available with the laser having a high-reflection coating of 90 % on one side and an anti-reflection coating of 0.005 % on the other. The laser cavity is formed by this high-reflection coated side of the gain chip and the mirrors defining the emitting wavelengths $\lambda_1$ & $\lambda_2$. The gain chip is based on a quantum-well structure with a gain width of about 150 nm. The high-reflective output is used to apply the optical feedback while the zeroth order of the grating is used for measurements together with an optical isolator (not shown).

The first challenge has been the adjustment of the individual wavelengths to emit on single modes. The arrangement and the required space for each component results in a relatively long laser cavity and subsequently a small mode separation. Selecting individual modes with the broadband mirrors was therefore challenging. An additional issue was to obtain an equal optical power between the wavelengths and has been achieved using neutral density filters in front of each mirror (not shown). Another challenge is related to the optical feedback strength which has also been controlled by a neutral density filter. However, to study the relative-phase shifts between the modes, the piezo actuator has to be moved along the optical axis of the laser beam. This requires a high level of adjustment to avoid varying feedback strengths. The alignment procedure revealed that mechanical or thermal factors result in either in a multi-mode emission or in a single-wavelength emission after a short amount of time. Nevertheless, we were able to obtain the results shown in Fig. 5.3. In (a), the spectral evolution of the individual wavelengths

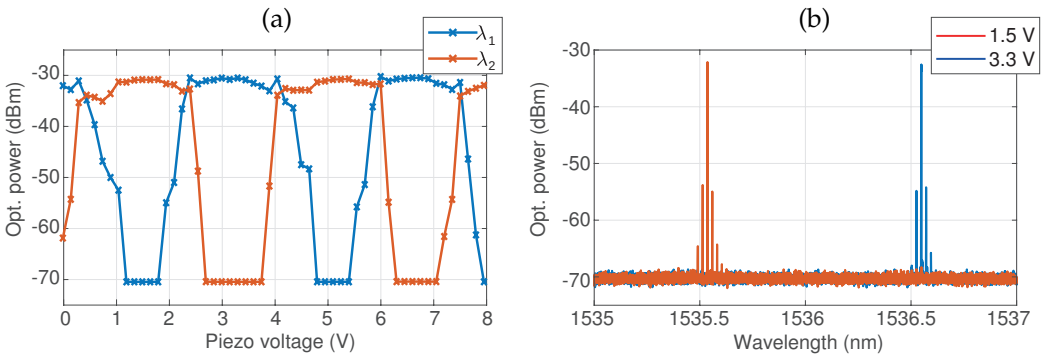


Figure 5.3: Experimental results for the external cavity diode laser. In (a), the spectral evolution of $\lambda_1$ & $\lambda_2$ is shown when the feedback delay is tuned. In (b), the optical spectra are shown at 1.5 V & 3.3 V for $\lambda_1$ & $\lambda_2$, respectively.

as a function of the feedback delay and in (b), the optical spectra for piezo voltages of 1.5 V and 3.0 V are shown. With our control approach, we achieved an extinction ratio of 40 dB and completely suppressed the emission of each wavelength.

After the laser lost its alignment, a thorough readjustment was required, making the current laser setup not suitable for any systematic measurements. Either time demanding or costly improvements of the setup can be considered for improvement. As already mentioned, an encapsulation into a thermally stabilized housing could overcome these limitations. Ideally together with individual mounting solutions for every component to obtain a very compact layout which would ease the selection of individual modes due to the larger mode separation. Controlling the mirrors via piezo-actuators would allow for a fully remote controlled laser with highest precision and stability. Another solution would the implementation of volume Bragg-gratings, but would come with a reduced flexibility for different wavelength separations. However, volume Bragg-grating with the required parameters for the selection of single modes are very costly and in the range of a MPW participation and are left for future investigations at this stage.

### 5.1.3 *Impact of DBR tuning on the spectral separation*

In chapter 3, the advantage of a DBR tuning to achieve a dual-wavelength emission or to reduce the number of emitting side modes has been discussed. Here the limited impact of the DBR tuning on the wavelength separation will be highlighted. We use laser II of PIC (C) with a feedback length of 4850 µm. We aim to detune the DBRs to study extinction ratios with varying relative-phase shifts. For this, we tune the wavelength separation and subsequently the beat-frequency. Detuning the spectral separation by about 0.3 nm is sufficient to tune the beat-frequency by one full period and allows to map the extinction ratios for different relative phase shifts. The exact tuning range depends on the length of the feedback cavity as this determines the number of beat-nodes. This approach can be used directly in the PIC: Tuning both DBRs could change the implemented wavelength separation in both directions by $\Delta\lambda \pm 1$ nm for 500 µm long DBRs. Moreover, this would

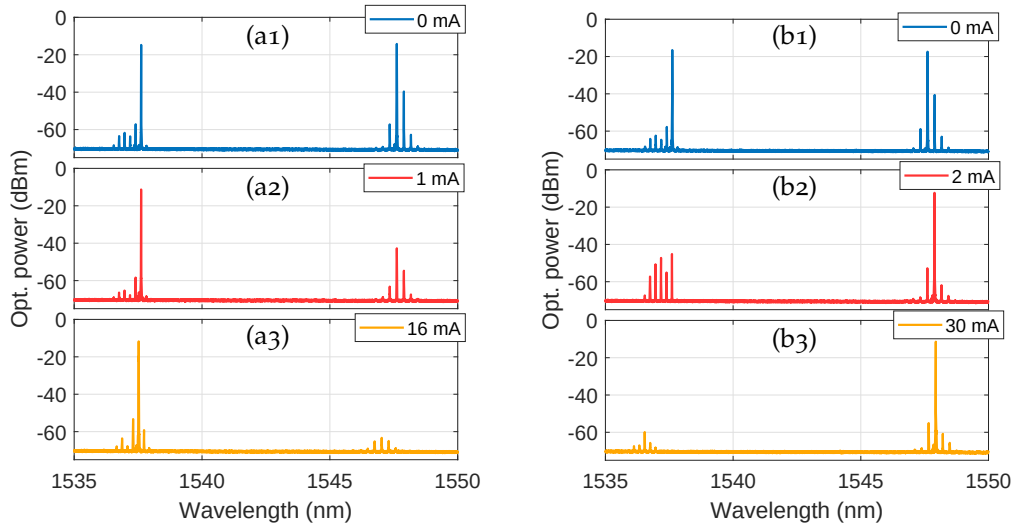


Figure 5.4: Limited tuning of the spectral separation between the two wavelength when the DBRs are tuned. In (a), a current of up to 16 mA applied to $DBR_1$ leads to a suppression of the corresponding wavelength while a current of 30 mA applied to $DBR_2$ leads to the same outcome in (b). Single-mode emission is obtained in both cases and results from the reduction in reflectivity when the DBRs are tuned.

provide a direct indication if the implemented feedback delays have the correct length or if they can be improved. If the implemented length is not optimal, a larger extinction ratio could be expected when detuning the spectral separation. Furthermore, it would also provide an indication of the required precision in length when implementing the feedback section on the PIC. Unfortunately, the peculiarities of our laser concepts did not allow to conduct this experiment.

To elaborate, we used laser concept II with an operating point exhibiting dual wavelength emission with equal optical powers as shown in the upper spectra of Fig. 5.4 (a1) & (b1). Both spectra are identical without any current applied to the DBRs and serve as the reference. In (a), only the $DBR_1$ was tuned up to a maximal current of 16 mA while in (b), only the $DBR_2$ was tuned to a current of 30 mA. With increasing DBR currents, the reflectivities of the DBRs are reduced such that only a single wavelength remains. Already at a current of 1 mA applied to $DBR_1$, the emission on the longer wavelength is suppressed by about 30 dB. At a current of 16 mA, the emission is suppressed by 50 dB. Similar results are obtained when tuning $DBR_2$ in (b), a suppression of about 30 dB are obtained at a current of 2 mA and about 45 dB are achieved at 30 mA. For a laser supposed to emit only on one single mode, the reduction in DBR reflectivity would potentially only affect the optical output power but represent no real limitation. Due to the coupled wavelengths in our laser concepts, the mode with the lowest losses takes over which consequently result in a single-wavelength emission. Although we find good results on the spectral shifts of the DBR wavelengths of 0.6 nm for the shorter $DBR_1$ and 1.1 nm for the longer $DBR_2$, the laser concept does not allow for a simultaneous dual-wavelength emission.

Nevertheless, it is possible to compensate for the suppressed wavelength by also tuning the second DBR. Tuning both DBRs results in a reduction in reflectivity for both of them and simultaneous dual-wavelength emission is maintained. In particular, the dual-wavelength emission for the spectrum shown in (a3) with 16 mA applied to $DBR_1$ can be restored by increasing the current of $DBR_2$ to about 15 mA. Although this results in a spectral shift for both DBRs to shorter wavelengths, it does not change the spectral separation significantly. Hence, applying DBR currents for the purpose of changing the spectral separation has been avoided as this is also adds heat to the system. The DBRs have only been tuned to either achieve a simultaneous dual-wavelength emission whenever a single-wavelength emission occurred, or to suppress the emission of undesired side modes as the bandwidth is reduced as well. About 8 mA would have been required to either tune $DBR_1$ or $DBR_2$ to achieve the required change in spectral separation of 0.3 nm. As this was not feasible in our laser concepts, we left these studies for future work.

## 5.2 LIMITATIONS OBSERVED

### 5.2.1 *Variability on different PICs*

We studied multiple lasers from five PICs, originating from three wafers. Four PICs (A-D) have been packaged originating from the locations J8 & B8 from two wafers. These locations are at about half the radius of the wafer and are considered as center cells. These four PICs showed good and reproducible results. Most lasers on these PICs, excluding laser I, showed a dual-wavelength emission and allowed a control of their emission via optical feedback. Although their performance varied, depending on DBR or laser currents, considering the limitations discussed, high extinction ratios and a control of up to 3 modes could be achieved across different PICs. Only the fifth PIC (E), located on position F11 on a third wafer, exhibited poor results. Although it is located in the center of the wafer, most lasers showed only single-wavelength emission or required optical feedback together with a tuning of the feedback phase to exhibit a dual-wavelength emission. This particular wafer was manufactured in a different run and might have suffered from large manufacturing tolerances as the overall performance was poor compared to the two other wafers.

### 5.2.2 *Achieving dual-wavelength emission in concept I*

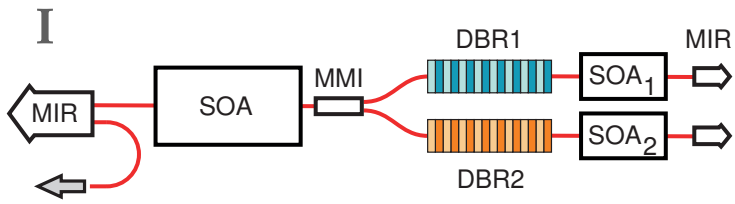


Figure 5.5: Laser concept I with additional SOA boosters to control the losses for each wavelength. The MIRs reflect the light back to the laser cavity. Due to the transparency to each other wavelength of the DBRs, a boost of $\lambda_1$ generated by $DBR_1$ is achieved by tuning $SOA_2$

For laser I on PIC (A), the solitary laser presented in chapter 3 was the only laser exhibiting an equal optical power. However, it showed no response to optical feedback or the feedback phase due to a broken EOPM section. We therefore used another laser based on concept I with additional boosters implemented behind the DBRs to control the losses for each wavelength as shown in Fig. 5.5, located on PIC (B). With the experience of the failing dual-wavelength lasers implemented on our first PICs, we included this concept as a backup solution in case we encounter similar issues in our improved concepts. The additional components make the operation of this laser more complex as it requires up to 5 currents, therefore we did not include this concept in our initial studies. MIRs behind the boosters reflect the light back towards the laser cavity. As the DBRs are transparent to each others wavelength, achieving emission on $\lambda_1$ generated by $DBR_1$ requires a boost of $SOA_2$ and vice versa. To obtain the LI curve shown in Fig. 5.6 (a), a current of 8.4 mA was applied to $SOA_2$. Multiple exchanges between the wavelengths were obtained with

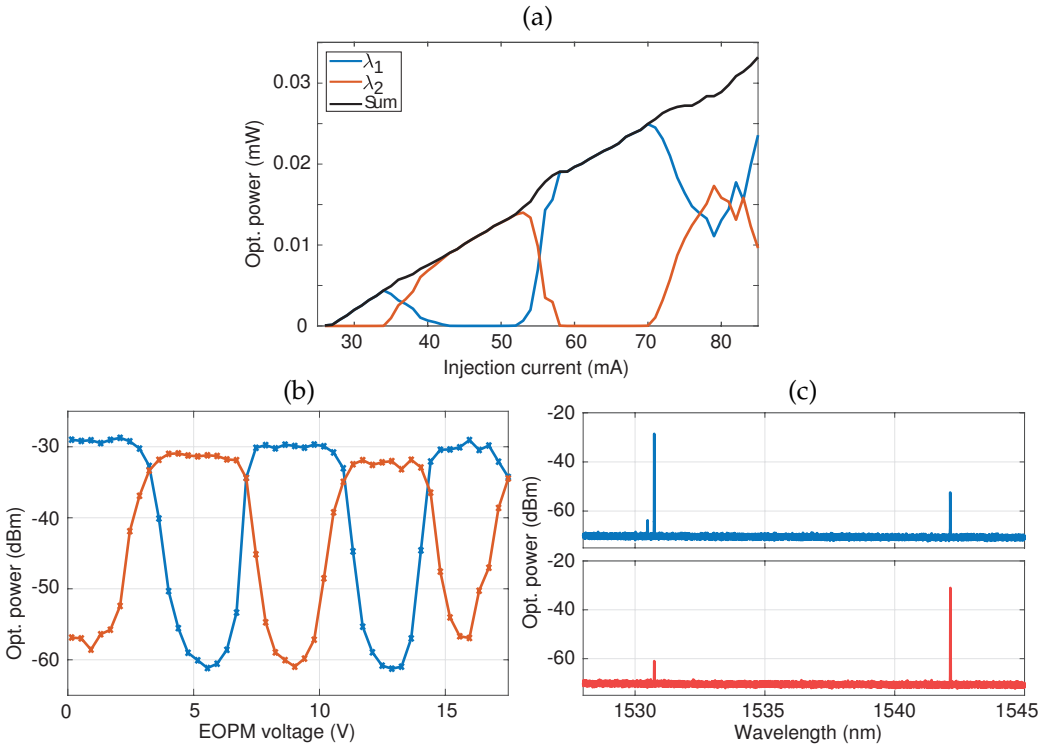


Figure 5.6: Characterisation for laser I: In (a), the LI curve exhibiting multiple power exchanges with increasing injection currents. To restrict the number of side modes, the laser current is chosen to be 36 mA in (b) & (c). In (b), the spectral evolution for each wavelength is shown when the feedback phase is tuned. In (c), the optical spectra at a voltage of 2 V and 5.5 V.

increasing injection currents, without the additional boost, only single-wavelength emission on $\lambda_2$ was achieved. However, the boost of the wavelengths also resulted in the trigger of multiple side modes. Therefore, this laser had to be operated at a low injection current of 36 mA to limit the number of modes together with large $DBR_3$ current of 30.2 mA to suppress the remaining modes. In a next step, we applied optical feedback onto the laser to obtain the spectrally resolved evolution shown in 5.6 (b). We were able to achieve an extinction ratio of up to 30 dB, the optical spectra for 2 V and 5.5 V are shown in (c). A feedback current of 19.8 mA had to be applied to obtain the optical feedback required for an emission control in this laser. The feedback current is higher than in other concepts and might result from the additional boost which has to be compensated by a higher feedback strength. The low laser current results in low output powers, although higher laser currents improve the output power, multiple side modes appear. This lowers the achievable extinction ratio between the wavelengths as undesired modes participate in the emission and will be discussed in detail in the following.

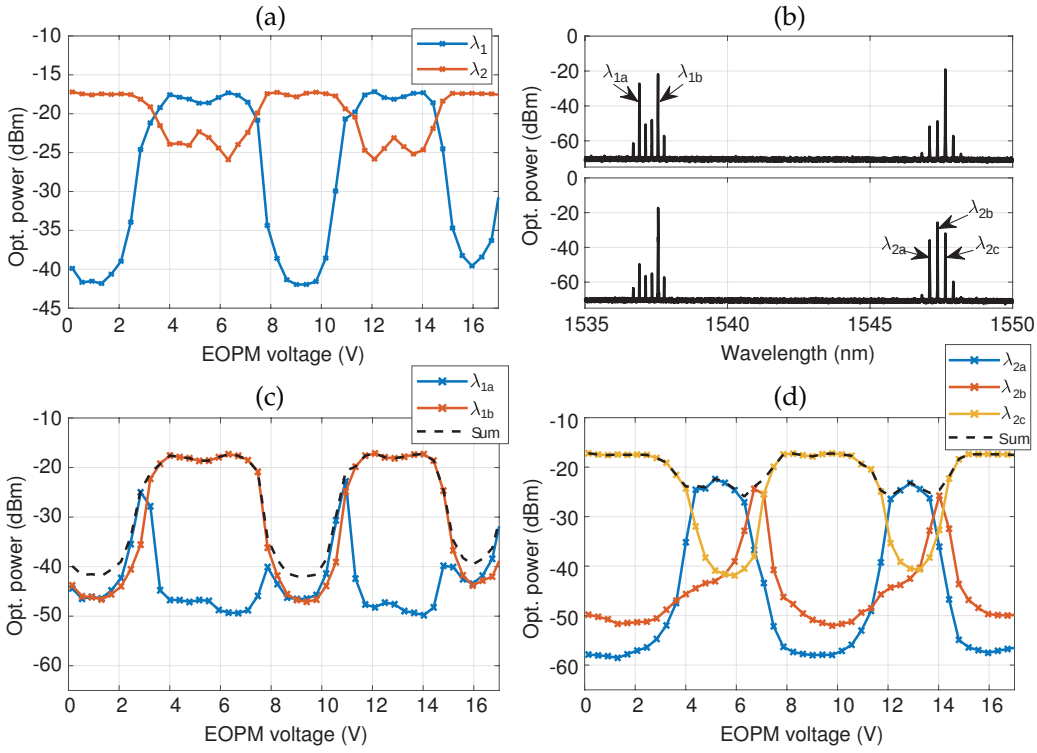


Figure 5.7: In (a), the limited suppression ratio of the two wavelength regions $\lambda_1$ & $\lambda_2$ is shown. The origin is the appearance of multiple side-modes shown in (b). In (c) & (d), the evolution and the energy exchange between the individual modes is shown. Tuning the feedback phase results in the undesired selection of the side-modes which hampers the suppression ratio.

### 5.2.3 *Longitudinal modes*

In this section, we will discuss the negative impact that neighbouring longitudinal modes can have on the proposed control approach. In some of the dual-wavelength lasers based on an MIR, i.e. laser concepts I & II, the selectivity of the DBRs is not sufficient to select one individual mode. Either multiple modes emit at once or a sequential selection of different modes occurs if the laser current or the EOPM voltage is tuned. Applying a current to the DBRs can counteract this behaviour as discussed in chapter 3. Here we use a laser concept II with a feedback cavity length of 4850 µm from PIC (A), which showed an emission on up to five modes and will be used to demonstrate the interaction between the modes when the EOPM voltage is tuned. In Fig. 5.7 (a), the spectral evolution of the two wavelength regions are shown in red and blue, i.e. for each wavelength region $\lambda_1$ & $\lambda_2$, the emitting modes were summed up to achieve this result. In (b), the optical spectra at an EOPM voltage of 3.2 V and 14 V are shown, showing all five emitting modes indicated by $\lambda_{1a}$ to $\lambda_{2c}$. The wavelength region of 1537 nm comprises of two modes $\lambda_{1a}$ & $\lambda_{1b}$ exchanging their energy depending of the EOPM voltage. This can be seen in (c), where the individual modes are plotted together with their sum, correspond-

ing to $\lambda_1$ in (a). It is visible that $\lambda_{1b}$ is the dominant mode, emitting for most of the EOPM voltages. However, around 2-4 V, 8 V and between 10-12 V, $\lambda_{1a}$ shows a parasitic emission whenever $\lambda_{1b}$ is turned on or off. As both modes can still be suppressed at the same time, the disturbance is limited to a small voltage range. For the wavelength region around 1547 nm shown in (d), three modes compete about the available gain and can not all be suppressed at the same time. While $\lambda_{2c}$ seems to dominate the emission for most of the EOPM voltages with $\lambda_{2a}$ & $\lambda_{2b}$ being suppressed by up to 40 dB, when $\lambda_{2c}$ is suppressed, the remaining modes take over the emission. Although the individual modes can be suppressed to a large degree, their sum shows only a modulation of about 10 dB. We find that the less modes are involved into the emission, the better our control capabilities are, resulting in higher suppression ratios and also in full switches between the wavelengths. The reduction of emitting modes to a minimum has also been pointed out in previous work on quantum-dot lasers [48] and was identified as a crucial parameter for this work. The emergence of multiple modes can be circumvented by either reducing the gain current and subsequently the available gain, or by tuning the DBR currents. However, this restricts our lasers to a small operation range and suggests an improvement of the DBR selectivities.

### 5.2.4 *Transient dynamics for switching*

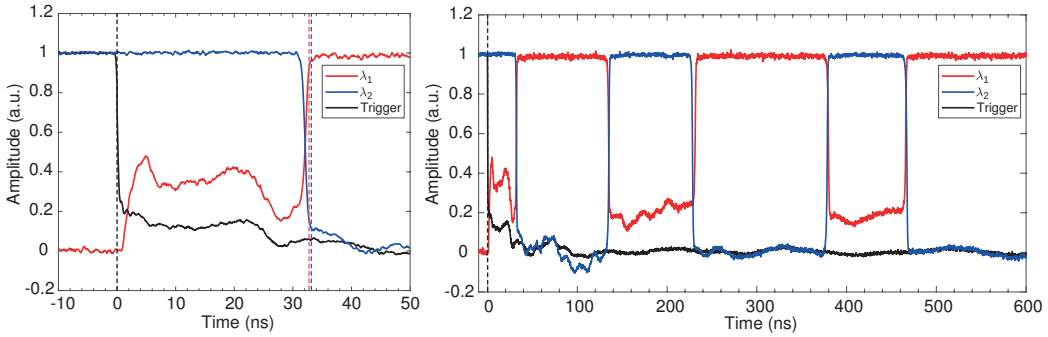


Figure 5.8: Transient behaviour with multiple switches between the two wavelengths $\lambda_1$ & $\lambda_2$ in red and blue, respectively, before reaching a stable state. The switch is initiated with the trigger signal shown in black and indicated by the dotted line.

In chapter 4 the switching performances with switching times of a few nano-seconds have been demonstrated. However, these excellent performances are not observed for all lasers and operating conditions. In some cases, we observed that the laser could exhibit long transients with several switches between $\lambda_1$ & $\lambda_2$ before reaching a stable state. A typical example is shown in Fig. 5.8 (a) & (b) for laser III from PIC (B) with two different time scales. The reaction time for $\lambda_1$ to initiate the switch is about 1 ns, visible in (a), however, it only exhibits a partial switch between 0 and 32 ns. Within this time, $\lambda_2$ shows no reaction. Only after 32 ns a full switch between both wavelengths occurs. Unexpectedly, after about 100 ns, another switch back to $\lambda_2$ occurs with $\lambda_1$ only being partially suppressed, visible in (b). These unexpected switches occur multiple times until reaching stable conditions beyond 500 ns. These switches are repetitive and do not change over

time. The repetition times do not correspond to any round-trip lengths in the feedback cavity or reflections due to cable length in the setup as they are in the range of tens of meter.

To gain more insights on this issue, we used a Fourier-Transform-Interferometer to record time-resolved optical spectra. A special add-on for this interferometer allows to obtain the optical spectra of repetitive signals stepwise with a low nano-second time resolution $\Delta t$. Each trigger step $n$ serves as a reference time $t_0$, the optical spectrum is recorded at different times $t = t_0 + n \cdot \Delta t$ to scan the spectral evolution over time. This would have allowed us to observe the whole optical spectrum and would have given valuable insights on the switching dynamics and potential undesired side modes being triggered. Unfortunately, the dedicated control setup did not work as intended and only allowed for time resolutions in the µs-range. We therefore left these studies for future work.

Moreover, the current setup is not optimized for high-frequency modulation. Although a probe was used to bias the EOPM, the bond wires were connected to the electronic boards at all times to operate the laser and feedback SOAs. Hence, implementing an RF EOPM might overcome this limitation and could lead to a stable switch by using a GSG probe. The RF EOPM allows for a frequency bandwidth of up to 8 GHz and could potentially lead to even faster switching times.

## 5.3 IMPROVEMENTS ON LASERS AND FEEDBACK SECTION

### 5.3.1 *Improvements of dual-wavelength laser concepts*

In this section, possible improvements for the solitary laser concepts will be discussed. Four different approaches have been implemented on the PICs to determine the most promising laser concepts but also to identify potential weaknesses. The goal of the improvements discussed here are to achieve dual-wavelength emission in each laser concept and to increase the optical output power.

Laser concept I is the simplest approach to design a dual-wavelength laser and requires the lowest design efforts. However, the emission on only a single wavelength showed a high demand on identical DBR parameters and manufacturing tolerances. Potential improvements should therefore aim to achieve a reliable dual-wavelength emission in the first place. However, this might still depend on the manufacturing tolerances if the precision on the parameters need to be too precise. Moreover, as discussed before, the parallel layout has higher losses originating from the transparencies of the DBRs to each other compared to the sequential layouts and is therefore disadvantaged. Overall, this structure showed to be less performant with low output powers and is not recommended for implementation on a PIC.

Laser concept II showed reproducible results throughout all PICs and wafers and is one of the most potent lasers implemented due to its compactness, variable wavelengths and high output powers. Yet, two different improvements can be envisioned, firstly, reducing the DBR length to improve the wavelength selectivity and to improve the output power at the same time. This reduces the number of emitting modes and channels the available gain into ideally one single mode. This should make the DBR tuning to reduce the number of side-modes unnecessary and also reduces the number the active controls to a minimum. The dual-wavelength emission without any side-modes will also lead to an improved extinction ratio as discussed in section 5.2.3 and consequently to a larger operation range for the laser. Due to the fixed DBR parameters by the foundry, a shortening of the DBR to increase the selectivity also reduces the reflectivity at the same time as the coupling coefficient can not be changed. However, we already saw that output powers of 2.2 mW are achievable in the test lasers discussed in chapter 3. Their SOA lengths are identical to our dual-wavelength lasers, but have much shorter DBR. Hence, a shortening of the DBRs in our dual-wavelength lasers is also beneficial to achieve higher optical output powers. A second improvement concerns the overall arrangement of the laser components and is shown in Fig. 5.9, II. Currently, the MIR serves as a laser output with a transmittance of about 50 %. If shorter DBRs with a length of about 200 µm are implemented, a transmittance of about 42 % would be achieved. In this case, the DBR output could be used as a laser output as shown in the proposed layout in Fig. 5.9 on the left. Moreover, without the need for the MIR as a outcoupling mirror, a 1-port MIR with a much higher reflectivity could be implemented. This MIR could be implemented right next to the SOA to reduce the laser cavity length by about 300 µm. The spectral separation of the modes would increase and allow for an easier selection of individual modes by the DBRs. The higher reflectivity together with the omitted transition section and waveguides would also contribute to a higher optical output power.

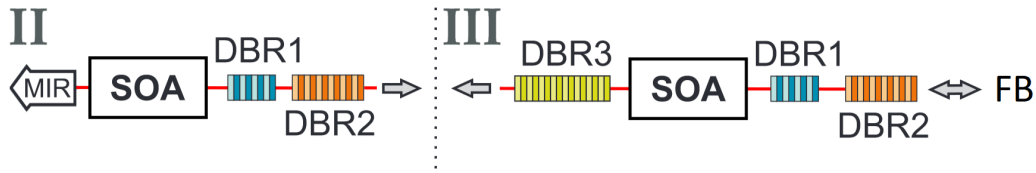


Figure 5.9: Proposed improvements for laser concept II & III. In II, a 1-port MIR closes the cavity which improves optical output power. Shorter lengths for $DBR_1$ & $DBR_2$ to improve wavelength selectivity, also allow the use as an optical output. In III, the feedback could be applied to the output of $DBR_1$ & $DBR_2$ to reduce the footprint to a minimum. This would also improve the output power via $DBR_3$ as no MMI-splitter is required to apply the feedback.

Laser concept III also showed reproducible results throughout all PICs and wafers with the highest extinction ratios and a control of up to three wavelengths. The optical powers are the highest achieved and might result from the shorter DBRs implemented. This is a good indication that other laser concepts could benefit from shorter DBRs to improve their output power. Nevertheless, in the design stage described in chapter 3, an equal optical power was favoured over a maximal power, leaving room for potential increase in optical power for future designs, i.e. circuit simulations could be performed with the goal of maximizing the optical power. For testing purposes, 0.3 nm detuned DBRs compared to the optimal results from the simulations have been implemented to achieve a large range of wavelength separations. This could be neglected in future designs to reduce the number of active control parameters and to ease the use for the laser operation. Moreover, for this particular concept, a much more compact layout could be implemented as shown in Fig. 5.9, III. Due to the transmittance of $DBR_1$ & $DBR_2$ of 42 % & 11 %, the feedback section could be implemented behind these two DBRs. The resulting feedback strength with about 5 % would be much stronger, but could be controlled with the SOA. This arrangement would be much more compact and could discard the MMI splitter in the current feedback section, hence improving the optical output power as well.

The parallel arrangement of the DBRs in laser concept IV performed well. Comparing it to the poor performing concept I, the active control of the DBR overlaps allowed to compensate for potential losses to achieve a dual-wavelength emission. Combining the outputs of the two DBRs was intended to improve of the optical power resulting from the parallel DBR arrangement, however has a major design flaw. The mutual transparency of the DBRs allows the feedback to fully enter the laser cavity. If the laser is emitting on the wavelength generated of $DBR_1$, the light is emitted through $DBR_2$ and vice versa. This also applies to the optical feedback phase. However, if the optical path lengths are not identical, different phases will be reflected into the laser cavity which can result in undesired dynamics. Different optical path lengths are highly possible, either due to manufacturing tolerances or due to different refractive indices due to different implemented DBR wavelength. To avoid this, the parallel outputs should not be combined and neither used as an optical output, nor to control the feedback strength. Nevertheless, this is the only laser concept capable of emitting simultaneously from two different wavelengths with a 1 nm separation as laser concept III only showed sequential emission.

Hence, shortening $DBR_3$ and using it as an outcoupling mirror could lead to a promising laser source. However, also with the drawback of lower optical output powers due to the parallel DBR arrangement.

### 5.3.2 *Optimization of the optical feedback cavity*

We were able to demonstrate a dual wavelength control in all laser concepts. For all of these demonstrators, we implemented very long EOPM sections of 1200 µm into all of our feedback sections for research purposes. This allowed for multiple wavelength switches corresponding to feedback delays of up to $4\pi$ at the highest EOPM voltages. However, in practice a phase shift of $\pi$ is sufficient to switch between two wavelengths once, hence, with a design voltage of 8 V, an EOPM length of 600 µm is sufficient. Considering the feedback strength required to achieve a full switch, the feedback SOAs were operated in the range of 10 mA. Hence, a shorter feedback SOA with a length around 100 µm would be sufficient to achieve the same feedback strength. Potentially the active control of the feedback SOA could be avoided once the optimal feedback strength is determined. This could be achieved in two ways, either in designing a customized MMI splitter to provide the optimal feedback strength, while also increasing the output power of the laser at the same time. However, this is connected to a large design effort as no predefined building blocks exist at this point. A simpler approach would be to include the ideal feedback SOA length to achieve the desired feedback strength without biasing, i.e. adding the right amount of losses for the feedback cavity.

Shortening the SOA and EOPM section would reduce the minimal required length for all components from 2400 µm to about 1600 µm, i.e. the feedback section can not be shorter than this. For a 1 nm wavelength separation, the optimal feedback length is multiples of about 700 µm, corresponding to the distance of one node of the beat-frequency to another. Hence, the feedback length could be reduced to about 1750 µm. For a 10 nm separation the distance between the nodes is about 70 µm which allows for a reduction of the feedback section to about 1645 µm. This is a significant reduction in footprint by a factor of about 1.8. Moreover, a shorter cavity is more robust against dynamical behaviours and allows for larger injection currents and faster switching times as discussed in the simulations in chapter 2. However, the precise length of the feedback section has to be adapted to the expected wavelength for each laser individually. This applies in particular for laser concepts III & IV where the overlapping DBRs define the emitting wavelengths and have to be determined by simulations.

## 5.4 CONCLUSION

To conclude, in this chapter we highlighted several limitations of our lasers and the feedback control. In the beginning, we highlighted the open question on how the extinction ratio scales with varying spectral separation and suboptimal feedback phases to evaluate the limitations of the control approach. To get further insights on this, we presented experimental work using a discrete device, an external cavity diode laser as well as the DBR tuning of our dual-wavelength lasers. However, performance and stabilisation issues limited these studies and are therefore left for future work. Nevertheless, we were able to get additional insight on the limited tuning capability of the spectral separations between the wavelengths. Tuning one DBR results in a single-wavelength emission due to the reduction in reflectivity of the DBR whereas a tuning of both DBRs results in a shift of both wavelengths to shorter wavelengths while maintaining the spectral separation. Another limitation is the appearance of undesired side modes which hampers the performance, limits the extinction ratios and requires improvements on the selectivity of the DBRs. Overall we experienced dynamics very rarely , however, when investigating the switching speed we found unexpected switches in some lasers before reaching a stable state. This might be possible to prevent by optimizing the feedback section towards an RF compatible system. Finally, we discussed and proposed improvements for the most promising laser concepts and the feedback section. Whereas improvements for the feedback section aimed to reduce the footprint, the improvements for the lasers are more comprehensive and aim to improve the general performance with more compact devices and less control parameters for a successful next MPW participation.

# 6 CONCLUSION

In this final chapter, we will summarize the essential points of this thesis and highlight the main achievements. We proposed a new technique to shape the emission of a dual-wavelength laser based on a phase controlled optical feedback approach. To demonstrate this approach, we designed custom dual-wavelength lasers and implemented them together with our control approach successfully onto a PIC. We demonstrated high performances with this proof of concept and achieved extinction ratios of up to 50 dB with switching times below 4 ns. In the first section 6.1 we will recapitulate the goal and achievements made in each chapter. Finally, in the second section 6.2 we will draw possible perspectives for future work.

## 6.1 MAIN ACHIEVEMENTS

In the second chapter, we highlighted the fundamental working principle of the control approach.

- First, we presented the approach to control the amplitudes of two different wavelengths using a phase controlled optical feedback. The underlying idea is to achieve a relative phase shift of $\pi$ between the wavelengths after a full round trip in the feedback cavity. This way, one wavelength is in phase and will benefit from an extra boost while the other wavelength is out of phase and suffers from extra losses. Detuning the feedback cavity on the wavelength scale changes the round-trip time in favour of the suppressed wavelength to achieve a switch.

- Then, we introduced the simulation model to obtain the best parameters to implement an optimal feedback cavity onto a PIC. We studied the phase space given by the two wavelengths and highlighted that a switch is possible for a large range of relative phase shifts and that even suboptimal conditions allow a full control over the laser emission. Moreover, we discussed that the control approach is dependent on intrinsic laser parameter like the coupling coefficient $\beta$ and the gain differences between the two wavelengths. Then, we showed that the optical feedback strength is a crucial parameter and emphasized that it allows to actively compensate for possible bad intrinsic laser parameters appearing in a manufactured laser to achieve a full control. Furthermore, we also identified a short feedback cavity to be beneficial as it leads to the fastest switching times.

In the third chapter, we presented different solitary dual-wavelength laser concepts, discussed the design and optimization process and presented their characteristics.

- First, we presented four different laser concepts with varying spectral separations and optimized them using a circuit simulator. We optimized each concept for an equal optical power as well as for a high side mode suppression ratio. We also determined the exact wavelengths each laser will emit on as this is a crucial parameter for the implementation of corresponding feedback cavities.

- Second, we characterized each laser concept and discussed their peculiarities: We demonstrated a dual-wavelength emission in all concepts. However, we also identified the concepts II & III to perform the best across different PICs and wafers as they showed to be the most reliable sources with the highest optical output powers.

- At last, we characterized DBRs under varying currents and temperatures and connected the observed effects to three different behaviours in our lasers. First we observed a shift to shorter wavelengths, which was to be expected. The second effect was a reduction in the spectral width by about 0.3 nm and the third effect was a reduction in reflectivity by 1.2 dB. The two latter effects were unexpected but on the one hand we exploited them to trigger dual-wavelength emission or to limit the number of emitting side modes. On the other hand, we connected the reduction in reflectivity to our limited capability of tuning the spectral separations of the two wavelengths.

In the fourth chapter, we discussed the design of the optical feedback cavity and presented experimental results on the tuning of the feedback phase.

- First, we discussed the layout of the feedback cavity and implemented individual feedback cavities for each laser. We implemented an identical arrangement with an SOA and an EOPM for each of them and adapted the feedback cavities by variations in the waveguide lengths.
- Second, we presented and discussed the control of two as well as three wavelengths by tuning the optical feedback phase via the EOPM. We demonstrated extinction ratios of up to 35 dB for lasers with a 10 nm separation and even higher extinction ratios of 50 dB for lasers with a 1 nm separation. We highlighted that the repetitive switching cycles correspond to a $4\pi$ phase shift. Hence, we could confirm the underlying control mechanism to be the expected phase dependent loss modulations.
- Then, we explored the switching performance for different laser and feedback currents and mapped their parameter space. We found that adapting the feedback strength enables for full switches for a large laser current range. However, the current limitations on the laser concepts prevent us form efficiently operating the laser for most set of parameters.
- At last, we investigated the switching speed and obtained switching times of 3.5 ns with a non-optimized setup. These excellent results show that the feedback based control approach is capable of reaching very fast and competitive switching times and could reach even faster switching considering a dedicated RF-setup.

In the last chapter, we identified different limitations of our laser concepts and proposed several improvements.

- First, we aimed to demonstrate our control approach using either a quantum-dot laser or an external cavity diode laser and to benefit from the flexibility of their external feedback arrangement. We conducted these experiments with the intention to identify possible limitations of our control approach by studying different wavelength separations as well as different feedback phase shifts. Although we obtained a 40 dB extinction ratio in the external cavity diode laser, limited performance of both sources did not allow for these studies and we therefore left them for future work.
- We then studied the impact of the DBR tuning onto the spectral separation of the dual-wavelength laser. We showed that a DBR tuning lowers the DBR reflectivity which results in a single wavelength emission and severely limits the flexibility of our lasers.
- Moreover, we emphasized that a multi-modes emission has a major impact on the maximal extinction ratios. We showed that an energy exchanges between different modes appear as each of them experiences different feedback phases. We connected this to a low wavelength selectivity of the DBR which can be improved by a shortening of the DBR lengths.

- Next, to overcome the weaknesses identified, we proposed different improvements to enhance the performance, reliability and compactness towards advanced laser sources. We identified shorter DBRs to be beneficial to improve output powers and the wavelength selectivity.
- At last, we identified potential improvements also for the external feedback cavity. First, we proposed a GSG connection to avoid the spurious signals discussed and to benefit from the fast electro-optic effect to reach highest switching speeds. Then, we proposed a reduction of the feedback SOA and EOPM lengths to achieve the most compact control approach. Moreover, implementing an optimal length for the feedback SOA could provide the precise feedback strength for a passive SOA and thus, could reduce the control parameter to just a single voltage for the EOPM.

## 6.2 PERSPECTIVES FOR FUTURE WORK

The photonic integration technology is constantly growing and mainly driven by telecommunication applications. The higher demand on PICs and the further development towards standardized electrical and optical connections lowers the costs and PICs become more appealing for customers in other branches. Applications in the medical technologies like optical coherence tomography, measurement tasks like fibre or gas sensing, image processing like LIDAR for drones and self-driving cars and spectrometers for agriculture to analyse the condition of seeds, fruits and vegetables are just a few examples of the current market shares [70]. The benefits of a compact, cost effective and flexible design makes this technology interesting for various applications. With the control approach presented in this thesis, we hope to contribute with an compact, energy efficient and easy to use method to control the emission of multi wavelength lasers for potential applications. The compactness of the approach allows to implement optical sources including our control approach together with analysis devices onto one single chip. The single control voltage and the low requirements on the EOPM voltage makes the operation very simple.

Nevertheless, to reach a mature level of this control approach, several improvements have to be made and open research questions still have to be answered. As already pointed out in chapter 5, various improvements on the lasers have to be made towards sources with high output powers and reliable two-wavelength emission. Also improvements have been proposed for the feedback control, first to reduce the footprint on the PIC and second to implement GSG contacts to improve the switching performance. Moreover, additional test structures are required to determine the amount of feedback send back towards the laser cavity. To get insights on these issues, a new multi-project-wafer participation is required. In addition, a participation to a different generic foundry platform like HHI could be envisioned: This would allow to compare the performances and to identify what impact the foundry specificities have on the control approach. A different coupling coefficient $\beta$ or a different gain spectrum and consequently different gain differences could be expected.

Moreover, as we have already been able to demonstrate the control of three modes, the question arises of how many mode could be controlled using one feedback cavity. The first step would be to determine a limitation on the number of modes, this could for example be the precision on the required feedback phase to select a specific mode. Then, a major challenge would be to generation more than two uniformly separated and well defined wavelengths to be able to implement a corresponding feedback delay length. The required development stages might require several MPW participations to gain enough insights to obtain a demonstrator. An interesting aspect is also if an asymmetric wavelength separation could be controlled, e.g. three modes with a 1 nm & 2 nm separation between them. This could potentially require the implementation of multiple feedback cavities with different feedback delays to achieve the required relative phase shifts. The challenge would then be, to implement the different feedback cavities onto the PIC and to address the desired feedback cavity in practice. A simple Mach-Zehnder-Interferometer to guide the light to a particular feedback cavity would fail: These interferometers select a specific output by achieving a precise relative phase shift in their two arms, the emission of a multi-wavelength laser is therefore not compatible as each mode would require

a different relative phase shift. An MMI splitter with multiple outputs to select specific cavities with additional SOA gates could be one solution. Coupling the laser light out of the PIC and routing the light to different feedback channels via optical fibres could be another solution. Both options could be feasible, but would suffer from high losses.

On another note, the proposed control approach can be adapted for every platform or dual-wavelength laser with a sufficient coupling and similar gain. The implementation on the PIC provided a high thermal and mechanical stability to build a demonstrator. The limitations of the control approach could however not be determined due to the fixed components. For this, an external cavity diode laser has been presented to study the suppression ratio under different feedback delays and different spectral separations. This might reveal potential limitations which could also limit the implementation for specific applications, e.g. for very large spectral separations. To conduct these experiments, an encapsulation of the setup into a mechanically and thermally stabilized box could be successful.

# LIST OF PUBLICATIONS

Some of the materials, ideas and figures in this dissertation have appeared previously in the following publications:

### PUBLICATIONS IN PEER REVIEWED JOURNALS

1. M. Virte, R. Pawlus, M. Sciamanna, K. Panajotov, and S. Breuer, "Energy exchange between modes in a multimode two-color quantum dot laser with optical feedback", Optics letters, 264955, 3205-3208 (2016)
2. R. Pawlus, S. Breuer, M. Virte, "Relative intensity noise reduction in a dual-state quantum-dot laser by optical feedback", Optics Letters, Vol. 42, Issue 21, pp. 4259-4262 (2017)
3. R. Pawlus, L. L. Columbo, P. Bardella, S. Breuer, M. Gioannini, "Intensity noise behaviour of an InAs/InGaAs quantum dot laser emitting on ground and excited states", Optics Letters, Vol. 43, Issue 4, pp. 867-870 (2018)
4. R. Pawlus, R. de Mey, S. Breuer, M. Virte, "Dual-wavelength lasers on generic foundry platform", (Submitted on 14 Oct 2019), arXiv:1911.03533

### PATENTS

1. R. Pawlus, S. Breuer, H. Thienpont, M. Virte, "Wavelength control of multi-wavelength laser", submitted 08 Oct. 2019, Application number EP19201970.1

### CONTRIBUTIONS TO WORKSHOPS, NATIONAL AND INTERNATIONAL CONFERENCES

1. R. Pawlus, M. Gioannini, M. Virte, W. Elsässer, S. Breuer, "Investigations on the relative intensity noise of a two-state quantum dot laser", Oral, SPIE Photonics Europe, April 2016, 9892-29, Brussels, Belgium
2. M. Virte, R. Pawlus, W. Elsässer, K. Panajotov, M. Sciamanna, and S. Breuer, "Range-dependent effects of optical feedback on multimode two-color Quantum Dot Lasers", Oral, SPIE Photonics Europe, April 2016 , 9892-31, Brussels, Belgium
3. R. Pawlus, S. Breuer, M. Virte, "Relative intensity noise reduction in a two-color quantum-dot laser by optical feedback control", Oral, IS-PALD, Sept. 2016 , National Tsing Hua University, Hsinchu, Taiwan
4. R. Pawlus, S. Breuer, M. Virte, "Impact of optical feedback onto the relative intensity noise of a two-state quantum-dot laser", Oral, ESLW, Oct. 2016 , Technische UniversitÃ€t Darmstadt, Darmstadt, Germany

5. R. Pawlus, S. Breuer, M. Virte, "RIN improvement by optical feedback of a two-state emitting QD laser", Oral, IS-PALD, Nov. 2017, Paris, France
6. R. Pawlus, L. L. Columbo, P. Bardella, S. Breuer, M. Gioannini, "Intensity noise of a two-state quantum dot laser", Poster presentation, Deutsche Physikalische Gesellschaft e.V., March 2018, HL 13.84, Berlin, Germany
7. R. Pawlus, S. Breuer, and M. Virte, "Compact dual-wavelength lasers on InP generic foundry platform", Oral, Conference on Lasers and Electro-Optics, June 2019, CB-9.4, Munich, Germany
8. R. Pawlus, R. de Mey, S. Breuer, M. Virte, "Impact of DBR tuning on a dual-wavelength laser implemented on a generic foundry platform", Oral, IS-PALD, Nov. 2019, Metz, France
9. R. Pawlus, R. de Mey, S. Breuer, M. Virte, "Control of dual-wavelength laser using monolithically integrated phase-controlled optical feedback", Oral, SPIE Europe, April 2020, Strassbourg, France

## SUPERVISED MASTER THESIS

1. R. de Mey, "Tailoring Two-Color Laser Emission Using an Integrated Feedback Cavity", 2019
2. M. Skënderas, "Control of a Widely-Tunable Ring Laser Based On Cascaded Asymmetric Mach-Zehnder Interferometers", 2019

# BIBLIOGRAPHY


[1] A. Einstein, "The Quantum Theory of Radiation," *Physikalische Zeitschrift*, vol. **18**, no. 121, 1917.

[2] T. Numai, *Fundamentals of Semiconductor Lasers*. Springer-Verlag, 2004.

[3] Z. Alferov, "Double heterostructure lasers: Early days and future perspectives," *IEEE Journal on Selected Topics in Quantum Electronics*, vol. **6**, no. 6, pp. 832–840, 2000.

[4] J. Carroll, J. Whiteaway, and D. Plumb, *Distributed Feedback Semiconductor Lasers*. The Institution of Electrical Engineers, London, United Kingdom, 1998.

[5] E. U. Rafailov, *The Physics and Engineering of Compact Quantum Dot-based Lasers for Biophotonics*. John Wiley & Sons Inc., 2014.

[6] A. Markus, J. X. Chen, C. Paranthoen, A. Fiore, C. Platz, and O. Gauthier-Lafaye, "Simultaneous two-state lasing in quantum-dot lasers," *Applied Physics Letters*, vol. **82**, no. 12, pp. 1818–1820, 2003.

[7] Z. Zhang, Q. Jiang, and R. Hogg, "Simultaneous three-state lasing in quantum dot laser at room temperature," *Electronics Letters*, vol. **46**, no. 16, p. 1155, 2010.

[8] S. Ummethala, T. Harter, K. Koehnle, Z. Li, S. Muehlbrandt, Y. Kutuvantavida, J. Kemal, P. Marin-Palomo, J. Schaefer, A. Tessmann, S. K. Garlapati, A. Bacher, L. Hahn, M. Walther, T. Zwick, S. Randel, W. Freude, and C. Koos, "THz-to-optical conversion in wireless communications using an ultra-broadband plasmonic modulator," *Nature Photonics*, vol. **13**, no. 8, pp. 519–524, 2019.

[9] T. Nagatsuma, G. Ducournau, and C. C. Renaud, "Advances in terahertz communications accelerated by photonics," *Nature Publishing Group*, vol. **10**, no. 6, pp. 371–379, 2016.

[10] I. White, R. Penty, M. Webster, Y. J. Chai, A. Wonfor, and S. Shahkooh, "Wavelength switching components for future photonic networks," *IEEE Communications Magazine*, vol. **40**, no. 9, pp. 74–81, 2002.

[11] S. Latkowski, A. Hänsel, N. Bhattacharya, T. De Vries, L. Augustin, K. Williams, M. Smit, and E. Bente, "Novel Widely Tunable Monolithically Integrated Laser Source," *IEEE Photonics Journal*, vol. **7**, no. 6, 2015.

[12] T. Mohr, S. Breuer, G. Giuliani, and W. Elsäßer, "Two-dimensional tomographic terahertz imaging by homodyne self-mixing," *Optics Express*, vol. **23**, no. 21, p. 27221, 2015.

[13] D. M. Mittleman, "Twenty years of terahertz imaging [Invited]," *Optics Express*, vol. **26**, no. 8, p. 9417, 2018.

[14] T. F. K. Reed and E. Drive, "CW Terahertz Wave Generation By Photomixing Using A Two-longitudinal-mode Laser Diode," *Electronics letters*, vol. **33**, no. 24, pp. 2039–2040, 1997.

[15] M. Tani, O. Morikawa, S. Matsuura, and M. Hangyo, "Generation of terahertz radiation by photomixing with dual- and multiple-mode lasers," *Semiconductor Science and Technology*, vol. **20**, no. 7, pp. 151–163, 2005.

[16] S. Hoffmann and M. R. Hofmann, "Generation of Terahertz radiation with two color semiconductor lasers," *Laser and Photonics Reviews*, vol. **1**, no. 1, pp. 44–56, 2007.

[17] M. Theurer, T. Göbel, D. Stanze, U. Troppenz, F. Soares, N. Grote, and M. Schell, "Photonic-integrated circuit for continuous-wave THz generation," *Optics Letters*, vol. **38**, no. 19, pp. 3724–3726, 2013.

[18] M. D. Wheeler, I. R. Lambert, and M. N. R. Ashfold, "Two-colour laser-induced grating spectroscopy of iodine vapour," *Chemical Physics Letters*, vol. **211**, no. 4-5, pp. 381–384, 1993.

[19] J. Jágerská, P. Jouy, A. Hugi, B. Tuzson, H. Looser, M. Mangold, M. Beck, L. Emmenegger, and J. Faist, "Dual-wavelength quantum cascade laser for trace gas spectroscopy," *Applied Physics Letters*, vol. **105**, no. 16, 2014.

[20] J. Jágerská, P. Jouy, B. Tuzson, H. Looser, M. Mangold, P. Soltic, A. Hugi, R. Brönnimann, J. Faist, and L. Emmenegger, "Simultaneous measurement of NO and NO_2 by dual-wavelength quantum cascade laser spectroscopy," *Optics Express*, vol. **23**, no. 2, p. 1512, 2015.

[21] M. Majumder, T. K. Gangopadhyay, A. K. Chakraborty, K. Dasgupta, and D. K. Bhattacharya, "Fibre Bragg gratings in structural health monitoring-Present status and applications," *Sensors and Actuators A - Physical*, vol. **147**, no. 1, pp. 150–164, 2008.

[22] U. Nawrot, T. Geernaert, B. De Pauw, D. Anastasopoulos, E. Reynders, G. De Roeck, and F. Berghmans, "Development of a mechanical strain amplifying transducer with Bragg grating sensor for low-amplitude strain sensing," *Smart Materials and Structures*, vol. **26**, no. 7, p. 75006, 2017.

[23] S. Hancock, P. Lewis, M. Foster, M. Disney, and J. P. Muller, "Measuring forests with dual wavelength lidar: A simulation study over topography," *Agricultural and Forest Meteorology*, vol. **161**, pp. 123–133, 2012.

[24] E. S. Douglas, J. Martel, Z. Li, G. Howe, K. Hewawasam, R. A. Marshall, C. L. Schaaf, T. A. Cook, G. J. Newnham, A. Strahler, and S. Chakrabarti, "Finding leaves in the forest: The dual-wavelength Echidna lidar," *IEEE Geoscience and Remote Sensing Letters*, vol. **12**, no. 4, pp. 776–780, 2015.

[25] M. Gioannini, M. Dommermuth, L. Drzewietzki, I. Krestnikov, D. Livshits, M. Krakowski, and S. Breuer, "Two-state semiconductor laser self-mixing velocimetry exploiting coupled quantum-dot emission-states: experiment, simulation and theory," *Optics Express*, vol. **22**, no. 19, p. 23402, 2014.

[26] B. Mason, G. A. Fish, S. P. DenBaars, and L. A. Coldren, "Widely tunable sampled grating DBR laser with integrated electroabsorption modulator," *IEEE Photonics Technology Letters*, vol. **11**, no. 6, pp. 638–640, 1999.

[27] M. Nakao, K. Sato, T. Nishida, and T. Tamamura, "Distributed Feedback Laser Arrays Fabricated by Synchrotron Orbital Radiation Lithography," *IEEE Journal on Selected Areas in Communications*, vol. **8**, no. 6, pp. 1178–1182, 1990.

[28] J. Huang, C. Sun, B. Xiong, and Y. Luo, "Y-branch integrated dual wavelength laser diode for microwave generation by sideband injection locking," *Optics Express*, vol. **17**, no. 23, pp. 20727–20734, 2009.

[29] S. D. Roh, T. S. Yeoh, R. B. Swint, A. E. Huber, C. Y. Woo, J. S. Hughes, and J. J. Coleman, "Dual-Wavelength InGaAs-GaAs Ridge Waveguide Distributed Bragg Reflector Lasers with Tunable Mode Separation," *IEEE Photonics Technology Letters*, vol. **12**, no. 10, pp. 1307–1309, 2000.

[30] A. Hurtado, M. Nami, I. D. Henning, M. J. Adams, and L. F. Lester, "Two-wavelength switching with a 1310-nm quantum dot distributed feedback laser," *IEEE Journal on Selected Topics in Quantum Electronics*, vol. **19**, no. 4, 2013.

[31] S. Hoffmann, M. Hofmann, M. Kira, and S. W. Koch, "Two-colour diode lasers for generation of THz radiation," *Semiconductor Science and Technology*, vol. **20**, no. 7, pp. 205–210, 2005.

[32] J. W. Wu, B. Nakarmi, T. Q. Hoai, and Y. H. Won, "Tunable two-color lasing emission based on fabry-perot laser diode combined with external cavity feedback," *IEEE Photonics Journal*, vol. **5**, no. 1, 2013.

[33] C. C. Huang, C. H. Cheng, Y. S. Su, and C. F. Lin, "174-nm Mode Spacing in Dual-Wavelength Semiconductor Laser Using Nonidentical InGaAsP Quantum Wells," *IEEE Photonics Technology Letters*, vol. **16**, no. 2, pp. 371–373, 2004.

[34] M. L. Osowski, R. M. Lammert, and J. J. Coleman, "A dual-wavelength source with monolithically integrated electroabsorption modulators and Y-junction coupler by selective-area MOCVD," *IEEE Photonics Technology Letters*, vol. **9**, no. 2, pp. 158–160, 1997.

[35] J. H. Teng, S. J. Chua, Z. H. Zhang, Y. H. Huang, G. Li, and Z. J. Wang, "Dual-Wavelength Laser Source Monolithically Integrated with Y-Junction Coupler and Isolator Using Quantum-Well Intermixing," *IEEE Photonics Technology Letters*, vol. **12**, no. 10, pp. 1310–1312, 2000.

[36] M. Brunner, K. Gulden, R. Hövel, M. Moser, J. F. Carlin, R. P. Stanley, and M. Ilegems, "Continuous-Wave Dual-Wavelength Lasing in a Two-Section Vertical-Cavity Laser," *IEEE Photonics Technology Letters*, vol. **12**, no. 10, pp. 1316–1318, 2000.

[37] S. D. Roh, R. B. Swint, A. M. Jones, T. S. Yeoh, A. E. Huber, J. S. Hughes, and J. J. Coleman, "Dual-wavelength asymmetric cladding InGaAs-GaAs ridge waveguide distributed bragg reflector lasers," *IEEE Photonics Technology Letters*, vol. **11**, no. 1, pp. 15–17, 1999.

[38] H. Zhao, Y. Zhu, F. Li, and Y. Yu, "Wavelength bistability based on optical injection in a novel tunable dual mode laser," *Optics Express*, vol. **24**, no. 4, p. 3817, 2016.

[39] M. Gioannini, "Ground-state power quenching in two-state lasing quantum dot lasers," *Journal of Applied Physics*, vol. **111**, no. 4, p. 43108, 2012.

[40] A. Markus, M. Rossetti, V. Calligari, D. Chek-Al-Kar, J. X. Chen, A. Fiore, and R. Scollo, "Two-state switching and dynamics in quantum dot two-section lasers," *Journal of Applied Physics*, vol. **100**, no. 11, p. 113104, 2006.

[41] H.-Y. Wang, H.-C. Cheng, S.-D. Lin, and C.-P. Lee, "Wavelength switching transition in quantum dot lasers," *Applied Physics Letters*, vol. **90**, no. 8, p. 081112, 2007.

[42] N. A. Naderi, F. Grillot, K. Yang, J. B. Wright, A. Gin, and L. F. Lester, "Two-color multi-section quantum dot distributed feedback laser," *Optics Express*, vol. **18**, no. 26, p. 27028, 2010.

[43] S. Breuer, M. Rossetti, L. Drzewietzki, I. Montrosset, M. Krakowski, M. Hopkinson, and W. Elsässer, "Dual-state absorber-photocurrent characteristics and bistability of two-section quantum-dot lasers," *IEEE Journal on Selected Topics in Quantum Electronics*, vol. **19**, no. 5, pp. 1–9, 2013.

[44] J. Lee and D. Lee, "Double-state lasing from semiconductor quantum dot laser diodes caused by slow carrier relaxation," *J. Korean Phys. Soc.*, vol. **58**, p. 239, 2011.

[45] R. Pawlus, L. L. Columbo, P. Bardella, S. Breuer, and M. Gioannini, "Intensity noise behavior of an InAs/InGaAs quantum dot laser emitting on ground states and excited states," *Optics Letters*, vol. **43**, no. 4, p. 867, 2018.

[46] A. Kovsh, I. Krestnikov, D. Livshits, S. Mikhrin, J. Weimert, and A. Zhukov, "Quantum dot laser with 75nm broad spectrum of emission," *Optics Letters*, vol. **32**, no. 7, pp. 793–795, 2007.

[47] M. Virte, S. Breuer, M. Sciamanna, and K. Panajotov, "Switching between ground and excited states by optical feedback in a quantum dot laser diode," *Applied Physics Letters*, vol. **105**, no. 12, p. 121109, 2014.

[48] M. Virte, R. Pawlus, M. Sciamanna, K. Panajotov, and S. Breuer, "Energy exchange between modes in a multimode two-color quantum dot laser with optical feedback," *Optics Letters*, vol. **41**, no. 14, p. 3205, 2016.

[49] M. Smit, X. Leijtens, H. Ambrosius, E. Bente, J. Van Der Tol, B. Smalbrugge, T. De Vries, E. J. Geluk, J. Bolk, R. Van Veldhoven, L. Augustin, P. Thijs, D. D'Agostino, H. Rabbani, K. Lawniczuk, S. Stopinski, S. Tahvili, A. Corradi, E. Kleijn, D. Dzibrou, M. Felicetti, E. Bitincka, V. Moskalenko, J. Zhao, R. Santos, G. Gilardi, W. Yao, K. Williams, P. Stabile, P. Kuindersma, J. Pello, S. Bhat, Y. Jiao, D. Heiss, G. Roelkens, M. Wale, P. Firth, F. Soares, N. Grote, M. Schell, H. Debregeas, M. Achouche, J. L. Gentner, A. Bakker, T. Korthorst, D. Gallagher, A. Dabbs, A. Melloni, F. Morichetti, D. Melati, A. Wonfor, R. Penty, R. Broeke, B. Musk, and D. Robbins, "An introduction to InP-based generic integration technology," *Semiconductor Science and Technology*, vol. **29**, no. 8, 2014.

[50] K. A. Williams, E. A. J. M. Bente, D. Heiss, Y. Jiao, K. Ławniczuk, X. J. M. Leijtens, J. J. G. M. van der Tol, and M. K. Smit, "InP photonic circuits using generic integration [Invited]," *Photonics Research*, vol. **3**, no. 5, pp. B60–B68, 2015.

[51] R. Soref, "Tutorial: Integrated-photonic switching structures," *APL Photonics*, vol. **3**, no. 2, pp. 1–18, 2018.

[52] F. Kish, V. Lal, P. Evans, S. W. Corzine, M. Ziari, T. Butrie, M. Reffle, H. S. Tsai, A. Dentai, J. Pleumeekers, M. Missey, M. Fisher, S. Murthy, R. Salvatore, P. Samra, S. Demars, N. Kim, A. James, A. Hosseini, P. Studenkov, M. Lauermann, R. Going, M. Lu, J. Zhang, J. Tang, J. Bostak, T. Vallaitis, M. Kuntz, D. Pavinski, A. Karanicolas, B. Behnia, D. Engel, O. Khayam, N. Modi, M. R. Chitgarha, P. Mertz, W. Ko, R. Maher, J. Osenbach, J. T. Rahn, H. Sun, K. T. Wu, M. Mitchell, and D. Welch, "System-on-Chip Photonic Integrated Circuits," *IEEE Journal of Selected Topics in Quantum Electronics*, vol. **24**, no. 1, pp. 1–24, 2018.

[53] M. Smit, K. Williams, and J. Van Der Tol, "Past, present, and future of InP-based photonic integration," *APL Photonics*, vol. **4**, no. 5, pp. 1–10, 2019.

[54] G. Carpintero, E. Rouvalis, K. Ławniczuk, M. Fice, C. C. Renaud, X. J. M. Leijtens, E. A. J. M. Bente, M. Chitoui, F. Van Dijk, and A. J. Seeds, "95 GHz millimeter wave signal generation using an arrayed waveguide grating dual wavelength semiconductor laser," *Optics Letters*, vol. **37**, no. 17, pp. 3657–3659, 2012.

[55] B. Docter, J. Pozo, S. Beri, I. V. Ermakov, J. Danckaert, M. K. Smit, and F. Karouta, "Discretely tunable laser based on filtered feedback for telecommunication applications," *IEEE Journal on Selected Topics in Quantum Electronics*, vol. **16**, no. 5, pp. 1405–1412, 2010.

[56] I. V. Ermakov, S. Beri, M. Ashour, J. Danckaert, B. Docter, J. Bolk, X. J. Leijtens, and G. Verschaffelt, "Semiconductor ring laser with on-chip filtered optical feedback for discrete wavelength tuning," *IEEE Journal of Quantum Electronics*, vol. **48**, no. 2, pp. 129–136, 2012.

[57] M. J. R. Heck, A. La Porta, X. J. M. Leijtens, L. M. Augustin, T. de Vries, B. Smalbrugge, R. Notzel, R. Gaudino, D. J. Robbins, and M. K. Smit, "Monolithic AWG-based Discretely Tunable Laser Diode With Nanosecond Switching Speed," *IEEE Photonics Technology Letters*, vol. **21**, no. 13, pp. 905–907, 2009.

[58] M. Kanskar, T. Earles, T. J. Goodnough, E. Stiers, D. Botez, and L. J. Mawst, "73% CW power conversion efficiency at 50 W from 970 nm diode laser bars," *Electronics Letters*, vol. **41**, no. 5, pp. 245–247, 2005.

[59] Junji Ohtsubo, *Semiconductor Lasers: Stability, Instability and Chaos*. Springer-Verlag, 3 ed., 2013.

[60] R. W. Tkach and A. R. Chraplyvy, "Regimes of feedback effects in 1.5-um distributed feedback lasers.," *Journal of Lightwave Technology*, vol. **LT-4**, no. 11, pp. 1655–1661, 1986.

[61] N. Schunk and K. Petermann, "Stability Analysis for Laser Diodes with Short External Cavities," *IEEE Photonics Technology Letters*, vol. **1**, no. 3, pp. 49–51, 1989.

[62] M. Khoder, R. M. Nguimdo, X. Leijtens, J. Bolk, J. Danckaert, and G. Verschaffelt, "Wavelength switching speed in semiconductor ring lasers with on-chip filtered optical feedback," *IEEE Photonics Technology Letters*, vol. **26**, no. 5, pp. 520–523, 2014.

[63] I. V. Koryukin and P. Mandel, "Dynamics of semiconductor lasers with optical feedback: Comparison of multimode models in the low-frequency fluctuation regime," *Physical Review A - Atomic, Molecular, and Optical Physics*, vol. **70**, no. 5 B, pp. 1–6, 2004.

[64] M. Khoder, M. Radziunas, V. Tronciu, and G. Verschaffelt, "Study of wavelength switching time in tunable semiconductor micro-ring lasers: experiment and travelling wave description," *OSA Continuum*, vol. **1**, no. 4, p. 1226, 2018.

[65] G. Verschaffelt, M. Khoder, R. M. Nguimdo, X. Leijtens, J. Bolk, and J. Danckaert, "Wavelength tuning speed in semiconductor ring lasers using on-chip filtered optical feedback," *Proc. of SPIE*, vol. **26**, no. 5, p. 913319, 2014.

[66] L. A. Coldren, S. W. Corzine, and M. L. Masanovic, *Diode Lasers and Photonic Integrated Circuits*. John Wiley & Sons Inc., 2012.

[67] Technobis, "www.technobis.com," March 2020.

[68] R. de Mey, R. Pawlus, and M. Virte, *Tailoring two-color laser emission using an integrated feedback cavity*. Master thesis, Vrije Universiteit Brussel - TONA/B-PHOT, 2019.

[69] R. Pawlus, S. Breuer, and M. Virte, "RIN reduction in a dual-state QD laser by optical feedback," *Optics Letters*, vol. **42**, no. 21, pp. 4259–4262, 2017.

[70] Jeppix, "www.jeppix.eu/vision," March 2020.

# ACKNOWLEDGMENTS

Looking back 12 years ago, I was working as a technician for chromatography systems. Although I was an expert on the technical specificities, I never fundamentally understood how light could be used to distinguish different substances. I felt being hold back to understand certain aspects of my work which kept me intrigued to learn more. Studying physics and following the path of optics opened my eyes and led to a unique experience which now peaked in obtaining my PhD degree. Along this journey I had the joy to meet different people and I would like to take the opportunity to thank them.

First, I would like to thank Klaus Renner, who not only taught me a great deal about all kind of manual skills, but also opened my horizon to possible career paths to continue to grow. You believed in me and motivated me to follow an academic path to find all the answers and the satisfaction I was looking for. You were the driving person who got the ball rolling, without you, I would have missed countless experiences, opportunities and friendships in all these years. Obviously, you are also the one I like to blame for all the stress, struggle and pain I went through in my studies, but the benefits clearly out wage the downsides. Thank you for believing in me, supporting me and being my mentor ever since!

Throughout my studies I was more and more intrigued by semiconductor lasers. To learn more and get my hands on them, I joined the group of Stefan Breuer in 2014 for my Bachelor and Master thesis. At that time, I could not have imagined the path this would lead to. I got the opportunity to improve my experimental skills, deepen my understanding of semiconductor lasers and became a member of an amazing team I enjoyed being part of. Thank you very much for including me into your group, guiding and support me in all these years and giving me the opportunity to grow.

Next I would like to thank Martin Virte, who was the mastermind behind all this work. I appreciate your balance of applying pressure whenever necessary, but also providing support and positive words when I needed them the most. I could always count on your full support whenever something was not going as planned. Your guidance and advices were invaluable and always helped me to see the bigger picture. Please keep your attitude and your enthusiasm so future generations of students may have the same positive experience throughout their studies as I did. Thank you!

I would also like to thank Hugo Thienpont, the head of the Department of Applied Physics and Photonics, for the opportunity to join your group and becoming a part of B-PHOT. Thank you for your support and all the motivational words throughout the years.

Changing the country for my studies was a difficult and worrying decision. However, arriving at B-PHOT, I had the joy to share an office with Sidney Goossens, Urszula Nawrot and Agnieszka Gierej. You were the ones welcoming me, helping me to get settled and showing me around in the city. You always created a nice atmosphere in the office I enjoyed being a part of. Throughout the years of our studies, we all went through different phases, good ones and bad ones. We were celebrating the good times together and supporting each other in the bad ones. This clearly grew us together as a team and became true friendship which I hope will last for decades to come! The discomfort of changing the country quickly turned into a great experience. Thank you for your support, your trust and your friendship!

Next I would like to thank Robbe de Mey who joined B-PHOT doing his Master thesis. Thank you for putting your trust in our small group and joining our team. Your work helped me to understand different aspects of my project and found a nice place in this thesis. Thank you very much!

I would also like to thank the whole B-PHOT team for the pleasant working environment. Special thanks go to the secretary team and the administrative & IT support who always took care of all needs and issues I faced throughout these years. Without all your support, achieving this goal would have been much more difficult, thank you all!

Next I would like to thank my jury for taking the time to carefully read my thesis and evaluating my work. I would also like to include the jury of my committee who supported and guided me throughout these years. Although the annual evaluations have not been the most pleasant times, the questions I faced always opened up a new way of thinking and showed me a new point of view on the challenges I faced. This helped me to continuously develop my critical thinking, my approaches to solve issues and helped me to grow as a person. Thank you!

Special thanks go also to SmartPhotonics in The Netherlands for their outstanding work of manufacturing the Photonic Integrated Circuits I was able to demonstrate my PhD project with. I also thank the COBRA research institute for allowing me to use their layout of a 85:15 MMI splitter to improve my designs.

Next I would like to thank my colleagues Christoph Weber, Andreas Herdt and Dominik Auth at the Technische Universität in Darmstadt of who I was a member of for about 9 months. Thank you for welcoming me in your group, the friendly environment and the help to find myself around in the lab. I would also like to take the opportunity to thank my former colleagues Sébastien Blumenstein, Andreas Molitor and Till Mohr who introduced me into the work of a PhD student which motivated me to pursue my own PhD. Thank you all!

In all these years, there have been a few constants in my life who supported me unconditionally, my friends and family.

Ständig mit Wissenschaftlern umgeben zu sein kann schon manchmal ganz schön anstrengend sein. Ich möchte mich daher bei meinen Freunden bedanken, die es mir immer wieder erlaubt haben, den Kopf frei zu bekommen und Kraft zu tanken. Ich habe mich immer auf unsere regelmäßigen Treffen gefreut, es war immer eine ideale Möglichkeit dem Alltag zu entfliehen und die Heimat zu besuchen. Vielen Dank für all die schöne Zeit!

Ich möchte mich auch bei Tim Ratajczyk für sämtliche Sporteinheiten und speziell den Mountainbike Touren in all den Jahren bedanken. Diese Touren waren immer die ideale Lösung, um den alltäglichen Stress mit jeder Menge Spaßabzubauen. Vielen Dank dafür und ich freue mich auf unsere zukünftigen Touren!

Zu guter Letzt möchte ich mich bei meinen Eltern Bedanken die mich bei allen meinen Wünschen, Vorhaben und Phasen bedingungslos unterstütz haben. Ihr habt mir jederzeit allen Rückhalt gegeben, den ich während meiner Studienzeit gebraucht habe, in den letzten 4 Jahren mehr denn je. Leider wart es auch ihr, die meine schlechten Launen unmittelbar miterlebt haben wenn mal etwas mal nicht nach Plan lief. Für euer Verständnis und eure Geduld in dieser Zeit möchte ich mich herzlich bedanken! Speziell in den finalen Monaten der Doktorandenzeit, die zur Fertigung dieser Thesis geführt haben, habt ihr mir jederzeit den Rücken freigehalten und mich in allem unterstützt. Ohne euch wäre dieses Projekt nicht möglich gewesen, herzlichen Dank dafür!

**Robert Pawlus**
Brussels, 15th June 2020

# CURRICULUM VITAE

| | |
|---|---|
| 2016-2020 | Joint PhD candidate at the Vrije Universiteit Brussels, Belgium and the Technische Universität Darmstadt, Germany.<br>Working on tailoring multi-wavelength laser emission in semiconductor lasers via optical feedback. |
| 2009-2016 | Studies of Physics at the Technische Universität Darmstadt, Germany.<br>**Master degree in Physics**<br>Thesis title "Investigations on the relative intensity noise of two-state quantum-dot semiconductor lasers" |

TECHNISCHE
UNIVERSITÄT
DARMSTADT

**Erklärung gemäß §9 Promotionsordnung**

Hiermit versichere ich, dass ich die vorliegende Dissertation selbstständig angefertigt und keine anderen als die angegebenen Quellen und Hilfsmittel verwendet habe. Alle wörtlichen und paraphrasierten Zitate wurden angemessen kenntlich gemacht. Die Arbeit hat bisher noch nicht zu Prüfungszwecken gedient.

12.05.2020

Datum und Unterschrift